INVESTIGATION OF THERMOPHYSICAL PROPERTIES OF ENHANCED MOLTEN SALT NANOFLUIDS FOR THERMAL ENERGY STORAGE (TES) IN CONCENTRATED SOLAR POWER (CSP) SYSTEMS

by

JOOHYUN SEO

Presented to the Faculty of the Graduate School of

The University of Texas at Arlington in Partial Fulfillment

of the Requirements

for the Degree of

DOCTOR OF PHILOSOPHY

THE UNIVERSITY OF TEXAS AT ARLINGTON

December 2017

Copyright © by Joohyun Seo 2017

All Rights Reserved

Acknowledgements

My Ph.D. life would not have been possible without my LORD who determines my every steps and knows the number of hairs on my head.

First of all, I wish to express my deep sense of gratitude to Dr. Donghyun Shin, my advisor, for providing me an opportunity to complete my Ph.D. program in Nanomaterials Research Lab (WH 110). I also sincerely thank him for the invaluable guidance, direction, and encouragement in carrying out my project work as well as this dissertation. I would like to thank GE (General Electric) for giving me an opportunity to carry out this research and for their financial support during my Ph.D. program. I express my sincere gratitude to my committee members, Dr. Hyejin Moon in MAE, Dr. Yaowu Hao, and Dr. Kyungsuk Yum in MSE, and I would never have been able to complete my dissertation without their professional advice, guidance, and help. I would like to thank my lab members, Dr. Hani Tiznobaik, Vidula Pawar, Sumeet Changla, Sriram Sambasivam, Aditya Pinto, Zahra Pournorouz, Amirhossein Mostafavi, and Vamsi Kiran Eruvaram. I will never forget our valuable time together in research day and night in WH 110.

I would like to express my heartfelt thanks to my father, Dr. Seung-Jik Suh, and my mother, Mrs. Jiyeon Lee, for their almost unbelievable support, prayers, and unconditional love. My deepest appreciation belongs to my father-in-law, Mr. Minsik Kim, and my mother-in-law, Mrs. Hyojung Lee, for their patience, understanding, and prayers during my Ph.D. life. I would like to thank my brother, Mr. Chang Hyun Seo (will be Ph.D. soon), and my sister-in-law, Mrs. Eunkyung Shin, my first nephew, Taerang Aiden Seo, and my second nephew, Harang Ian Seo, for always cheering me up in Arlington. I will also never forget the wonderful home-cooked meals in my brother's house when I missed Korean food. I would also like to thank my brother-in-law, Mr. Jisoo Kim, for having an interest in me in hard times.

Finally, I owe thanks to my beloved wife, Jeewon Kim, who always encouraged me, for her continued and unfailing support, love, understanding, and prayers during my Ph.D. life. This dissertation would not have been completed without my wife's infinite patience, an unfailing source of solace, and encouragement. I dedicated this dissertation to my beloved wife, Jeewon Kim.

Abstract

INVESTIGATION OF THERMOPHYSICAL PROPERTIES OF ENHANCED MOLTEN SALT NANOFLUIDS FOR THERMAL ENERGY STORAGE (TES) IN CONCENTRATED SOLAR POWER (CSP) SYSTEMS

Joohyun Seo, PhD

The University of Texas at Arlington, 2017

Supervising Professor: Donghyun Shin

Concentrated solar power (CSP) technologies have a great economical and technical potential for energy production in future. Its incorporation with thermal energy storage (TES) overcomes one of the biggest challenges in most renewable energy technologies, the intermittency of energy supply by natural resources. TES with 15-hour storage capacity is already commercialized to operate a CSP plant for 24 hours a day. When the sunlight is concentrated by mirrors into a small focal point, a heat transfer fluid (HTF) transfers the collected heat to a turbine or an engine to produce electricity and any surplus heat to a TES unit for later use. Typical CSP plants used two different materials for HTF and TES, and thus several heat exchangers were necessary between HTF and TES. These heat exchangers can cause a significant temperature drop and associated thermodynamic penalties. The potential capital cost increase is also not negligible.

Using a binary nitrate salt (termed as “solar salt”) as a single storage fluid for both HTF and TES can not only simplifies the heat transport/storage system but also minimize a potential energy loss. Its high-temperature stability (over 500 °C) can also increase the overall thermodynamic efficiency. However, solar salt has a relatively high melting point (220 °C), and it is likely to freeze under a harsh condition such as nighttime,

rainy, or cloudy day. As a result, an auxiliary heater is required for a freeze protection and can significantly decrease the power output. Hence, it is necessary to investigate alternative storage fluid whose melting point is low enough to minimize the energy loss. A ternary nitrate salt mixture ($LiNO_3$-$NaNO_3$-KNO_3) has a very low melting point (~100 °C). Using this mixture as a single storage fluid for both HTF and TES in a CSP can significantly reduce the energy loss by the freeze protection but also enhance CSP's energy conversion efficiency. However, the heat storage density of these molten salts is typically low. Literature study shows that dispersing appropriate nanoparticles can enhance salts' heat capacity. This can not only reduce the required HTF and TES amount, but also reduce the size of thermal transport and storage systems (e.g., pipes, heat exchanger, and storage tanks).

In this study, several commercial SiO_2 nanoparticles were first dispersed into a ternary nitrate salt to see if it can enhance its effective heat capacity. Several SiO_2 nanoparticles at different sizes were tested to investigate the effect of nanoparticle size. Fresh nanoparticles, then, were *in-situ* synthesized in a binary and ternary nitrate salts. $Al(NO_3)_3 \cdot 9H_2O$ (aluminum nitrate nonahydrate) and $Mg(NO_3)_2 \cdot 6H_2O$ (magnesium nitrate hexahydrate) were induced to decompose in a molten nitrate salt to produce Al_2O_3 and MgO nanoparticles. The new method (Liquid to Liquid) for the sample preparation was used to increase the enhancement of specific heat of a binary nitrate salt with SiO_2 nanoparticle. A modulated differential scanning calorimeter (MDSC; Q20, TA Instrument Inc.) was used to measure the effective heat capacity. A discovery hybrid rheometer (HR-2, TA Instruments Inc.) was employed to measure the mixture's viscosity. A customized apparatus was built to measure its effective thermal conductivity. A figure of merit analysis was performed to predict the performance of the mixture. A scanning electron microscope (SEM: Hitachi S-3000N and S-5000H) was used for material

characterization. Moreover, molecular dynamics simulation was performed to investigate the effect of nanoparticles on the observed property measurements.

Table of Contents

List of Illustrations

List of Tables

Chapter 1

Introduction

Concentrated Solar Power (CSP) System

There are different types of concentrated solar power (CSP) systems to collect and focus sunlight as shown in figure 1 [1]. The dish type solar concentrator includes a parabolic dish and stirling engine to convert energy from sunlight to electricity. The solar power tower consists of several solar collector (e.g., heliostats) and concentration component (e.g., central receiver) to produce high system efficiency using concentrated sunlight. The parabolic trough solar concentrator tracks the sun with a single axis and it produces less efficient than other types of CSP systems. This type of CSP systems operates at low temperature compared to other types.

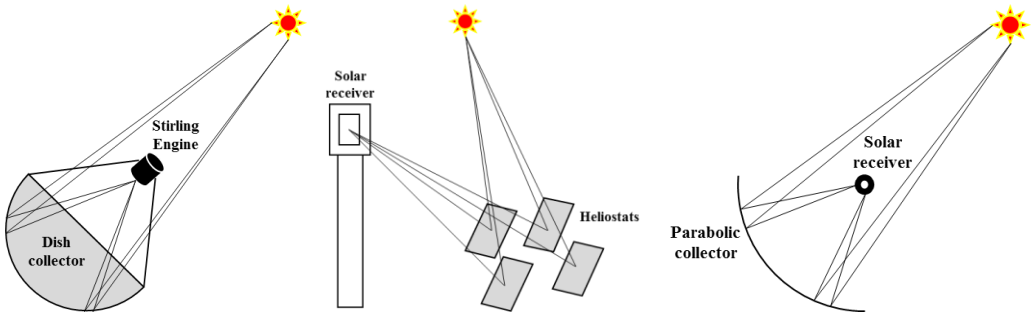

Figure 1 Dish type solar concentrator (left), solar power tower (middle), and parabolic trough solar concentrator (right) [1]

As shown in figure 2 [2], the CSP system consists of several components such as the solar receiver and heliostats, thermal energy storage (TES), heat transfer fluid (HTF), and power conversion module (e.g., turbine engine). The solar receiver and heliostats collects and focuses sunlight and a large number of heliostats provides high concentrated solar flux. TES has two storage tanks (hot tank and cold tank) to store solar energy at high temperature as shown in figure 3 [3]. It provides several desired properties. First, it can enhanced efficiency of thermodynamic cycle due to high operating

temperature. Second, it has the high heat capacity (e.g., high heat storage capability) and thus it can reduces cost of the structure and material. Third, TES can reduce cost of heat exchanger because it has the high thermal conductivity (e.g., high heat transfer capability). Moreover, it shows properties such as low pressure, non-toxic, and less reactive and thus it is appropriate for the side of safety and economics. HTF delivers the working fluid to the heat exchanger from two storage tanks.

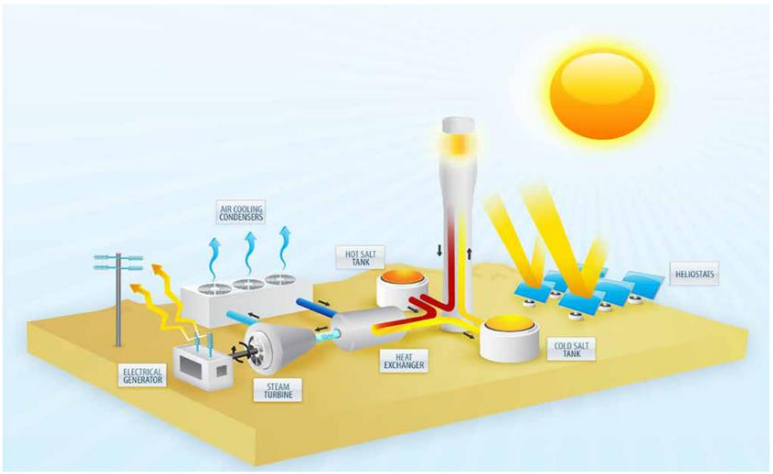

Figure 2 Schematic of the concentrated solar power (CSP) system [2]

Figure 3 Two storage tanks at Andasol CSP system in Spain [3]

Single Storage Fluid for Heat Transfer Fluid (HTF) and Thermal Energy Storage (TES)

In the CSP system field, different working fluids have been used for heat transfer fluids (HTF) and thermal energy storage (TES) as shown in figure 4 [4]. Heat exchangers are required for the conventional CSP to transfer heat energy between HTF and TES. However, the addition of the heat exchanger in CSP causes increased total production cost of electricity and decreased exegetic efficiencies.

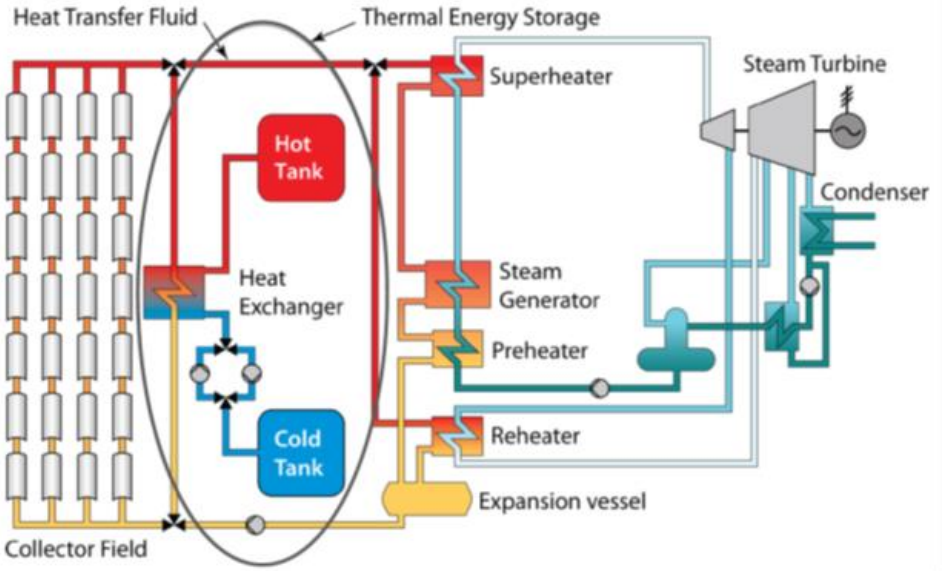

Figure 4 Different fluid for HTF and TES [4]

To prevent thermodynamic penalties related to the heat exchangers, the single working fluid is used for HTF and TES in the most advanced TES system as shown in figure 5 [4]. In general, the binary nitrate molten salt eutectic (e.g., $NaNO_3$-KNO_3; 60:40 by weight ratio) shows 220 °C for the melting temperature [5]. However, the auxiliary heater is required to operate the CSP system with HTF and TES over the melting point to prevent freeze protection [6]. According to the current research [7], it suggested the ternary nitrate molten salt eutectic (e.g., $LiNO_3$-$NaNO_3$-KNO_3) due to the low melting temperature (~100 °C) for the advanced TES medium. For example, when this ternary

molten salt eutectic is used for the working fluid as the single storage fluid for HTF and TES, there are several benefits. First, it can considerably cut down the total production cost of electricity due to no heat exchangers between HTF and TES and it shows the high exergy efficiency. Second, it can reduce the heat load is related to the freeze protection and it provides cost-effective controls for HTF and TES in the CSP system. However, CSP systems are insufficiently competitive compared to coal-fired power plants without a government subsidy even though this ternary molten salt eutectic has the advantages. According to the report [8], solar power plants received government supports in 2013, and the overall support was around 30 % for power production. Enhanced specific heat capacity of the TES material can primarily reduce the total production cost of electricity from the current CSP workshop in 2011 [4]. It can not only reduce the required HTF and TES amount, but also reduce the size of thermal transport and storage systems (e.g., pipes, heat exchanger, and storage tanks). Therefore, these days many studies have focused on enhanced specific heat capacity of different molten salt eutectic with nanoparticles.

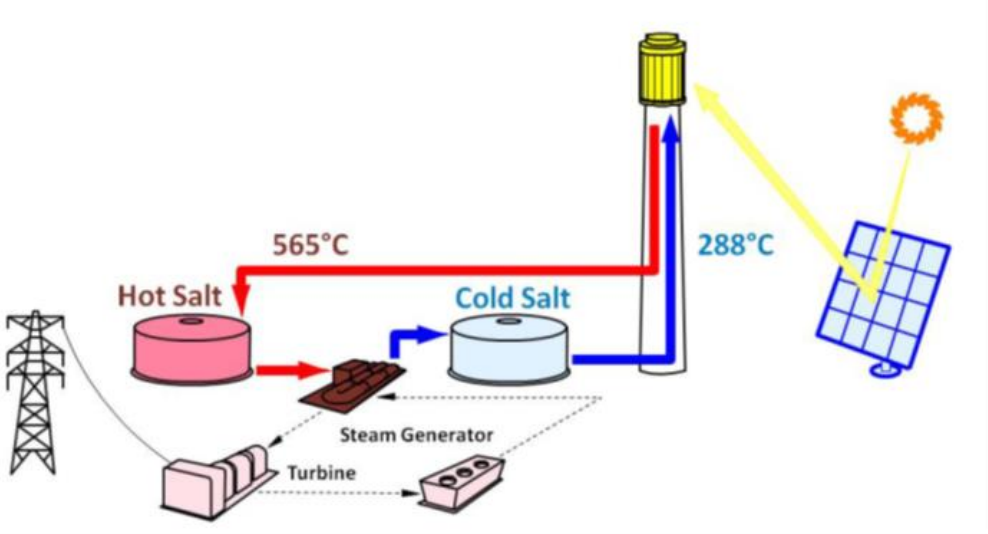

Figure 5 Single storage fluid for HTF and TES [4]

Thermal Energy Storage Media: Molten Salt Eutectic

The molten salt eutectic is currently regarded as a promising material among others to operate renewable energy systems. In the current industrial field, it can be used as heat transfer fluids (HTF) [9]-[11] in thermal energy storage (TES) [12]-[14] as well as phase change materials (PCM) [15]-[17] in renewable energy systems. In practice, a molten salt eutectic can be used as the working fluid in concentrated solar power (CSP) systems [9]-[13], [15], [16] and nuclear power system [18]. They have been proven effective to enhance the system efficiency compared to other energy systems without a molten salt eutectic. According to the literature, alkali carbonate salt eutectic has high thermal stability with high temperature over 600 °C [5], and it can be used as a substitute for the working fluid in advanced TES material. The molten salt eutectic-carbonate based (e.g., Li_2CO_3-K_2CO_3) has high temperature stability up to 565 °C, and thus it can allow CSP plants to operate at a high temperature in comparison with other conventional plants [19]. The power conversion efficiency of the thermodynamic cycle (e.g., Rankine cycle, Stirling cycle, etc.) can be considerably enhanced due to high operating temperature compared to other CSP plants' working fluid such as mineral oils (its operating temperature is about 350-400 °C) [20]. The molten salt eutectic allows structures of a system to be decreased mechanical stress due to a lower vapor pressure [5]. In other words, this lower vapor pressure can reduce a potential risk of breakage or leakage significantly in the TES due to efficient TES designs without pressurized vessels [21]. The molten salt eutectic is economically feasible compared to mineral oils for the TES [20]-[22]. Most molten salt eutectics are non-toxic and abundant [23], [24]. It means the molten salt eutectic can allow a low environmental and material cost [19]-[25]. Nevertheless, typically molten salt eutectic shows poor thermo-physical property such as specific heat capacity (C_p) is less than 2 kJ/kg °C [5]. This poor property is responsible for

an increase in the scale of a storage system. Material and environmental costs of the system also naturally increase. Hence, there is a need to find better performing TES technologies and materials. Novel materials (e.g., nanomaterial additives) can become cost-effective if they increase the operating range of the storage facilities to a higher range of temperatures.

Classical Nanofluids: Enhancing Thermal Conductivity

The thermal conductivity of a nanofluid has been reported in a number of experimental studies [26]-[42] since nanofluids were first introduced in 1995 [26]. Two different solutions (e.g., water and ethylene glycol) were used to dissolve nanoparticles. With water, the nanofluid with Al_2O_3 nanoparticle showed 23 % enhancement with 4.0 % concentration by volume [43] and nanofluid with SiC nanoparticle was reported by 17 % enhancement of thermal conductivity at 4.18 % concentration by volume [44]. The nanofluid with Cu (7.5 % concentration by volume) and CuO nanoparticle with 4.0 % concentration by volume were dissolved in water, and they showed enhanced thermal conductivity by 75 % and 36 % respectively [31], [45]. With ethylene glycol, the nanofluid with Fe (0.55 % concentration by volume) and CuO with 14.8 % concentration by volume showed 18 % and 54 % enhancement of thermal conductivity respectively [34], [46]. The multi-walled carbon nanotubes with ethylene glycol were used for the measurement of thermal conductivity, and it showed 13 % enhancement of thermal conductivity with 1.0 % volume fraction [47]. According to the literature [35]-[39], they suggested several mechanisms (Brownian motion, semi-solid layering of liquid molecules, interfacial thermal resistance, and heat transfer in nanoparticles) to explain how thermal conductivity of nanofluids is enhanced. The conventional approach cannot fully explain why nanofluids show effective thermal conductivity and thus literature suggested possible mechanisms such as liquid-layering, particle aggregation, particle Brownian motion, and Brownian motion induced convection [48]. According to the figure of merit (FOM2) [49], performance of the system can be analyzed as heat transfer fluid (HTF). The density, specific heat, thermal conductivity, and viscosity of HTF are used to evaluate performance of the system.

Molten Salt Nanofluids: Enhancing Specific Heat

Specific heat capacity of a nanofluid has been reported in the recent literature. For polyalphaolefin (PAO) with graphite nanofluid (0.6 %) doped with nanoparticles, specific heat capacity of this nanofluid was enhanced by 50 % [50]. Specific heat capacity of a binary nitrate salt eutectic with SiO_2 nanoparticle was enhanced by 20 % [51]. In comparison with the bulk material, obviously specific heat capacity of nanoparticles can be increased. However, the concentration of a nanoparticle in those molten salt nanofluids is very small (~1 %) with a conventional water and specific heat capacity of water (4.18 kJ/kg °C) in general is higher than enhanced specific heat capacity of a nanoparticle. Therefore, many studies (experimental and theoretical aspects) have been reported enhanced specific heat capacity of a nanoparticle [51]-[55]. They showed a nanoparticle could make an extremely large specific surface compared to their bulk material and thus the effect of a surface phonon can be dramatically enhanced due to the enlarged specific surface area. Recent studies have been reported a molten salt eutectic doped with the nanoparticle to obtain enhanced specific heat capacity in a nanofluid. Thus, several nanofluids (e.g., molten-based) reported highly enhanced specific heat capacity [20]-[23], [56]-[67]. In general, there are two groups for a molten salt eutectic such as nitrate-based and carbonate-based molten salts with different nanoparticles. For a nitrate-based molten salt eutectic, a binary molten nitrate salt eutectic ($NaNO_3$:KNO_3= 60:40 by weight ratio) with SiO_2 nanoparticle was reported by 20 % enhanced specific heat capacity, and its nanoparticle was dispersed in salt eutectic at 1% concentration by mass [23]. Also, doping with a different concentration ratio of SiO_2 nanoparticle (0.5 % to 2 % by mass) in the same binary molten nitrate salt eutectic ($NaNO_3$-KNO_3) was reported by 25 % enhanced specific heat capacity at 1 % concentration by mass [57]. At the same base material (binary nitrate salt- $NaNO_3$-KNO_3), doping with several nanoparticles such

as SiO_2, Al_2O_3, TiO_2, and SiO_2-Al_2O_3 at 0.5, 1.0, and 1.5 % concentration by mass was reported enhanced specific heat capacity by ~20 % at 1 % concentration by mass among others [58]. Al_2O_3 nanoparticle at 0.78 % concentration by mass in the same binary molten nitrate salt eutectic ($NaNO_3$-KNO_3) was reported by 30.6 % enhancement of specific heat capacity [59]. Also, two different nanoparticles (CuO at 0.1 to 1.5 % concentration by mass & TiO_2 at 0.1 to 1.5 % concentration by mass) were dispersed in a binary nitrate molten salt eutectic ($NaNO_3$-KNO_3) and 11 % enhanced specific heat capacity was shown at 0.1 % concentration by mass of CuO nanoparticle and 5 % enhanced specific heat capacity was shown at 0.5 % concentration by mass of TiO_2 nanoparticle, respectively [60]. A ternary molten nitrate salt eutectic ($LiNO_3$:$NaNO_3$:KNO_3= 38:15:47 by molar ratio) doped with SiO_2 nanoparticle at 1.0 % concentration by mass was reported by 13 % enhanced specific heat capacity and this salt shows 15-16% enhanced specific heat capacity of three different particle size (10nm, 30nm, and 60nm) [20], [21]. Another ternary molten nitrate salt eutectic ($NaNO_3$:KNO_3:$Ca(NO_3)_2$= 49:30:21 by molar ratio) with SiO_2 nanoparticle was reported by 19 % enhanced specific heat capacity and its concentration was fixed at 1 % by mass [61]. For a carbonate-based molten salt eutectic, a binary molten carbonate salt eutectic (Li_2CO_3:K_2CO_3=62:38 by molar ratio) doped with SiO_2 nanoparticle (1 % by mass concentration) were shown enhanced specific capacity by ~26 % [62], [63] and doping with SiO_2 nanoparticle (1.5 % by mass concentration) were shown enhanced specific capacity by ~124 % [64]. The same binary molten carbonate salt eutectic (Li_2CO_3:K_2CO_3=62:38 by molar ratio) with the different nanoparticle (Al_2O_3 with 1.0 % mass concentration) was shown enhanced specific heat capacity by ~32 % for a nanofluid [65]. For other chemicals-based molten salt eutectics, quaternary alkali metal chloride salt ($BaCl_2$-$CaCl_2$-LiCl-NaCl) with SiO_2 nanoparticle at 1.0 % mass concentration

was reported by 15 % enhanced specific heat capacity [66]. HITEC conventional eutectic salt (KNO_3:$NaNO_2$:$NaNO_3$=53:40:7 by molar ratio) doped with Al_2O_3 nanoparticle at 0.063 % mass concentration shown enhanced specific heat capacity by ~20 % [67].

Molten Salt Nanofluids: Enhancing Viscosity

The viscosity of a nanofluid has been reported in the recent literature. The molten salt eutectic and ethylene glycol were used as the base fluid with a nanoparticle. The nanofluid of Li_2CO_3-K_2CO_3 with the multi-walled carbon nanotubes (2.0 % weight fraction) showed 90 % enhancement of viscosity [68] and CuO nanoparticle (1.0 % weight fraction) was added to $NaNO_3$-KNO_3 and it showed enhanced viscosity by 18 % [69]. The nanofluid of ethylene glycol with TiO_2 nanoparticle showed increased viscosity by 22.75 % at 8.0 % weight fraction [70]. However, when the viscosity of the heat transfer fluid (HTF) is enhanced in the thermal energy storage (TES), the total cost of the CSP system is increased due to the high pumping power. To estimate the required pumping power in the system, the evaluation of thermophysical properties of nanofluids is necessary for the system to maintain the temperature difference between the inlet and outlet of the storage fluid. According to the figure of merit (FOM1) [71], performance of the system can be analyzed as thermal energy storage using density, specific heat, and viscosity of the working fluid. The required pumping power of different fluids is evaluated, and the density of the storage fluid is constant in this case.

Molecular Dynamics (MD) Simulation

As I mentioned earlier, the enhanced specific heat of a molten salt nanofluid can reduce the total production cost of electricity from concentrate solar power (CSP) systems. This cost-effective control relates to the effect of enhancement in the specific heat of heat transfer fluids (HTF) and thermal energy storage (TES) systems. However, there are a number of restrictions on the practical use of the ionic liquid-based nanofluid. For example, HTF and TES systems require a large amount of a working fluid to operate the CSP system at high temperature in the field. It is difficult to predict the effect of enhancement in the specific heat of a molten salt nanofluid in the CSP system. In other words, current technology makes it difficult to control and model the formation of different phases at nanoscale interfaces of a molten salt nanofluid in experiments. Molecular Dynamics (MD) simulation can be a powerful tool for confirming results before conducting experiments. For example, we can easily build the formation of different phases at nanoscale interfaces in a simulation domain under a molecular modeling tool to confirm the practical use of the ionic liquid-based nanofluids (e.g., molten salt nanofluid) of HTF and TES systems. According to the recent studies [72]-[74], researchers have questioned variable factors to approve the formation of different phases at nanoscale interfaces of the molten salt nanofluid. They have only conducted the effect of the enhanced specific heat on a nanoparticle in a molten salt nanofluid. Therefore, the computational approach is required to explain the formation of a different phase at nanoscale interfaces in nanofluids. It is the key factor for understanding enhanced conventional the heat transfer fluid (HTF) and thermal energy storage (TES) systems.

Chapter 2

Proposed Mechanisms for Enhanced Specific Heat in the Literature

According to the previous chapter, the cost-effective control relates to the effect of enhancement in the specific heat capacity of heat transfer fluid (HTF) and thermal energy storage (TES) systems in a solar thermal power plant. However, there are a number of restrictions on the practical use of the ionic liquid-based nanofluids. Current technology makes it difficult to control and model the formation of different phases at nanoscale interfaces in experiments. According to the current research [31], [34], [43]-[47], they have recently identified enhanced thermophysical properties of ionic liquid-based nanofluids by modeling the formation of a different phase at nanoscale interfaces. They have focused on enhancing thermal transport properties of nanofluids for many years. However, much of the research has only shown enhanced thermal conductivities of nanofluids using effective medium theory [40]-[42]. By thermal equilibrium, they reported that specific heat capacity agreed with conventional effective specific heat capacity models. Subsequently, they have generally agreed that a significant impact on specific heat capacity is not related to the addition of nanoparticles into a fluid. However, according to recent studies [20], [21], [43], [45], [46], [57]-[66], proper dispersal of oxide nanoparticles can increase thermophysical properties (e.g., specific heat capacity and thermal conductivity) for ionic liquid-based nanofluids. For ionic liquid-based nanofluids, researchers observed 25-30 % enhanced specific heat capacity and 35-40 % enhanced thermal conductivity. From the current research on material characterization of these nanofluids, enhanced thermophysical properties (e.g., specific heat capacity) of ionic liquid-based nanofluids (e.g., molten salt nanofluid) closely relates to the formation of a different phase at nanoscale interfaces. Therefore, the formation of a different phase at

nanoscale interfaces in nanofluids is the key factor for understanding enhanced conventional the heat transfer fluid (HTF) and thermal energy storage (TES) systems.

Increased Nanoparticle's Specific Heat than its Bulk Material

According to the literature [39], [55], [66], [75]-[77], they proposed three different mechanisms of enhanced specific heat of nanofluid as shown figure 6-8. The case 1 is the higher specific heat of nanoparticles than bulk value of nanoparticle. Since the surface energy of the nanoparticle per unit mass is high, specific heat of particles is enhanced by 25 % compared to the bulk value of particle. According to the theoretical study [55], it proposed the theoretical model to analyze specific heat of nanoparticle. Specific heat of nanoparticle was increased when its size is decreased. According to the experimental research [52], specific heat of Al_2O_3 nanoparticle was enhanced by 25 % compared to the bulk value of Al_2O_3 nanoparticle. As shown in figure 6, it shows the high surface energy near a nanoparticle due to the higher amplitudes and lower natural frequency that are related to the vibration of the surface atoms. Therefore, discrete value of the phonon of nanoparticle are constrained by its size and it shows quantized phonon spectrums of nanoparticles. However, typical nanoparticle concentrations are very small (~1% by mass) and thus the effect of the enhanced specific heat of nanoparticles on the effective specific heat of their mixture is small. Hence, this cannot fully explain the enhanced specific heat of molten salt nanofluids. In other words, although the size of the nanoparticle is related to the enhanced its specific heat, it is hard to say that specific heat of nanofluid has a close connection with nanoparticle's size. Other mechanisms are required to explain this phenomenon in more detail [78]-[80].

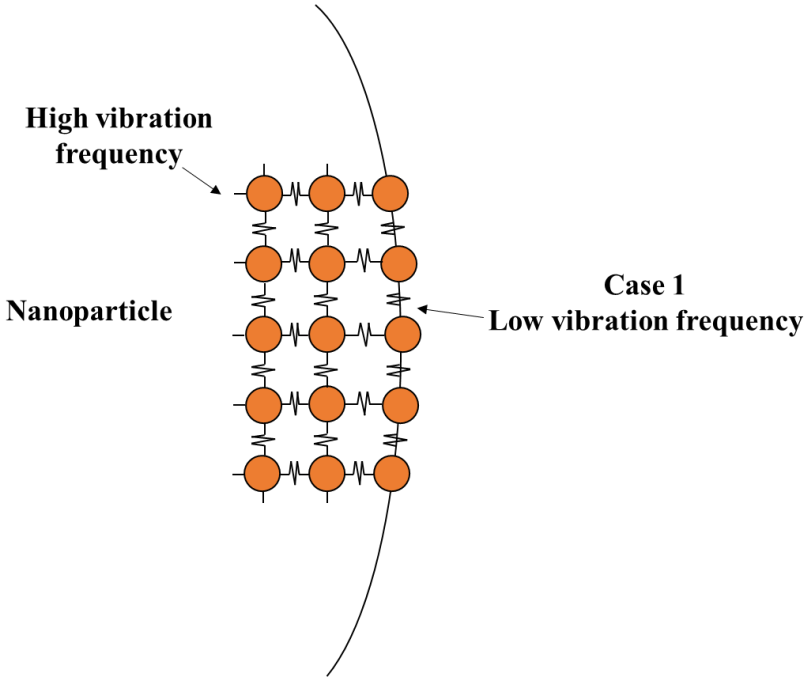

Figure 6 Case 1: higher specific heat of nanoparticles than bulk value of nanoparticle [66]

Interfacial Thermal Resistance

The case 2 is the solid-fluid interaction energy between two different layers in liquid as shown in figure 7. The interfacial thermal resistance is increased between nanoparticles and liquid molecules due to the high surface area per unit volume of nanoparticles. In other words, specific heat of nanofluid is increased when the nanoparticle is added in the liquid solution because of the enlarged surface area. According to previous studies [39], [75], enhanced interfacial thermal resistance functions as the additional thermal storage between nanoparticles and liquid molecules. Since the interfacial interaction between interfacial molecules and nanoparticle atoms is increased, the interfacial thermal resistance is increased between interfaces. Therefore, this phenomenon may be responsible for the enhanced specific heat of nanofluid (nanoparticle and liquid). However, interfacial thermal resistance exists both in classical nanofluids and molten salt nanofluids. If this mechanism is responsible for the enhanced specific heat of molten salt nanofluids, classical nanofluids should also show enhanced specific heat. However, literature shows that the specific heat of classical nanofluids (water, oil, or ethylene glycol-based) decreased with the addition of nanoparticles [78]-[80] and thus it may not be primarily responsible for the observed enhanced specific heat of molten salt nanofluids.

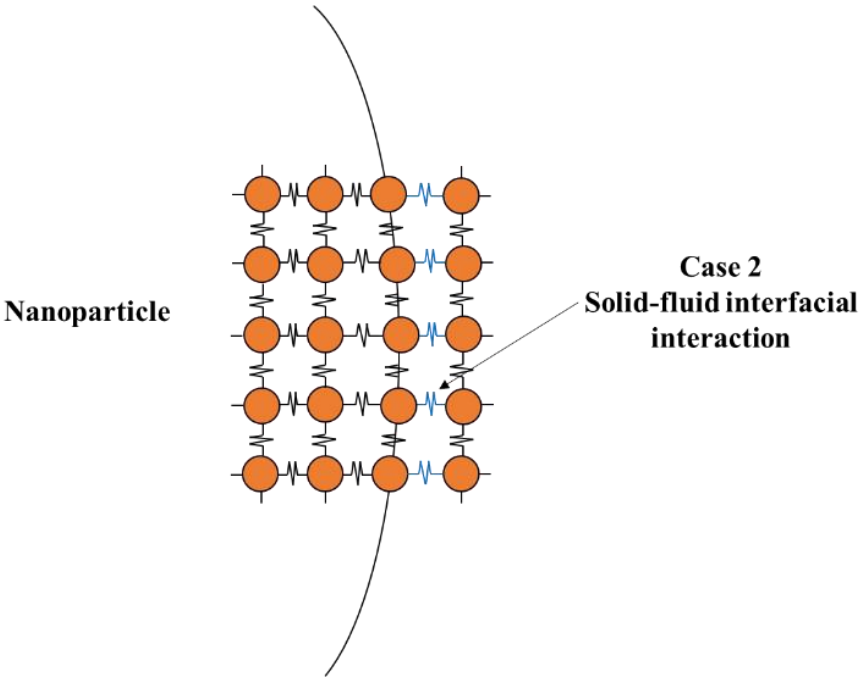

Figure 7 Case 2: solid-fluid interaction energy [66]

Semi-Solid Layering of Liquid Molecules

The case 3 is the liquid molecules layer at the surface (e.g., semi-solid layer) as shown in figure 8. Liquid molecules adhere to the surface of the nanoparticle and it forms a semi-solid layer between the surface of the nanoparticle and liquid molecules. The surface energy of the nanoparticle is responsible for the thickness of a semi-solid layer of liquid molecules (e.g., adhesion layer). The semi-solid layer contributes to enhanced thermophysical properties (e.g., specific heat) of nanofluid compared to the bulk liquid. According to the simulation study [76], it proved that the semi-solid layer exists between the nanoparticle and liquid molecules using molecular dynamics (MD) simulation. According to the experimental study [77], the semi-solid layer was proved experimentally by TEM images and it demonstrated that ordering of liquid molecules exists between solid surface (sapphire) and liquid surface (liquid aluminum). Increased adhesion layer of liquid molecules is a major contributory factor in increasing the surface energy of the interface between the solid surface and liquid surface. When the size of the nanoparticle is decreased, the mass fraction of the adhesion layer (semi-solid) is increased on the nanoparticle surface and it is related to enhanced specific heat. However, semi-solid layering of liquid molecules near nanoparticles can exist both in classical nanofluids and molten salt nanofluids. If this mechanism is responsible for the enhanced specific heat of molten salt nanofluids, classical nanofluids should also show enhanced specific heat. However, literature shows that the specific heat of classical nanofluids (water, oil, or ethylene glycol-based) decreased with the addition of nanoparticles [78]-[80] and thus it may not be primarily responsible for the observed enhanced specific heat of molten salt nanofluids. It does not have to be and other mechanisms is required to explain that this semi-solid liquid layer between the solid and liquid interface has a close relation to enhanced specific heat of nanofluids [78]-[80].

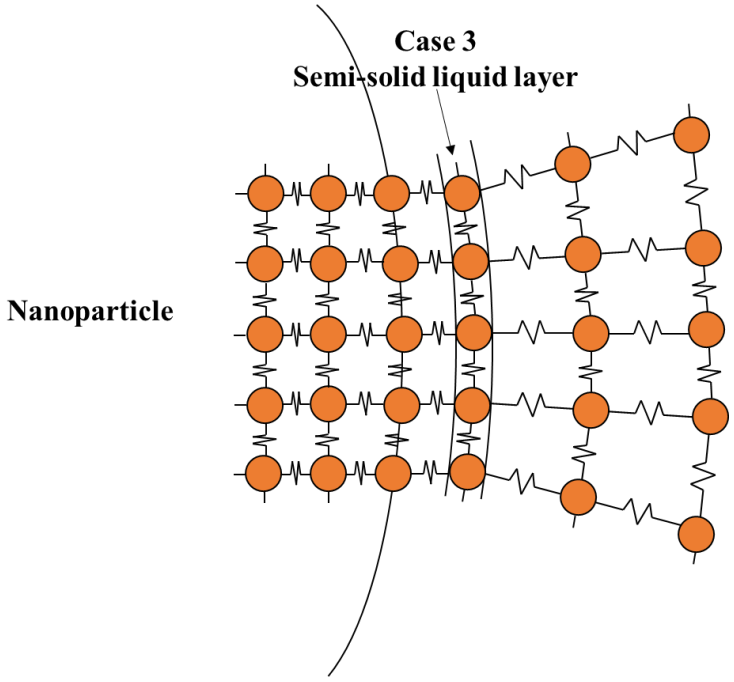

Figure 8 Case 3: semi-solid behavior (liquid molecules layer at surface) [66]

Summary

As I mentioned earlier, three different mechanisms such as increased nanoparticle's specific heat than its bulk value, enhanced interfacial thermal resistance, and semi-solid layer were proposed to explain why specific heat is increased in the liquid solution. These three cases do not have enough scientific evidence to prove this phenomenon clearly. According to the literature [78]-[80], different nanoparticles (e.g., SiO_2, Al_2O_3, and ZnO nanoparticle) was added to the liquid solution to measure its specific heat. Specific heat of SiO_2 nanoparticle with water was decreased by 12 % at 10 % concentration by volume [78]. Specific heat of Al_2O_3 nanoparticle with water was decreased by 40 % at 22 % concentration by volume [79]. Specific heat of ZnO nanoparticle with water/ethylene glycol was decreased by 20 % at 7 % concentration by volume [80]. When the nanoparticle is added to solution, specific heat of nanolfuids is decreased at different concentration by volume even though its concentration by volume is increased. The addition of nanoparticle is not related to enhanced specific heat of nanofluids. The case 1-3 may not be responsible for enhanced specific heat of nanofluids (nanoparticle and liquid solution) and other clear mechanisms are required to prove why nanofluid's specific heat is enhanced when the nanoparticle is added. In other words, literature shows that the specific heat of classical nanofluids (water, oil, or ethylene glycol-based) decreased with the addition of nanoparticles [78]-[80] and thus it may not be primarily responsible for the observed enhanced specific heat of molten salt nanofluids.

Possible Mechanisms of Fractal-Like Structure Formation

According to the literature [52], [55], [56], [81], [82], the mechanism was proposed from experimental and theoretical aspects to explain why the nanoparticle's specific heat capacity is increased. The specific heat capacity is enhanced by the enlarged interfacial area of nanostructure. For the experimental aspect, enhanced specific heat of nanoparticle was proven experimentally by the enlarged interfacial area and it was observed in the nanostructured particle compared to coarse grained materials [52]. For the theoretical aspect, the surface and interior atoms are related to the enhanced specific heat of nanoparticle and its specific heat was calculated by the Einstein and Debye models [55]. Atoms from two parts (surface and interior part) are contributed to the enlarged specific surface and it is responsible for the enhanced specific heat of nanoparticle. The specific heat of nanocrystals (solids to nanocluster) was calculated by the Einstein model [56]. The thermodynamic approach was used to prove the interfacial surface energy which is contributed to the specific heat capacity of nanoclusters. The enlarged interfacial area of nanoclusters (e.g., nanostructure) is the important factor to explain why its specific heat is enhanced. The bulk free energy and surface free energy of nanoparticles was calculated to obtain its specific heat [81]. The surface free energy of atoms is related to the enlarged interfacial area compared to the bulk free energy and it is responsible for the size effect of nanoparticle on its specific heat. In other words, the surface energy (e.g., enlarged area) of atoms has a close connection with enhanced specific heat of nanoparticles. The specific heat of nanoparticle was calculated to explain the relationship with its size and the surface effect on the specific heat of the bulk structure [82]. The specific heat of nanoparticle is enhanced when its size is decreased and its surface energy is increased. In other words,

the enlarged surface area of nanoparticle and enhanced specific heat correlate to each other.

The separation mechanism is needed to explain before describing how the fractal-like structure is formed. For the separation mechanism of the molten salt, the eutectic molten salt mixture may separate due to the difference in electrostatic interactions according to the literature [83], [84]. The specific mechanism of separation of the molten salt mixture that electrostatically interacts with oxide nanoparticles was used to explain how the non-eutectic molten salt mixture is created [83]. In other words, each ion in the eutectic molten salt mixture can move along the specific direction. This phenomenon makes the different formation of the structure in the same eutectic system due to electrostatic interaction. Ionic solids and melts are held together due to electrostatic interactions [84]. In general, ionic solid (e.g., eutectic molten salt mixture) consists of multiply charged cation and it is related to interaction potentials each other. The eutectic molten salt mixture includes two, three, or four ionic compounds. In other words, this interaction of this ionic compound is dominated by the difference in electrostatic interactions between the negative charge and positive charge. For example, when the specific particle (e.g., oxide particle) disperses into the eutectic molten salt mixture, one salt can be more attracted to this specific particle than another salt due to the difference in electrocstatic interactions. After that, it makes the different composition of the original eutectic moletn salt and it becomes the non-eutectic motlen salt mixture. However, this separation mechanisam (due to the electrostatic interaction) of the eutectic molten salt mixture are not enough to explain the formation of the fractal-like strucure in the micro-scale size level. Therefore, another mechanism which is relaterd the formation of the fractal-like structure is requried to explains how each ion separates over a good distance in the eutecitc molten salt mixture.

In general, the molten salt mixture consists of two, three, or four different salt compounds and thus specific separation mechanism is required to explain how the multi-component molten salt can be separated in the molten salt mixture system. According to the literature [85], the specific separation mechanism of molten salt were proposed by multi-component diffusion. The mechanism of multi-component diffusion was used in the binary molten salt. Although this binary molten salt has been studied in experimental and computational research about the separation mechanism, more research of the principle of multi-component diffusion is necessary to explain the separation mechanism in more detail. In general, the multi-component system shows different effects (e.g., inherent effects) compared to the single component system. In other word, the multi-component and single system have the different thermophysical properties as well as inherent effects in the mixture system. The Chemla effect is a prime example of collective effects to explain the separation mechanism in the multi-component system. This Chemla effect in melts and solutions was used to explain molten salts' separation [86]-[90]. According to this theory, the mobility of the larger ions is relatively faster than the smaller ions at the critical concentration of the larger ions and thus multi-component diffusion occurs on the binary molten salt as shown in figure 9. Therefore, multi-component diffusion (e.g., Chemla effect) may be responsible for the separation mechanism of the binary molten salt mixture in this case. However, it is difficult to explain the formation of fractal-like structure (e.g., microscale structure) in the molten salt nanofluid because the movement of ions by different mobility is only related to the atomic-scale level. Although the larger ion has the faster mobility, it can naturally move the small space (e.g., atomic-scale). Therefore, clear mechanisms are required to explain the formation of fractal-like structure in the micro-scale level size.

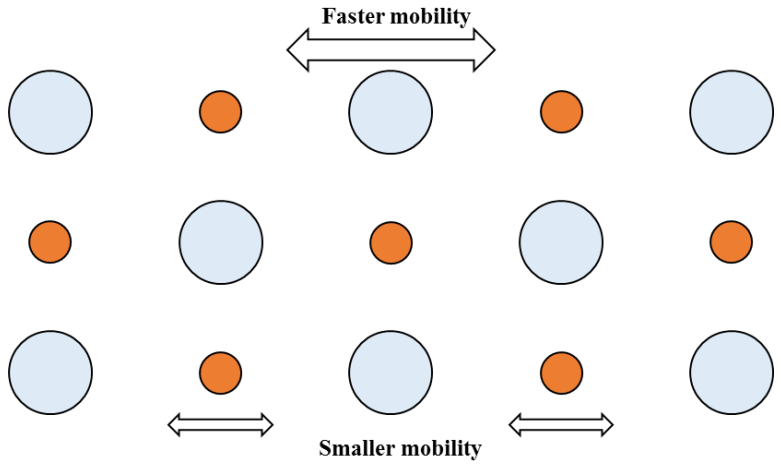

Figure 9 Basic concept of Chemla effect in multi-component system

As I mentioned earlier, the separation of the molten salt is related to its inherent effects and there will be different possible mechanism to explain the separation mechanisms in the molten salt mixture. According to the literature [84], ionic solids and melts are held together due to electrostatic effects. However, the polarization effect of the ions is an important factor in understanding how each ion separates in the molten salt. Here is the separation mechanism by the polarization effect in the molten salt mixture. As shown in figure 10, there is no electric field and induced dipole when the crystal has the perfect formation. In other words, this perfect crystal formation does not move the negative ion (anion). When the positive ion (cation) is away from the next nearest the anion, there will be the electric field. The induced dipole is also created and it moves the anion under this specific condition (e.g., the electric field). After that, the cation moves immediately into the empty space where there used to be the anion. The electrons are allowed to roam free around the empty space while the electric field occurs. This electric field pushes the electron away from the cation which is displaced off and this phenomenon is related to the induced dipole. Therefore, the polarization effect of the ions can be considered as a key factor for understanding the separation mechanism of molten

salt. However, this polarization effect occurs between ions (e.g., atomic-level) and it is hard to explain the formation of fractal-like structure in the micro-scale size level in more detail. Although the induced dipole which is related to the polarization effect occurs on the molten salt mixture, this separation mechanism has only relevance to the atomic-scale level. Therefore, clear separation mechanism which is related to the formation of fractal-like structure is required to prove the specific separation phenomenon in the molten salt mixture.

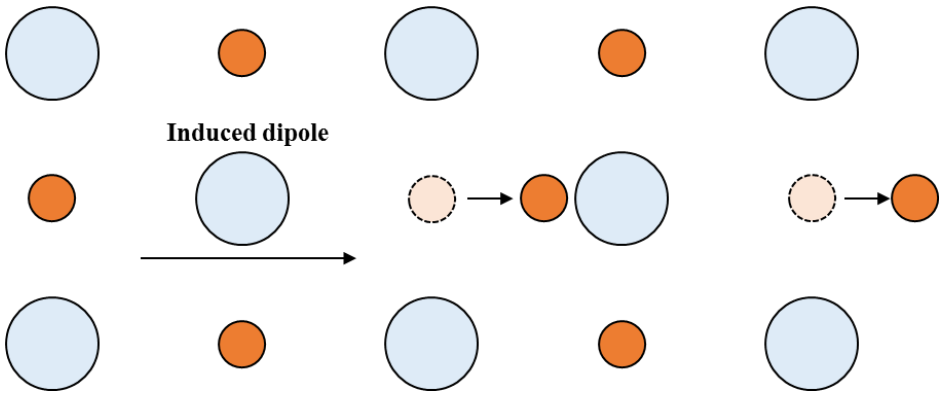

Figure 10 Basic concept of polarization effect of ions [84]

If the mixture is separated, the nucleation process may occur and the pre-existing crystal may begin to grow larger crystals in the lattice formation. After that, it develops the crystal dendrite with the specific structure form (e.g., tree-like). According to the literature [91], the dendrite structure forms under the specific condition between the solid interface and liquid interface. As shown in figure 11, the solid starts to grow into superheated liquid in the condition (e.g., different temperature gradient) that the solid interface and liquid interface are stable. Heat of liquid moves from liquid to solid due to the different temperature gradients between two interfaces. After that, the curvature of the protrusion in the solid interface starts form and the temperature gradient of liquid is increased when the solid's temperature gradient is decreased. More heat moves from the

liquid interface to the protruding solid. Finally, the growth rate of the solid interface is decreased and thus the protrusion in the solid interface is disappeared over time. As shown in figure 12, the solid starts to grow into supercooled liquid. When the temperature gradient of solid and liquid interface is decreased, heat moves from the solid interface and liquid interface. In other words, heat of the protruding solid is removed more effectively from the solid interface to liquid interface than other spaces and it creates a better environment for the protruding solid. The solid starts to grow into this supercooled liquid due to unstable condition. As shown in figure 13, there is the procedure explain how to form the thermal dendrite formation between interfaces (e.g., solid and liquid). The first solid particle is created in supercooled liquid and then nucleation happens as shown in figure 13 (a). The shape of the first solid is the spherical nucleus. After that, the solid interface and liquid interface are not stable and the protruding solid stars to grow over time as shown in figure 13 (b). The primary arms starts to develop in the specific directions (e.g., crystallographic direction) as shown in figure 13 (c). When the primary arm extends from the solid surface, the interfaces (solid and liquid) are not stable and it starts to break up into the secondary and tertiary arms as shown in figure 13 (d). Finally, the thermal dendrite formation appears in this case and this elongated arms (e.g., primary, secondary, and tertiary arms) develop in certain crystallographic direction. As I mentioned earlier, molten salts possibly start to crystallize on a nanoparticle surface. It grows away from the nanoparticles and and eventually form fractal-like fluid nanostructures [83]. In other words, the eutectic salt becomes the non-eutectic salt after specific molten salt starts to crystallize on a nanoparticle surface in this case. The non-eutectic molten salt means that it shows the different composition as well as its melting point compared to the eutectic molten salt. According to the literature [92], the non-eutectic molten salt ($NaNO_3$-KNO_3=70:30 by weight ratio) has a larger melting point

(about 260 °C) than the eutectic molten salt ($NaNO_3$-KNO_3=60:40 by weight ratio). It means that this thermal dendrite formation may occur on the interface between the molten salt and nanofluid when specific molten salt start to crystallize a nanoparticle surface after the separation process.

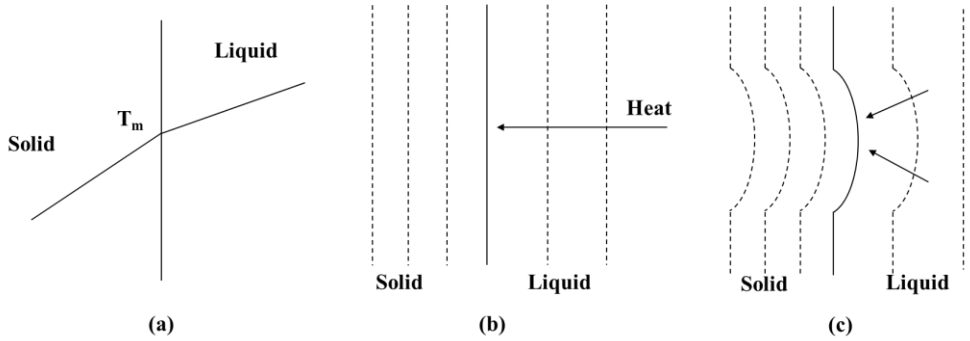

Figure 11 Procedure of direction of heat flow between interfaces ($T_S < T_L$) [91]

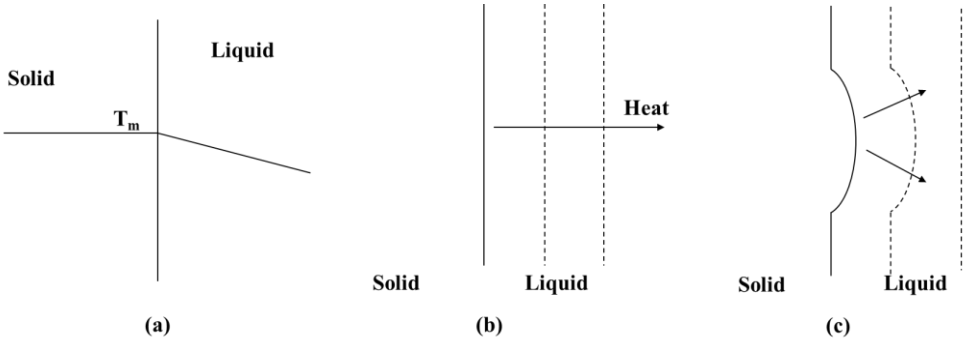

Figure 12 Procedure of direction of heat flow between interfaces ($T_S > T_L$) [91]

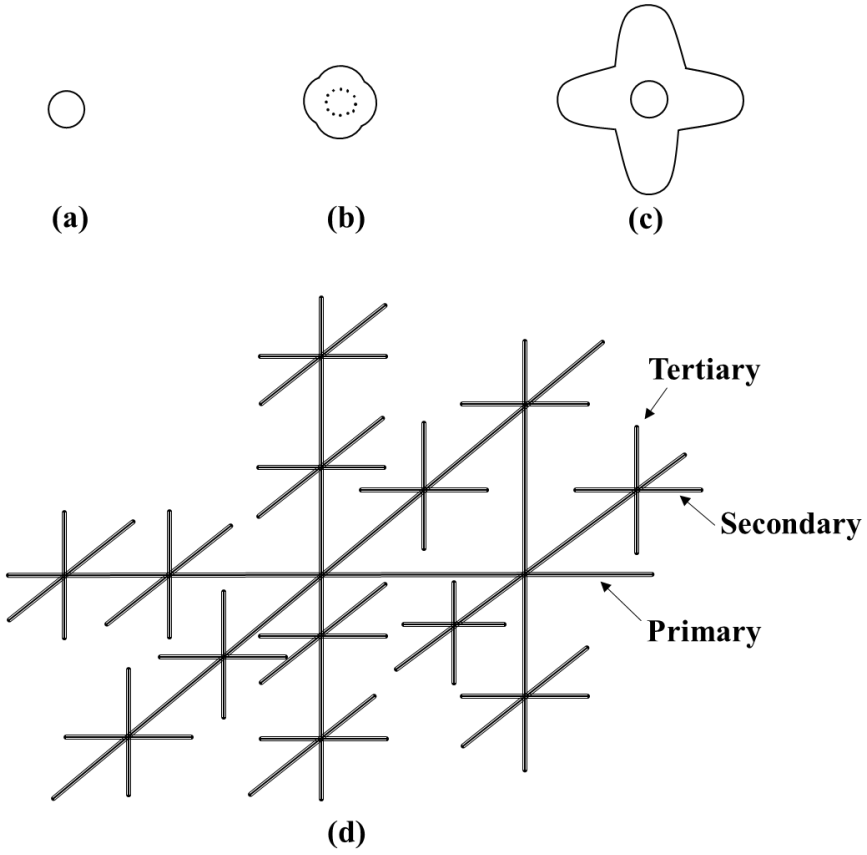

Figure 13 Procedure to form thermal dendrite formation [91]

The nanolfuid (molten salt eutectic + nanoparticle) shows enhanced specific heat compare to the molten salt eutectic. It means that the specific mechanism may be responsible for the enhanced thermophysical properties (e.g., specific heat capacity). In other words, the enhanced nanofluid has the specific formation which is related to enhanced specific heat than the molten salt eutectic. According to the literature research [83], the extraordinarily large specific surface area of a nanoparticle enhances its specific heat capacity. The contribution of surface phonons to the specific heat is negligible, because the number of surface atoms is much smaller than the number of interior atoms. However, for structures such as nanoparticles that have extraordinarily increased specific areas, the effect of surface phonons on the specific heat capacity is substantial, and thus the effective specific heat capacity of a nanoparticle can become greatly enhanced in comparison with its bulk material. Nanoparticle aggregates form the fractal-like structure as shown in figure 14.

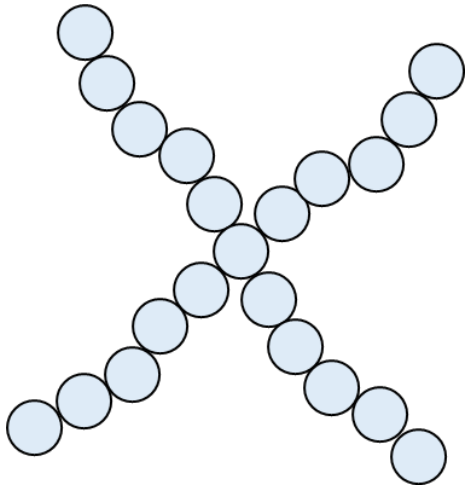

Figure 14 Formation of the fractal-like structure by the aggregated nanoparticle [83]

Much of the research has only shown enhanced thermal conductivities of nanofluids using effective medium theory [31], [34], [43]-[47]. By thermal equilibrium, they reported that specific heat capacity agreed with conventional effective specific heat

capacity models. Subsequently, they have generally agreed that a significant impact on specific heat capacity is not related to the addition of nanoparticles into a fluid. The fractal-like structure by the aggregated nanoparticle is responsible for the enhanced effective thermal conductivity of nanofluids as shown in figure 15 (a). However, as shown in figure 15 (b), fractal-like fluid nanostructure in a molten salt nanofluid are formed by separated base molten salt. This fractal-like nanostructure may be responsible for the enhanced effective specific heat capacity of nanofluids.

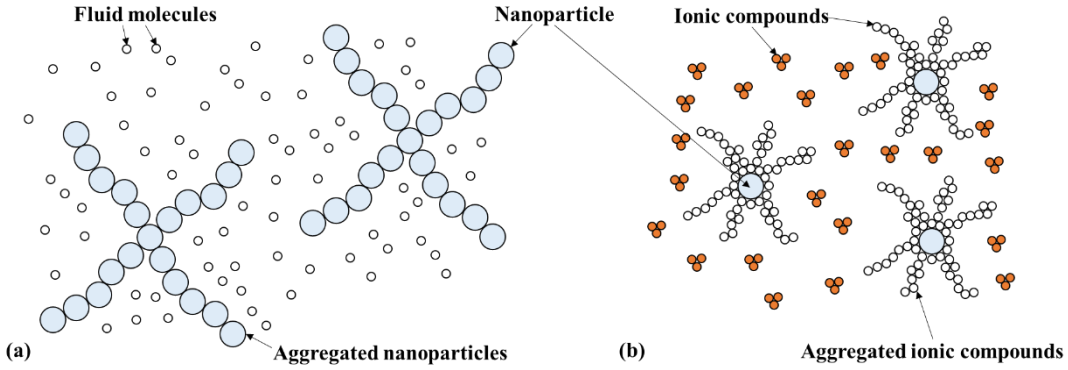

Figure 15 (a) Fractal-like fluid nanostructures in a conventional nanofluid are formed by nanoparticles. (b) Fractal-like fluid nanostructures in a molten salt nanofluid are formed by separated base molten salts [83]

A special separation phenomenon of molten salt mixture that electrostatically interacts with oxide nanoparticles explains the formation of the fractal-like nanostructure. As shown in figure 16 (a), a molten salt mixture consists of two or three ionic compounds, and each salt can interact differently with an oxide nanoparticle. When an oxide nanoparticle disperses into a mixture of two salts (white and yellow), salt A (white particle) can be more attracted to a nanoparticle than salt B (yellow particle) as shown in figure 16 (b). After that, there should be a concentration gradient within molten salts toward a nanoparticle because of the difference in electrostatic interactions between a

nanoparticle surface (negatively charged) and each ion of molten salts (positively charged). This difference will separate molten salts near nanoparticle at the nanoscale. When molten salts separate, they may crystallize and form solid structures. Because this phenomenon occurs locally near a nanoparticle at the nanoscale, molten salts possibly start to crystallize on a nanoparticle surface, grow away from the nanoparticles, and eventually form fractal-like fluid nanostructures as shown in figure 16 (c). Salt A is more attracted to a particle than salt B while an oxide nanoparticle disperses in ionic compound. Salt A possibly starts to crystallize on a nanoparticle surface as shown in figure 17.

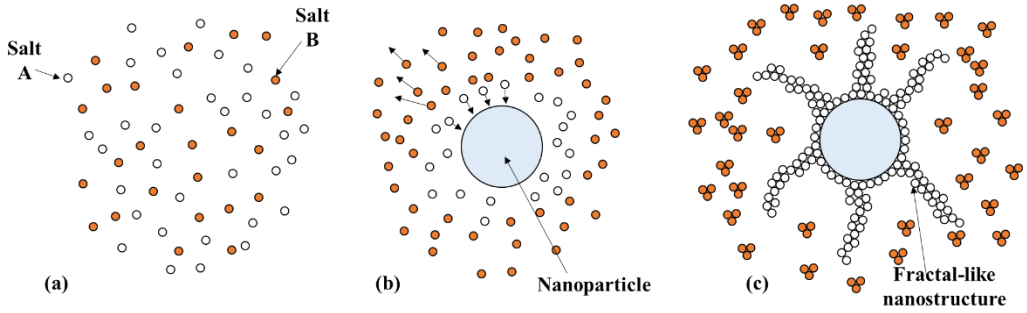

Figure 16 (a) Salt A and B (white particle and yellow particle) dispersed homogeneously. (b) When an oxide nanoparticle disperses, salt A (white particle) is more attracted to a nanoparticle than salt B (yellow particle) due to electrostatic interactions. (c) Molten salts start to crystallize on a nanoparticle surface, grow away from the nanoparticles [83]

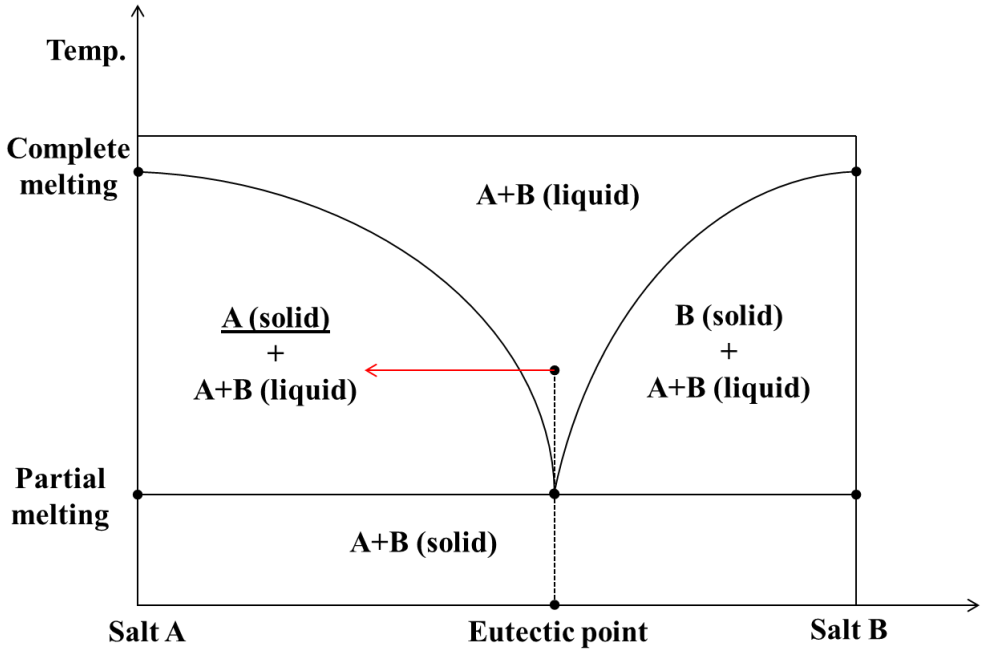

Figure 17 Phase diagram of binary salt mixture (salt A and salt B)

According to the literature [83], two TEM images show fractal-like nanostructures around the nanoparticle and it demonstrated how nanostructures formed in the molten slat nanofluid. As shown in figure 18 (top), separated salts grow up around one nanoparticle. This crystallized salts are reaching to another nanoparticle and fractal-like nanostructure are shaped by crystallized salt on the nanoparticle. As shown in figure 13 (bottom), the TEM image shows the nanoparticle (about 100 nm). There are aggregated nanoparticles and each small nanoparticle show about the size of ~20 nm. Therefore, this literature confirmed that molten salts start to crystallize on a nanoparticle surface, grow away from the nanoparticles, and eventually form fractal-like nanostructures. However, this separation and formation mechanism of structure have only relevance to the atomic-scale level. In other words, the separation process may occur on the molten salt nanofluid due to electrostatic interactions, but it is based on the atomic-scale level.

Therefore, clear separation mechanism, which is related to the formation of fractal-like structure, is required to prove the specific separation phenomenon in the molten salt nanofluid.

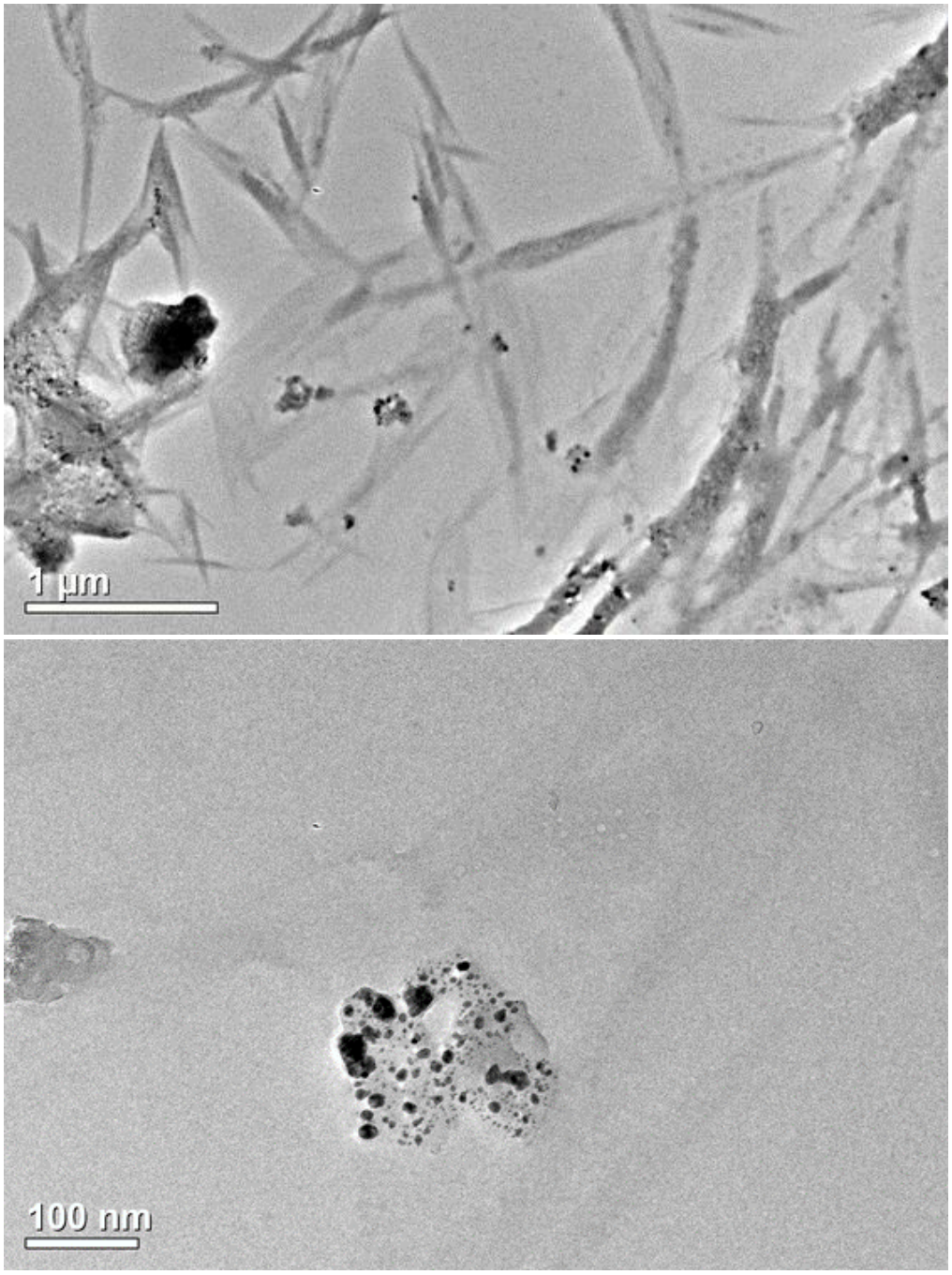

Figure 18 TEM images (top and bottom) of fractal-like nanostructures and nanoparticle

[83]

As I mentioned earlier, the electrostatic interactions may possibly separate molten salts near nanoparticle at the nanoscale. When molten salts separate, they may crystallize and form solid structures. Molten salts start to crystallize on a nanoparticle surface because this happen may possibly occur locally near a nanoparticle (inhomogeneous interface) at the nanoscale. This separated salt may grow away from the nanoparticles and eventually form fractal-like fluid nanostructures. This phenomenon occurs on the interface between the molten salt (solid) and nanofluid (liquid) and thus it is important to understand how the fractal-like structure is formed in the interface (inhomogeneous interface) between two different phases in the molten salt nanofluid. According to the literature [93], the titanium structure can be formed by the separation of mixture in the molten salt. This phenomenon is based on the chemical reaction between two different interfaces and it makes the needle-like structure. As shown in figure (a)-(b), the molten salt (titanium chloride) and magnesium liquid are dissolved together to create the titanium structure (needle-like structure). After that, the molten salt and titanium are separated. The rod type of the titanium structure can be formed at low temperature (without stirring process) because the interface between the molten salt and magnesium liquid is homogenous as shown in figure 19 (a). In other words, when the formation of two interfaces is quite uniform, this condition is less likely to form the needle-like structures in the molten salt. However, the different formation of the titanium structure can be formed at the specific condition with the stirring process (high temperature). As shown in figure 19 (b), the interface between the molten salt and magnesium liquid is inhomogeneous compared to the previous condition. Because of this specific condition, titanium starts to form the structure and it grows away from titanium and eventually form the needle-like structure from the molten salt eutectic. In other words, this inhomogeneous interface is likely to form the needle-like structure in the molten salt eutectic. As shown in figure 20

(a)-(b), SEM image shows clear needle-like structures. First, it was formed by inhomogeneous interface between two different layers and then the needle-like structure was created by the separation of mixture in the molten salt over time at the specific condition.

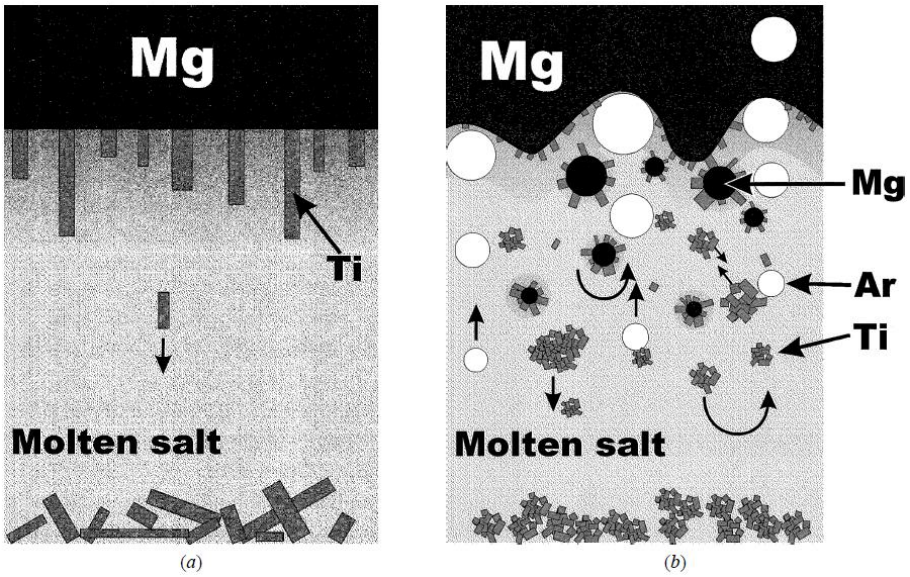

Figure 19 Interface between magnesium liquid and molten salt: (a) no stirring process-low temperature and (b) with stirring process-high temperature [93]

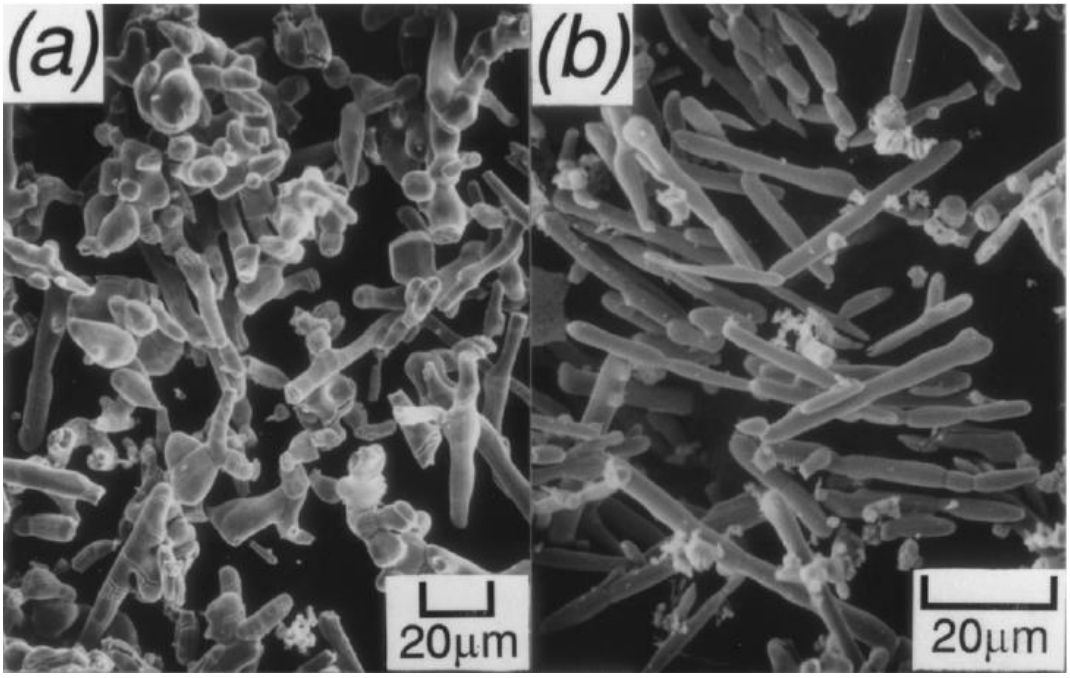

Figure 20 SEM image of needle-like structures of titanium from the molten salt eutectic [93]

As I mentioned earlier, this phenomenon occurs due to the chemical reaction between two different interfaces (inhomogeneous interface). This separation process (growing structure) may be used to explain how the fractal-like structure (micro-scale level) is formed physically in the molten salt nanofluid. When an oxide nanoparticle disperses into a mixture of two salts (e.g., the binray molten salt), the interface of the nanofluid between the nanoparticle and molten salt is inhomogeneous compared to the eutectic molten salt. Because of this inhomogeneous interface, molten salts separate and they possibly crystallize and form solid structures (e.g., fractal-like structure) as shown in figure 21. Molten salts possibly start to crystallize on a nanoparticle surface. It grows away from the nanoparticles and and eventually form fractal-like structures (micro-scale level) as shown in figure 22 [21].

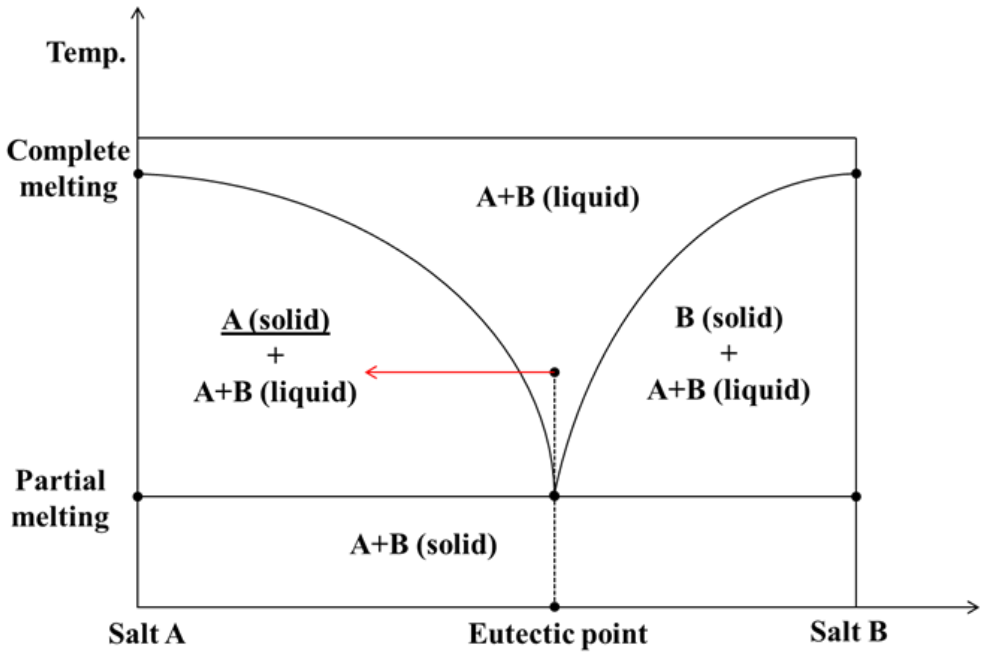

Figure 21 Phase diagram of binary salt mixture (salt A and salt B)

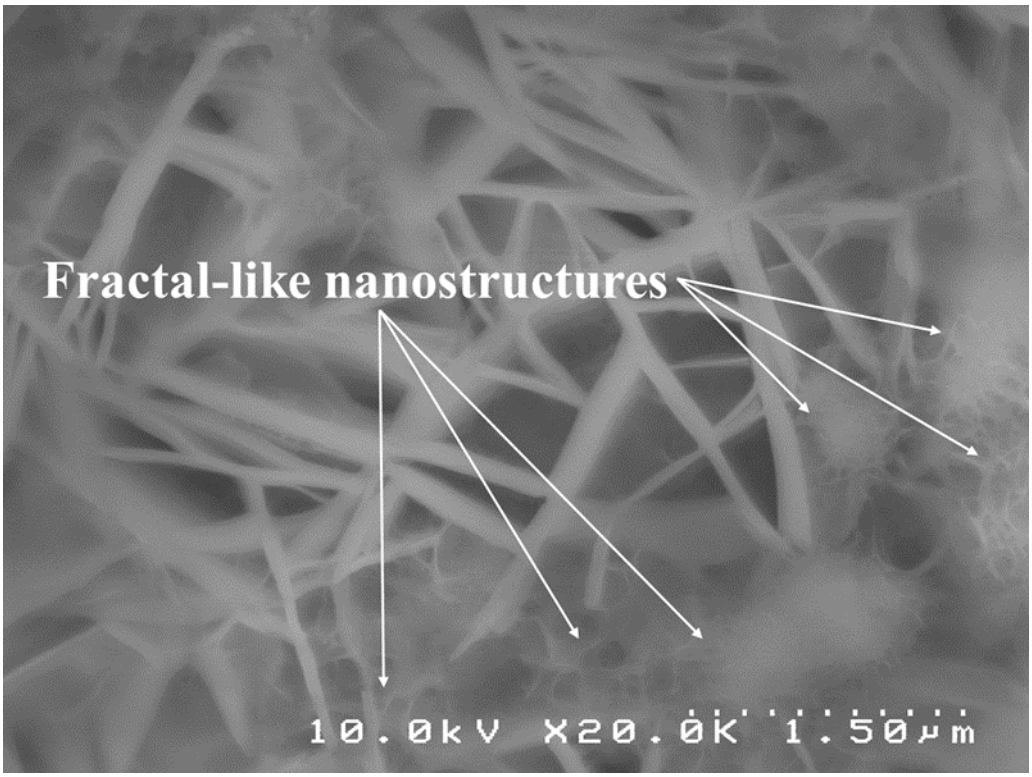

Figure 22 SEM image of the smaller nanostructure in the ternary nitrate molten salt ($LiNO_3$–$NaNO_3$–KNO_3) with SiO_2 nanoparticle [21]

Summary

There are several mechanisms to explain how the fractal-like nanostructure and micro-size structure are formed in the molten salt nanofluid or mixture. These mechanisms also explain how specific formation (or structure) has close correlation between the separation process and enhanced thermophysical properties. The specific mechanism was proposed from experimental and theoretical aspects to explain why the nanoparticle's specific heat capacity is increased. According to the results of this mechanism, the specific heat capacity is enhanced by the enlarged interfacial area of nanostructure. However, this mechanism are not enough to explain the formation of the fractal-like nanostructure as well as its growing micro-size structure from the separation of each ionic salt. The eutectic molten salt mixture may separate due to the difference in electrostatic interactions. Each ion in the eutectic molten salt mixture can move along the specific direction. This phenomenon may make the different formation of the structure in the same eutectic system due to electrostatic interaction. However, this separation mechanisams of the eutectic molten salt mixture are not enough to explain the formation of fractal-like strucure in the micro-scale size level. The multi-component diffusion (e.g., Chemla effect) may be responsible for the separation mechanism of the binary molten salt in this case. However, it is difficult to explain the formation of fractal-like nanostructure (e.g., microscale structure) in the molten salt nanofluid because the movement of ions by different mobility is only related to the atomic-scale level. The polarization effect of the ions is considered as a key factor for understanding the separation mechanism of molten salt. However, this polarization effect occurs between ions (atomic-level) and it is hard to explain the formation of fractal-like structure in the micro-cale size level in more detail. The dendrite structure forms under the specific condition between solid interface and liquid interface. The thermal dendrite formation can

occur on the molten salt nanolfuid when specific molten salt start to crystallize a nanoparticle surface. When molten salts separate, they may crystallize and form solid structures due to the differnce in the electrostatic interactions between two different ions. Because this phenomenon occurs locally near a nanoparticle at the nanoscale, molten salts start to crystallize on a nanoparticle surface. It grows away from the nanoparticles and eventually form fractal-like fluid nanostructures. However, this separation and formation mechanism of structure have only relevance to the atomic-scale level. In other words, the separation process may occur on the molten salt nanofluid due to electrostatic interactions, but it is based on the atomic-scale level. Therefore, clear separation mechanism, which is related to the formation of fractal-like structure, is required to prove the specific separation phenomenon in the molten salt nanofluid. The inhomogeneous interface between two different layers is likely to form the needle-like structure in the molten salt eutectic. First, it is formed by inhomogeneous interface between two different layers and then the needle-like structure is created by the separation of mixture in the molten salt. This separation process (growing structure) may be used to explain how the fractal-like structure (micro-scale level) is formed physically. Molten salts possibly start to crystallize on a nanoparticle surface after separation due to the inhomogeneous interface. It grows away from the nanoparticles (inhomogeneous interface) and possibly form fractal-like structures (micro-scale level).

Chapter 3

Molten Salt Nanofluids: doped with nanoparticles

Measurement of Specific Heat Capacity (C_p)

Sample Preparation

According to the previous research [20], [21], Four different SiO_2 (silica dioxide) nanoparticles (e.g., 5 nm, 10 nm, 30 nm, and 60 nm) were used for the additive in the molten salt mixture to confirm the enhanced specific heat capacity is responsible for the form of fractal-like nanostructures in the ternary nitrate molten salt ($LiNO_3$–$NaNO_3$–KNO_3). The ternary nitrate molten salt eutectic was prepared by the molar ratio (38:15:47) and the specific heat capacity of the ternary nitrate molten salt eutectic is 1.63 kJ/kg °C from the literature [94]. The sizes of the nanoparticle were verified by the photon correlation spectroscopy. To mix each chemical (total sample amoun; 200 mg), the microbalance (CPA26P, Sartorius AG) was used to measure the weight precisely. 59.99 mg of $LiNO_3$ (lithium nitrate), 29.19 mg of $NaNO_3$ (sodium nitrate), 108.81 mg of KNO_3 (potassium nitrate), and SiO_2 (silica dioxide) nanoparticle were mixed by the weight ratio. For the concentration of SiO_2 nanoparticle, 1% concentration by weight ratio was used it was 2 mg of the total weight (200 mg) of the molten salt nanofluid. As shown in figure 23 and 24, each chemical (lithium nitrate, sodium nitrate and potassium nitrate) is put on the hot plate at 200 °C for 3 hours with the different vial to prevent the effect of moisture. The mixed molten salt with SiO_2 nanoparticle was on the hot plate (Isotemp, Fisher Scientific) at 300 °C to melt the salt compounds homogeneously for 1 hour. The vial with the well mixed salts is on the hot plate at 100 °C to make it be solid after 1 hour.

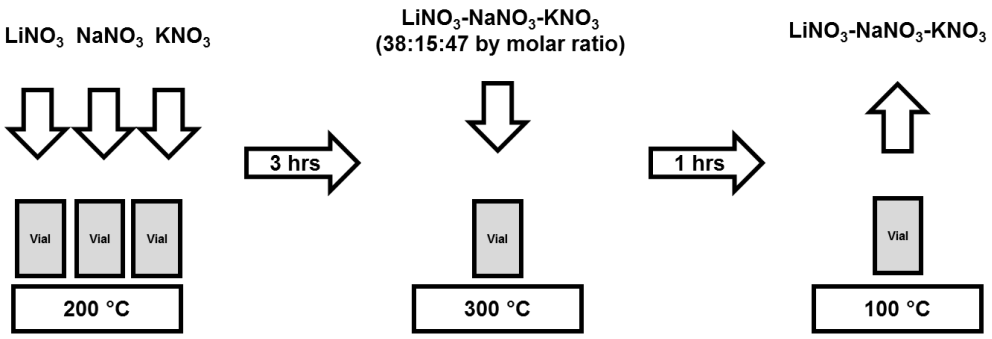

Figure 23 Procedure of the sample preparation of the ternary nitrate molten salt eutectic ($LiNO_3$–$NaNO_3$–KNO_3)

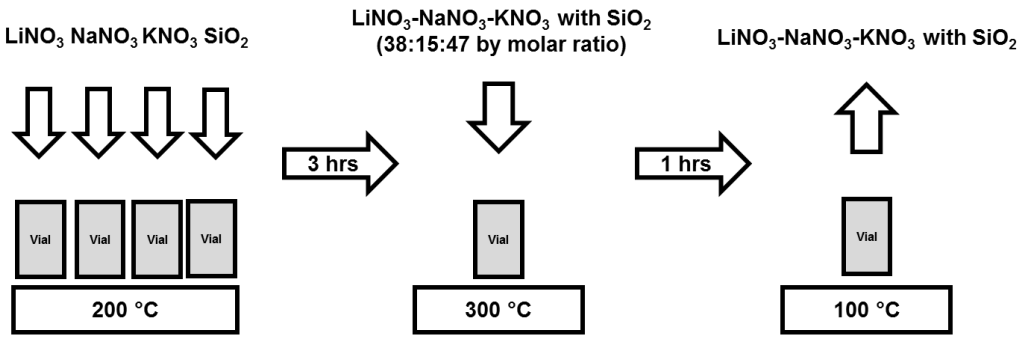

Figure 24 Procedure of the sample preparation of the ternary nitrate molten salt eutectic ($LiNO_3$–$NaNO_3$–KNO_3) with SiO_2 nanoparticle (5 nm, 10 nm, 30 nm, and 60 nm)

Experimental Setup

A modulated differential scanning calorimeter (MDSC; Q20, TA Instrument Inc.) was used to measure the specific heat capacity of the molten salt nanofluid as shown in figure 25. Each sample was hermetically sealed in a Tzero hermetic pan and lid (TA Instruments Inc.) to prevent sample losses during the measurement of the specific heat capacity as shown in figure 26. Each sample was loaded in the pan before the measurement starts in the MDSC. Before loading the sample into the MDSC, the pan and lid were on the hot plate (Isotemp, Fisher Scientific) at 100 °C for 30 minutes to avoid further effect of moisture before the measurement of the specific heat capacity. It means that possible errors (e.g., exploded sample inside MDSC) can be reduced during the measurement at high temperature (after sample's melting point).

Figure 25 Modulated differential scanning calorimeter (MDSC; Q20, TA Instruments Inc.)

Figure 26 Tzero hermetic pan and lid (TA Instruments Inc.)

Measurement Results

As shown in equation 1, the conventional effective specific heat model was used to compare the specific heat capacity of the nanomaterials. This model is related to the simple density weighted rule.

$$C_{p,nm} = \frac{\rho_{np} V_{np} C_{p,np} + \rho_e V_e C_{p,e}}{\rho_{np} V_{np} + \rho_e V_e} \qquad (1)$$

where ρ is density, V is volume, and C_p is the specific heat capacity respectively. Subscripts nm, np, and e denote the nanomaterial, nanoparticle, and pure molten salt eutectic respectively. The specific heat capacity of the pure ternary molten salt eutectic was 1.58 kJ/kg °C on average from the measurement and it is in good agreement with the literature (e.g., 1.63 kJ/kg °C) [94]. As shown in table 1 and figure 27, they show the specific heat capacity of the ternary nitrate molten salt eutectic and nanofluid with SiO_2 nanoparticles (e.g., 5 nm, 10 nm, 30 nm, and 60 nm) at 150 °C-400 °C. The specific heat capacity of the nanomaterials with 5 nm, 10 nm, 30 nm, and 60 nm nanoparticles were enhanced by an average of 13 %-16 % compared to the pure ternary molten salt eutectic. As shown in figure 28, it shows the variations in the specific heat capacity of the pure ternary molten salt eutectic ($LiNO_3$–$NaNO_3$–KNO_3) and nanofluids with SiO_2 nanoparticle using different sizes (e.g., 5 nm, 10 nm, 30 nm, and 60 nm). From the results, enhanced specific heat capacity are independent of the different size of SiO_2 nanoparticle. According to the results, in this ternary molten salt nanofluid with SiO_2 nanoparticle, nanostructures are formed by separated base molten salt. This nanostructure is responsible for enhanced specific heat of a molten salt nanofluid with SiO_2 nanoparticle. Therefore, the conventional effective specific heat model is not related to enhanced specific heat capacity due to the low concentration of the nanoparticle (e.g., 1 % by weight ratio).

Table 1 Specific heat capacity (average) of the ternary nitrate molten salt eutectic ($LiNO_3$-$NaNO_3$-KNO_3) and the nanofluid with four different SiO_2 nanoparticles (5 nm, 10 nm, 30 nm, and 60 nm) from 150 °C to 400 °C [21]

C_p (kJ/kg °C)	Pure salt	5 nm	10 nm	30 nm	60nm
#1	1.59	1.89	1.85	1.84	1.81
#2	1.59	1.84	1.87	1.82	1.79
#3	1.58	1.76	1.81	1.85	1.78
#4	1.54	1.73	1.78	1.80	1.79
Average	1.58	1.81	1.83	1.83	1.79
Enhancement (%)	-	15 %	16 %	16 %	13 %

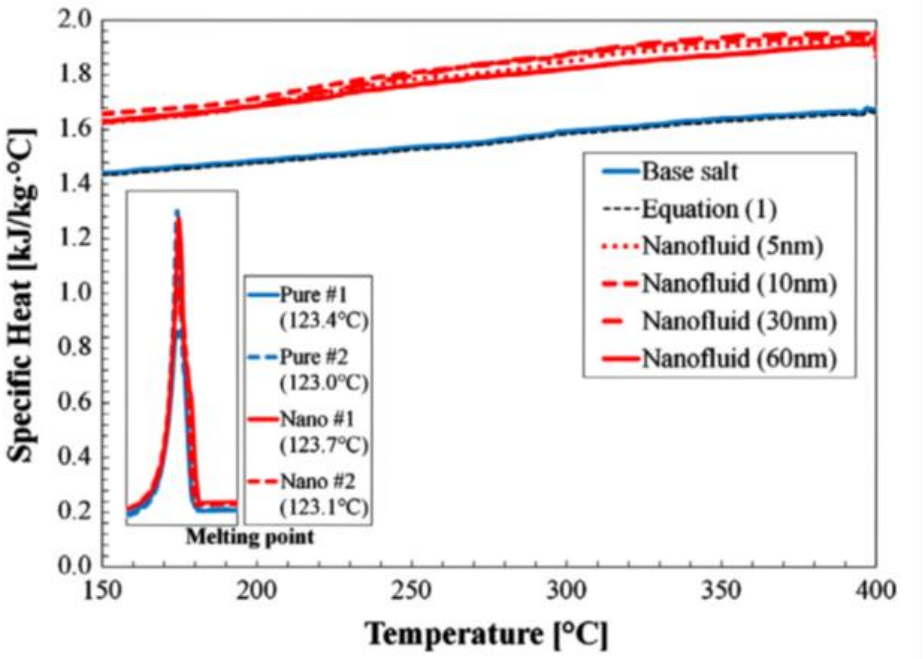

Figure 27 Specific heat capacity of the ternary nitrate molten salt ($LiNO_3$–$NaNO_3$–KNO_3) and the nanofluid with SiO_2 nanoparticle (5nm, 10nm, 30nm, and 60nm) [21]

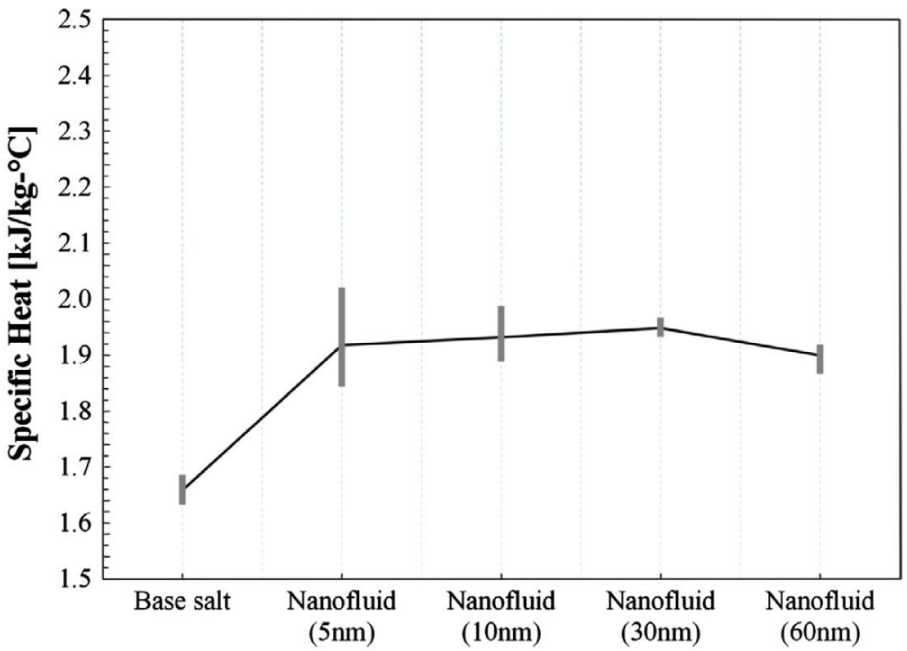

Figure 28 Variations in the specific heat capacity of the ternary nitrate molten salt eutectic ($LiNO_3$–$NaNO_3$–KNO_3) and the nanofluid with SiO_2 nanoparticle (5nm, 10nm, 30nm, and 60nm) [21]

Material Characterization (SEM) Results

Using a scanning electron microscope (SEM: Hitachi S-5000H), I observed a large amount of nanometer-sized structures that the salt compound (the ternary nitrate molten salt eutectic-$LiNO_3$-$NaNO_3$-KNO_3) formed around SiO_2 nanoparticles. According to figure 29 [21], figure 10 (a) shows the SEM image of the pure ternary nitrate molten and it is the classical pure ternary nitrate molten salt eutectic. Figure 29 (b) is the SEM image of the ternary nitrate molten nanomaterials with SiO_2 nanoparticle (5 nm). Figure 29 (c) shows the SEM image of the ternary nitrate molten nanomaterials with SiO_2 nanoparticle (10 nm) and figure 29 (d) and 29 (e) show SEM images of the ternary nitrate molten nanomaterials with SiO_2 nanoparticle (30 nm and 60 nm) respectively at 3000x magnification. Figure 29 (f) is the SEM image of the ternary nitrate molten nanomaterials at high magnification (20000x). It shows fractal-like nanostructures around salt compounds. According to figure 29 (f), fractal-like nanostructures consist of several smaller nanostructures and they are at a few nanometer scales. This fractal-like nanostructures are responsible for enhanced effect of surface energy. It is related to the overall effective specific heat capacity of this ternary molten salt nanofluid. From figure 29 (a-e), criss-crossed chain-like structures are shown in two different length scales with 100-150 nm diameter and 1-2 μm.

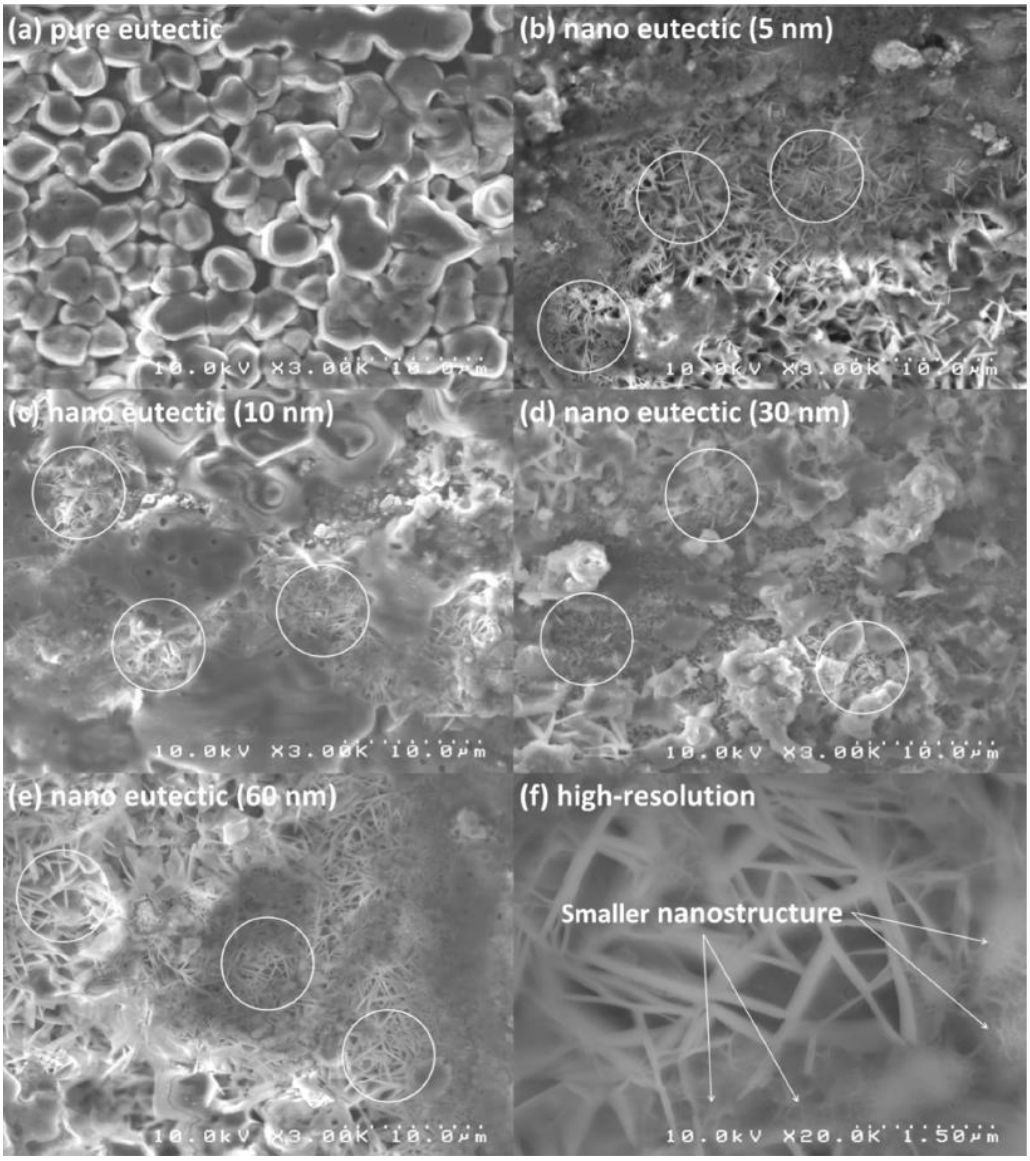

Figure 29 SEM images of fractal-like nanostructures of the ternary nitrate molten salt ($LiNO_3$–$NaNO_3$–KNO_3) with SiO_2 nanoparticle (5 nm, 10 nm, 30 nm, and 60 nm) [21]

As shown in Figure 29 (b)-(f), the nanostructure has an extremely large specific surface area, which can amplify the effect of surface energy on the effective specific heat capacity and can be primarily responsible for the enhanced specific heat capacity with doping nanoparticles. As shown in figure 30, it clearly shows the fractal formation of the

induced structure and the sizes of the nanostructures vary from 100 to 150 nm in diameter. It could be the first demonstration of the fractal-like nanostructures [21].

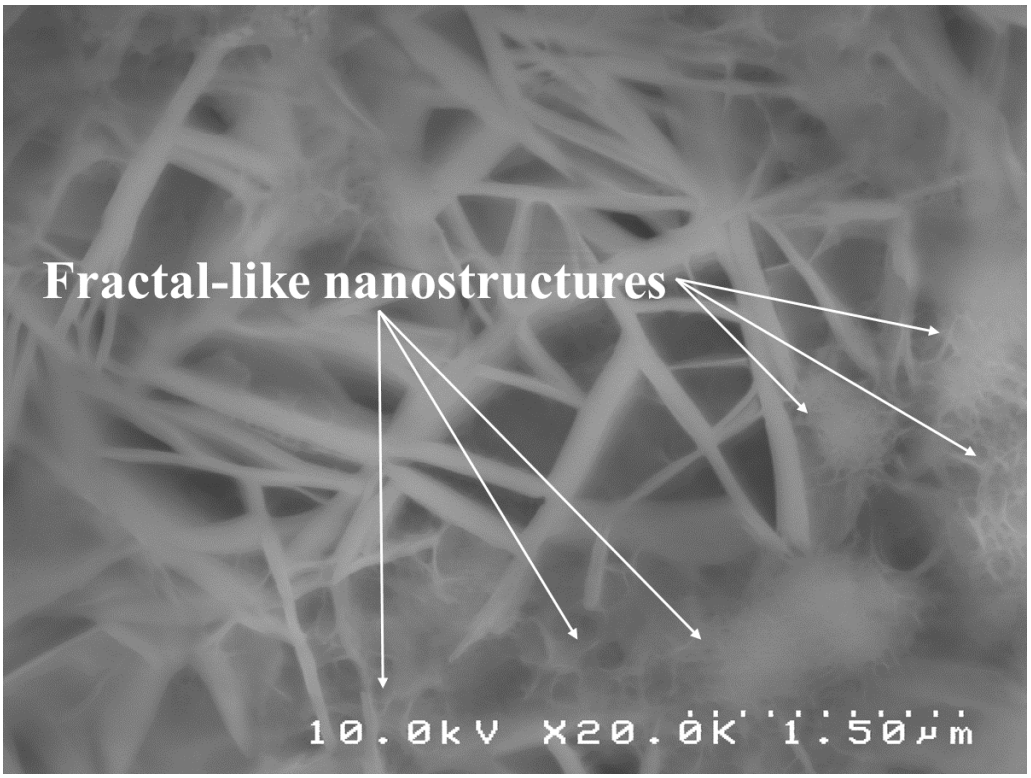

Figure 30 Enlarged SEM image of the smaller nanostructure in the ternary nitrate molten salt ($LiNO_3$–$NaNO_3$–KNO_3) with SiO_2 nanoparticle at 20000x magnification [21]

I also investigated the large amount of nanometer-sized structure (fractal-like) formed by the binary salt compound ($NaNO_3$-KNO_3; 60:40 by weight ratio) around SiO_2 (silicon dioxide) nanoparticle (30 nm). As shown in figure 31, it shows the SEM image of the pure binary molten salt eutectic ($NaNO_3$-KNO_3) (top) at 5000x magnification and it shows the classical salt compounds (e.g., crystal form). Figure 31 (bottom) shows the fractal-like nanostructure around the binary molten salt eutectic at 5000x magnification. Figure 31 (top, middle, and bottom) shows the SEM images of the binary nitrate molten salt eutectic ($NaNO_3$-KNO_3) and nanofluid with SiO_2 nanoparticle (30nm) at 3000x

magnification. They show the fractal-like nanostructures around the binary molten salt compounds. As shown in figure 31 and figure 32, this fractal-like nanostructure may be responsible for the enhanced specific heat capacity of the molten salt nanomaterial.

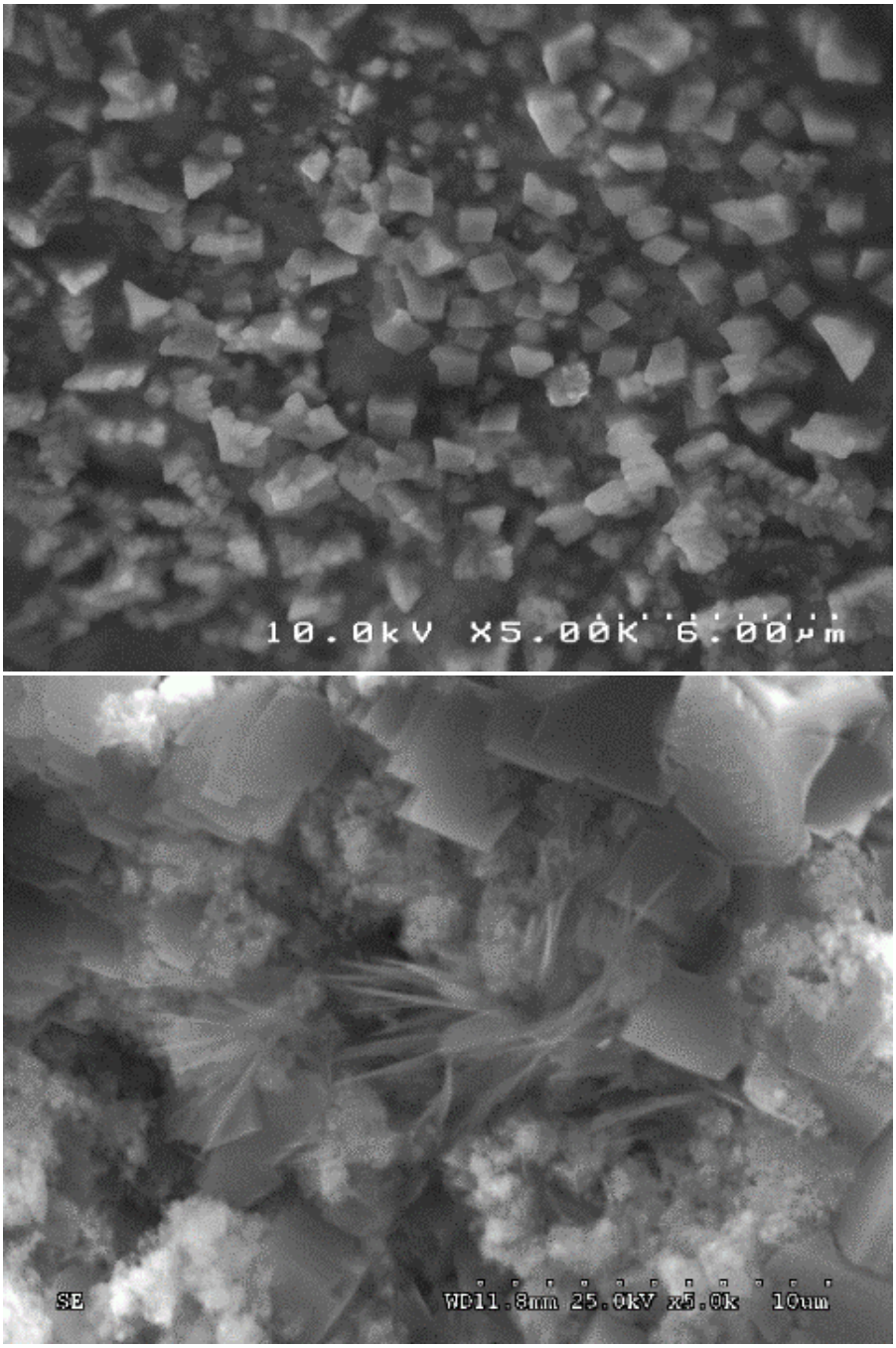

Figure 31 SEM images of the binary nitrate molten salt eutectic ($NaNO_3$-KNO_3) (top) and nanofluid with SiO_2 nanoparticle (30 nm) (bottom) at 5000x magnification

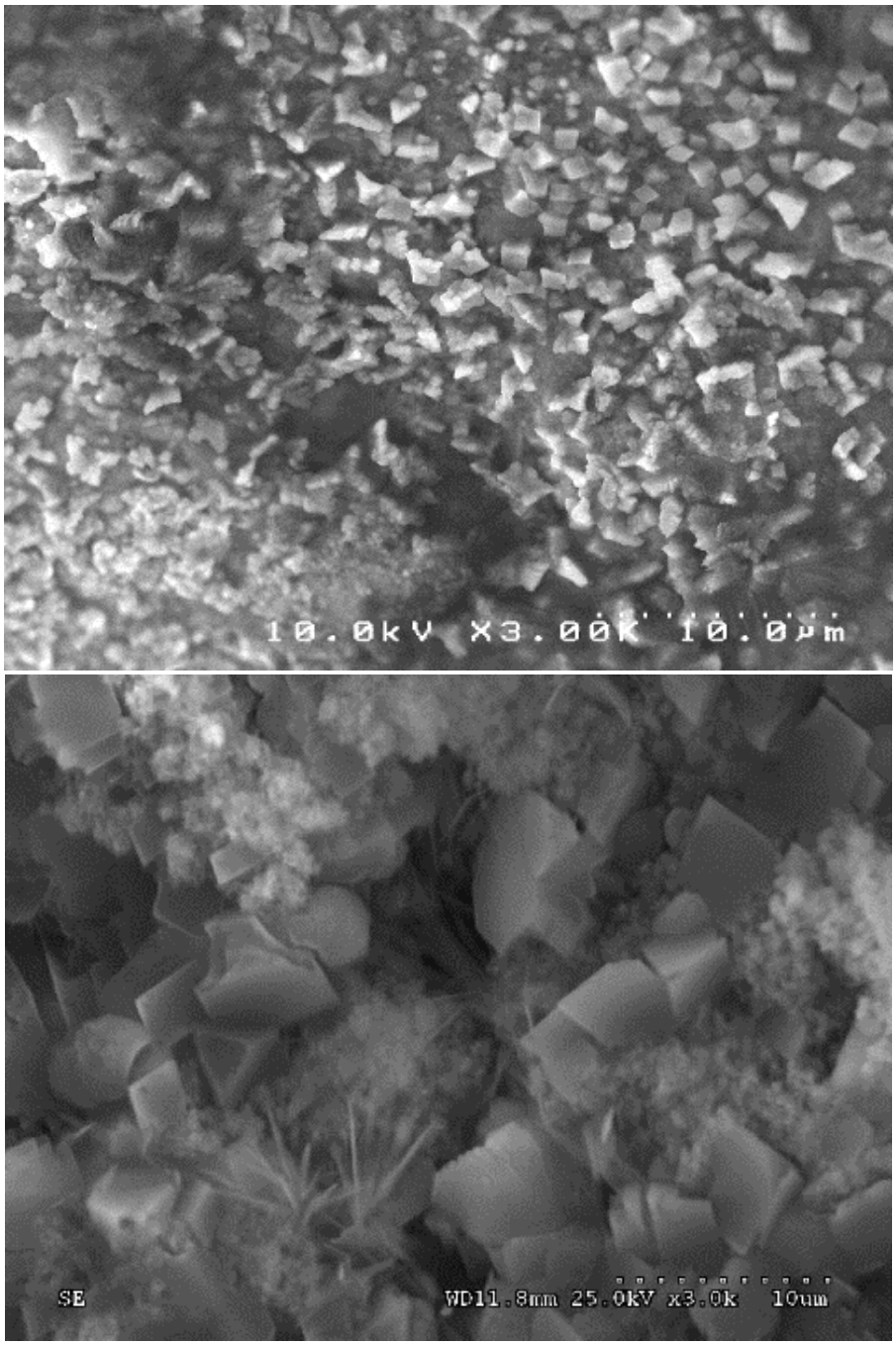
10.0kV X3.00K 10.0µm
SE
WD11.8mm 25.0kV x3.0k 10um

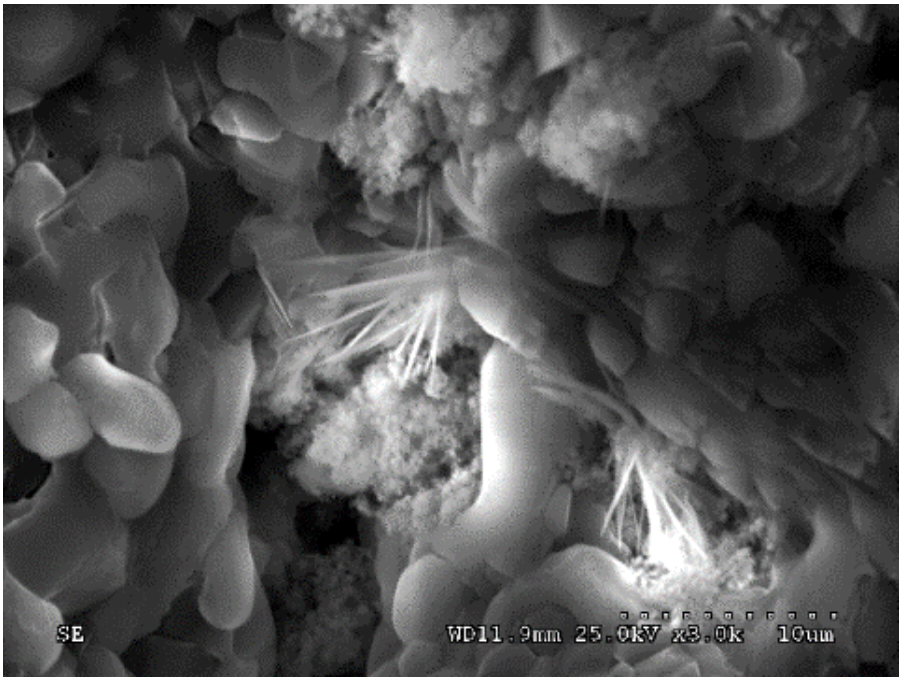

Figure 32 SEM images of the binary nitrate molten salt eutectic ($NaNO_3$-KNO_3) (top) and nanofluid with SiO_2 nanoparticle (30 nm) (middle and bottom) at 3000x magnification

Chapter 4

New Method Preparing Molten Salt Nanofluids: in-situ synthesis of nanoparticles

In general, the nanoparticle is a relatively expensive material compared to salt. According to the literature [95], the nanoparticle can be created by the thermal decomposition process of the hydrated salts as shown in equation 2

$$Al(NO_3)_3 \cdot 9H_2O \xrightarrow{-9H_2O} Al(NO_3)_3 \rightarrow \frac{1}{2}Al_2O_{3(s)} + \frac{3}{2}NO_{2(g)} + \frac{3}{2}NO_{(g)} + \frac{3}{2}O_{2(g)} \quad (2)$$

To produce the nanoparticle (1% concentration by weight) in the molten salt eutectic (e.g., $NaNO_3$-KNO_3), aluminum nitrate nonahydrate ($Al(NO_3)_3 \cdot 9H_2O$) is added to the eutectic salt and H_2O, NO_2, NO, and O_2 are vaporized during the thermal decomposition process. Al_2O_3 is also remained nanometer-sized particles in the salt mixture. Finally, the actual concentration of Al_2O_3 nanoparticle is approximately 1% by weight. The original mass fraction of $Al(NO_3)_3 \cdot 9H_2O$ that I used is 7.69 % to obtain the target concentration by weight (~1%).

Magnesium nitrate hexahydrate ($Mg(NO_3)_2 \cdot 6H_2O$) is added to the eutectic salt to produce the nanoparticle (1% concentration by weight). H_2O, NO_2, NO, and O_2 are vaporized during the thermal decomposition process and thus MgO is remained nanometer-sized particles in the salt mixture [96]. The eutectic salt is with the actual concentration of MgO nanoparticle is approximately 1% by weight. The nanoparticle can be created by the thermal decomposition process of the hydrated salts as shown in equation 3 [96]. The original mass fraction of $Mg(NO_3)_2 \cdot 6H_2O$ that I used is 6.37 % to get the target concentration by weight (~1%).

$$Mg(NO_3)_2 \cdot 6H_2O \xrightarrow{-6H_2O} Mg(NO_3)_2 \rightarrow MgO_{(s)} + NO_{2(g)} + NO_{(g)} + O_{2(g)} \quad (3)$$

The mixture of the molten salt eutectic ($NaNO_3$-KNO_3) with aluminum nitrate nonahydrate ($Al(NO_3)_3 \cdot 9H_2O$) was prepared to verify the thermal decomposition process. The target concentration of Al_2O_3 was 1.07 % by weight. $Al(NO_3)_3 \cdot 9H_2O$ (aluminum nitrate nonahydrate) was used to produce the specific nanoparticle (Al_2O_3) during the thermal decomposition process. The additive is put on the hot plate (50 °C) for 3 hours to prevent the further effect of moisture. After 3 hours, the pure molten salt eutectic and additive were mixed together. It was put into the laboratory furnace for 12 hours at 540 °C for the baking process (e.g., thermal decomposition process). Finally, Al_2O_3 was remained nanometer-sized particles (1.07 % weight concentration) in the salt mixture after the baking process in the laboratory furnace. The temperature of the furnace was maintained at 540 °C to make the isothermal condition for 12 hours during the baking process. For the material characterization, a scanning electron microscope (SEM: Hitachi S-3000N) was used to take images of the molten salt nanofluid sample. As shown in figure 33, nanometer-size particles are in the salt mixture and their size is relatively smaller than the salt mixture. As shown in figure 34, the size of each nanometer-size particle was measured and they show approximately 40 nm-60 nm size particle. The thermal decomposition process with the molten salt eutectic is proved by the material characterization (SEM) as shown in figure 33 and 34. Therefore, the creation of nanometer-sized particles in the binary molten salt eutectic was verified by this SEM images.

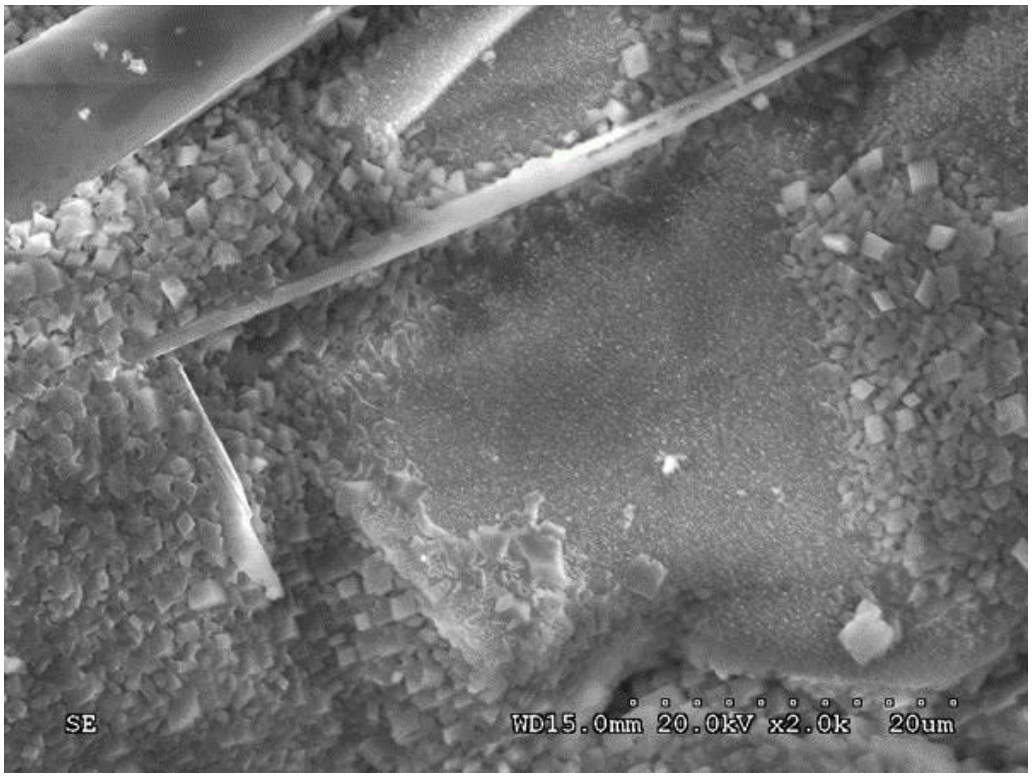

Figure 33 SEM image of $NaNO_3$-KNO_3+ $Al(NO_3)_3 \cdot 9H_2O$ with 1.07 % concentration of Al_2O_3 at 2000x magnification

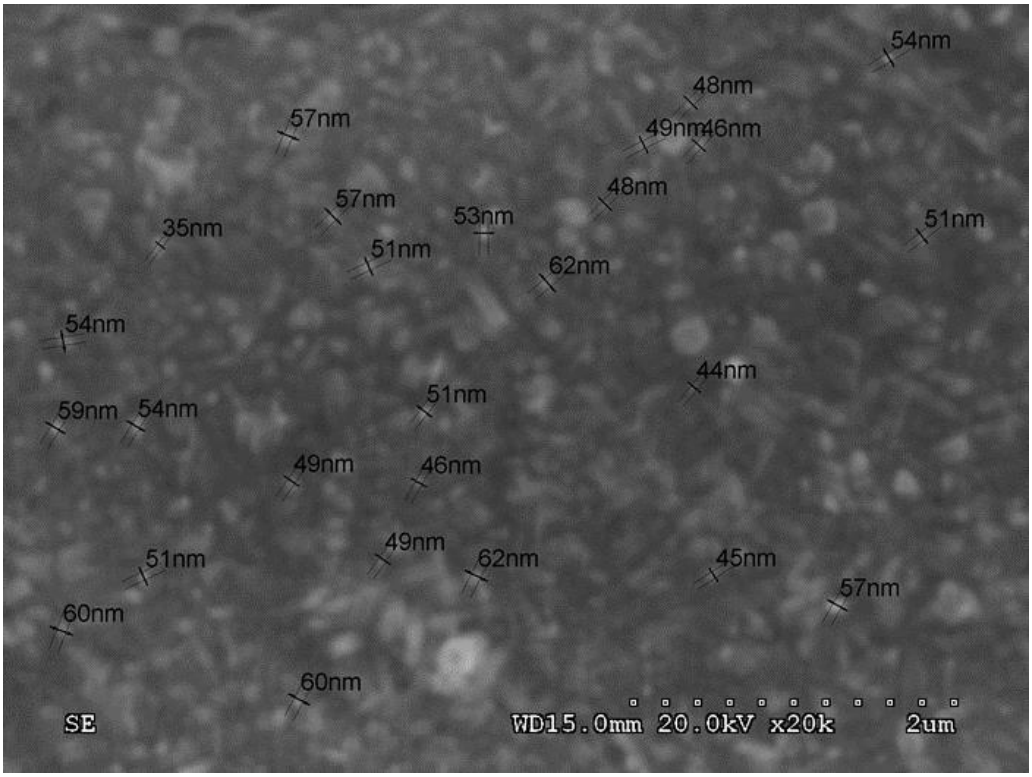

Figure 34 SEM image of $NaNO_3$-KNO_3+ $Al(NO_3)_3 \cdot 9H_2O$ with 1.07 % concentration of Al_2O_3 at 20000x magnification

Measurement of Specific Heat Capacity (C_p)

Sample Preparation

For measuring thermophysical properties of the pure molten salt eutectic, a mixture of $NaNO_3$ and KNO_3 (solar salt; 60:40 by weight ratio) was prepared. As shown in figure 35, each chemical (e.g., sodium nitrate and potassium nitrate) is put on the hot plate at 200 °C for 3 hours with the different vial to prevent the effect of moisture. After 3 hours, two chemicals ($NaNO_3$ and KNO_3) are mixed together with the 60:40 weight ratio in one vial. It was put on the hot plate at 300 °C for 1 hour to melt mixed the salt compounds homogeneously. After 1 hour, the vial with the well mixed salts was on the hot plate at 100 °C to make it be solid.

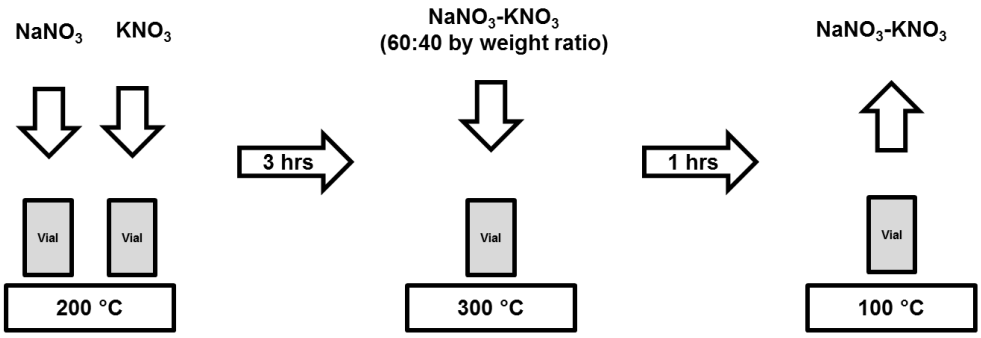

Figure 35 Procedure of the sample preparation of the molten salt eutectic ($NaNO_3$-KNO_3)

The mixture of $NaNO_3$ and KNO_3 (solar salt; 60:40 by weight ratio) is prepared to measure thermophysical properties of the nanofluid with the thermal decomposition process. As shown in figure 36, $Al(NO_3)_3 \cdot 9H_2O$ (aluminum nitrate nonahydrate) and $Mg(NO_3)_2 \cdot 6H_2O$ (magnesium nitrate hexahydrate) are used to create two different nanoparticles (e.g., Al_2O_3 and MgO). Two different additives ($Al(NO_3)_3 \cdot 9H_2O$ and $Mg(NO_3)_2 \cdot 6H_2O$) were put on the hot plate at 50 °C for 3 hours to prevent the further effect of moisture. After 3 hours, the pure molten salt eutectic and additive were mixed

together. It was put into the laboratory furnace for 12 hours at 540 °C for the baking process (e.g., thermal decomposition process). According to the literature [97], nitrate salt (e.g., $NaNO_3$) can be decomposed at 450 °C-550 °C. Finally, Al_2O_3 and MgO are remained nanometer-sized particles in the salt mixture after the baking process. This nanometer-sized particles had 1% weight concentration in the binary molten salt eutectic.

Figure 36 Procedure of the sample preparation of the nanofluid for the thermal decomposition process

Experimental Setup

A modulated differential scanning calorimeter (MDSC; Q20, TA Instrument Inc.) was used to measure the specific heat capacity of the pure molten salt as well as its nanofluids as shown in figure 37. Accurate measurement is the important factor in the MDSC at high temperature. The most important factor in all tests using the MDSC is to prevent loss of each sample. If a molten salt has leaked, a chamber of the MDSC may become contaminated during measurement. It is difficult to measure the accurate specific heat of molten salt eutectic and nanofluid at high temperature. Therefore, each sample was hermetically sealed in a Tzero hermetic pan and lid (TA Instruments Inc.) to prevent possible errors (e.g., exploded sample inside the MDSC) as shown in figure 38. For the loading sample, 12mg-15mg sample was prepared to prevent a leakage of a sample during measurement in MDSC.

Figure 37 Modulated differential scanning calorimeter (MDSC; Q20, TA Instruments Inc.)

Figure 38 Tzero hermetic pan and lid (TA Instruments Inc.)

Measurement Results

$Al(NO_3)_3 \cdot 9H_2O$ (aluminum nitrate nonahydrate) and $Mg(NO_3)_2 \cdot 6H_2O$ (magnesium nitrate hexahydrate) were used to produce nanometer-sized particle with the binary nitrate molten salt eutectic (solar salt: $NaNO_3$-KNO_3 with 60:40 weight ratio). Only 1 % of $Al(NO_3)_3 \cdot 9H_2O$ and $Mg(NO_3)_2 \cdot 6H_2O$ were added in the binary nitrate molten salt eutectic to measure the specific heat capacity. Figure 39 shows the specific heat capacity of the binary nitrate molten salt eutectic ($NaNO_3$-KNO_3) as well as nanofluid with $Al(NO_3)_3 \cdot 9H_2O$ (added 1 % by weight ratio). As shown in table 2, it shows the enhanced specific heat capacity by 14.8 % on average compared to the pure salt. As shown in figure 40, it shows the specific heat capacity of the binary nitrate molten salt eutectic (e.g., $NaNO_3$-KNO_3) and nanofluid with $Mg(NO_3)_2 \cdot 6H_2O$ (added 1 % by weight ratio). They also shows 17.1 % enhancement of the specific heat capacity on average compared to the based binary nitrate molten salt eutectic. As shown in table 2, two different pure samples were in good agreement with the literature.

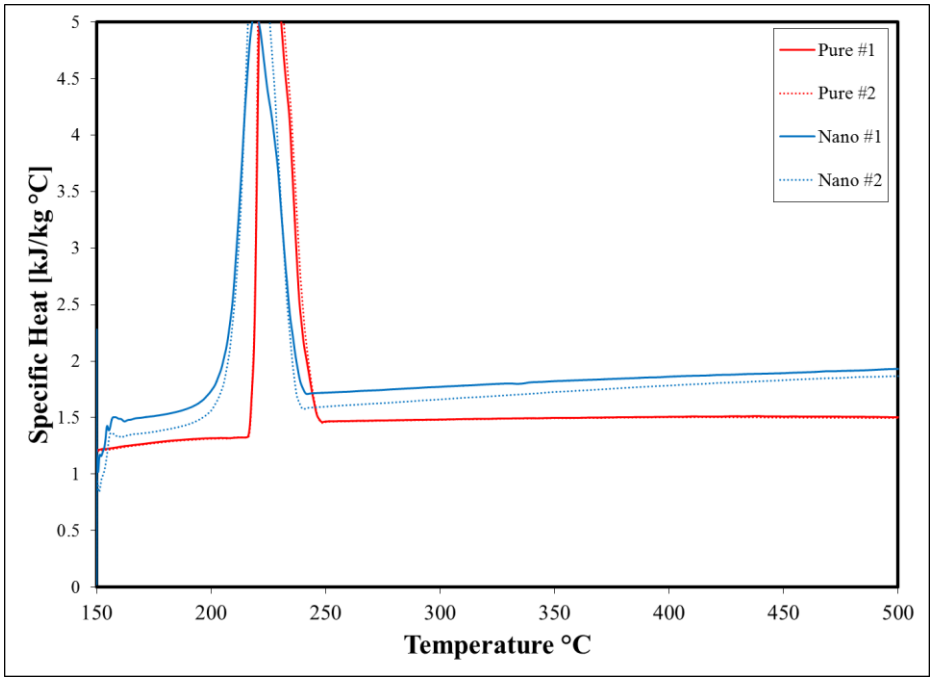

Figure 39 Specific heat capacity of the binary nitrate molten salt eutectic ($NaNO_3$-KNO_3) and nanofluid with $Al(NO_3)_3 \cdot 9H_2O$ (added 1 % by weight ratio)

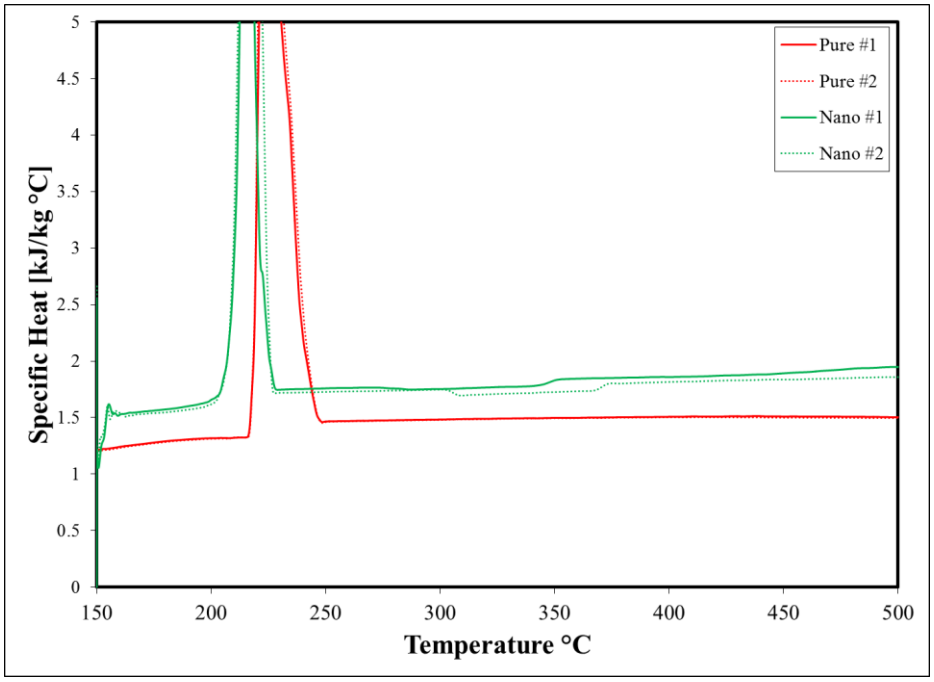

Figure 40 Specific heat capacity of the binary nitrate molten salt eutectic ($NaNO_3$-KNO_3) and nanofluid with $Mg(NO_3)_2 \cdot 6H_2O$ (added 1 % by weight ratio)

Table 2 Summary of the specific heat capacity of the binary nitrate molten salt eutectic and nanofluids ($Al(NO_3)_3 \cdot 9H_2O$ and $Mg(NO_3)_2 \cdot 6H_2O$) with added 1 % by weight ratio

	Solar salt + $Al(NO_3)_3 \cdot 9H_2O$ (added 1 % by weight ratio)		Solar salt + $Mg(NO_3)_2 \cdot 6H_2O$ (added 1 % by weight ratio)		Pure salt	
Sample	C_p at 300 °C (kJ/kg °C)	Enhancement (%)	C_p at 300 °C (kJ/kg °C)	Enhancement (%)	C_p at 300 °C (kJ/kg °C)	Ref [98]
#1	1.77	18.5	1.75	17.2	1.48	1.495
#2	1.66	11.0	1.75	16.9	1.48	
Average	1.72	14.8	1.75	17.1	1.48	

To produce Al_2O_3 and MgO nanoparticle with the thermal decomposition process, $Al(NO_3)_3 \cdot 9H_2O$ (aluminum nitrate nonahydrate) and $Mg(NO_3)_2 \cdot 6H_2O$ (magnesium nitrate hexahydrate) were used in the binary nitrate molten salt eutectic (solar salt: $NaNO_3$-KNO_3 with 60:40 weight ratio). The concentration of Al_2O_3 was 1.07 % by weight ratio and MgO was 1.06 % by weight ratio from the thermal decomposition process. Pure samples and nanofluid samples were prepared in the different days and they were tested to measure the specific heat capacity in MDSC. As shown in table 3, three different pure samples were in good agreement with the literature. As shown in figure 41, it shows the specific heat capacity of the binary nitrate molten salt eutectic and nanofluid with Al_2O_3 nanoparticle (1.07 % by weight ratio). Three different samples of molten salt nanofluids show the enhanced specific heat capacity compared to the binary pure eutectic salt. As shown in table 3, the maximum enhanced specific heat capacity is 2.15 kJ/kg °C and it shows 41.4 % enhancement. The average enhanced specific heat capacity is 2.12 kJ/kg °C and it shows 39.7 % enhancement compared to the pure eutectic salt. As shown in figure 42, it shows the specific heat capacity of the binary nitrate molten salt eutectic and nanofluid with MgO nanoparticle (1.06 % by weight ratio). Three different samples show the enhanced specific heat capacity compared to the binary pure eutectic salt. As shown in table 3, the average enhanced specific heat capacity is 2.08 kJ/kg °C and it shows 36.8 % enhancement. The maximum enhanced specific heat capacity is 2.14 kJ/kg °C and it shows 40.8 % enhancement compared to the binary nitrate molten salt eutectic.

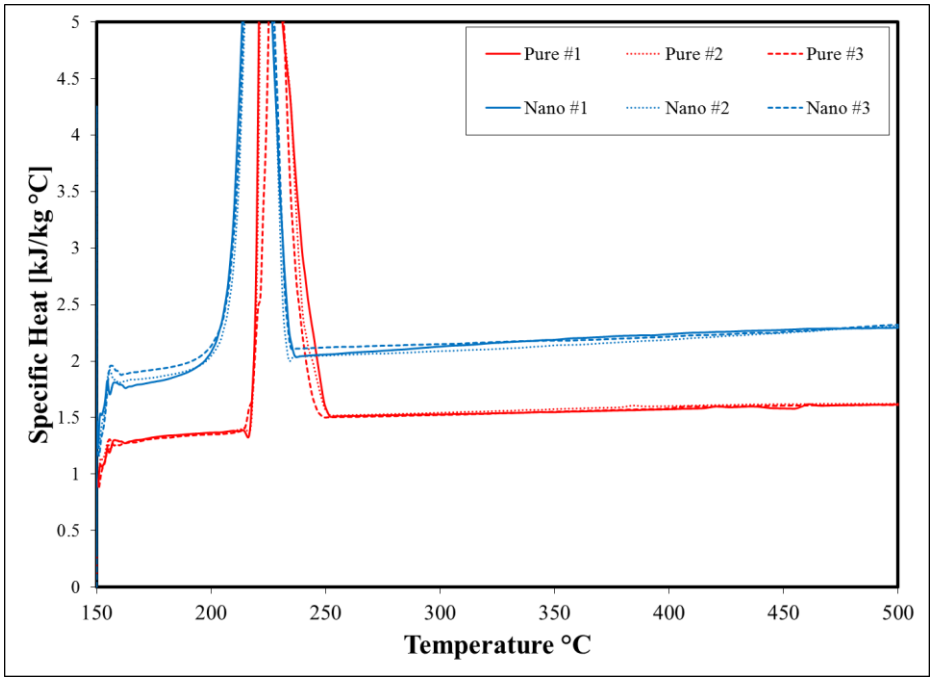

Figure 41 Specific heat capacity of the binary nitrate molten salt eutectic ($NaNO_3$-KNO_3) and nanofluid with Al_2O_3 nanoparticle (1.07 % by weight ratio)

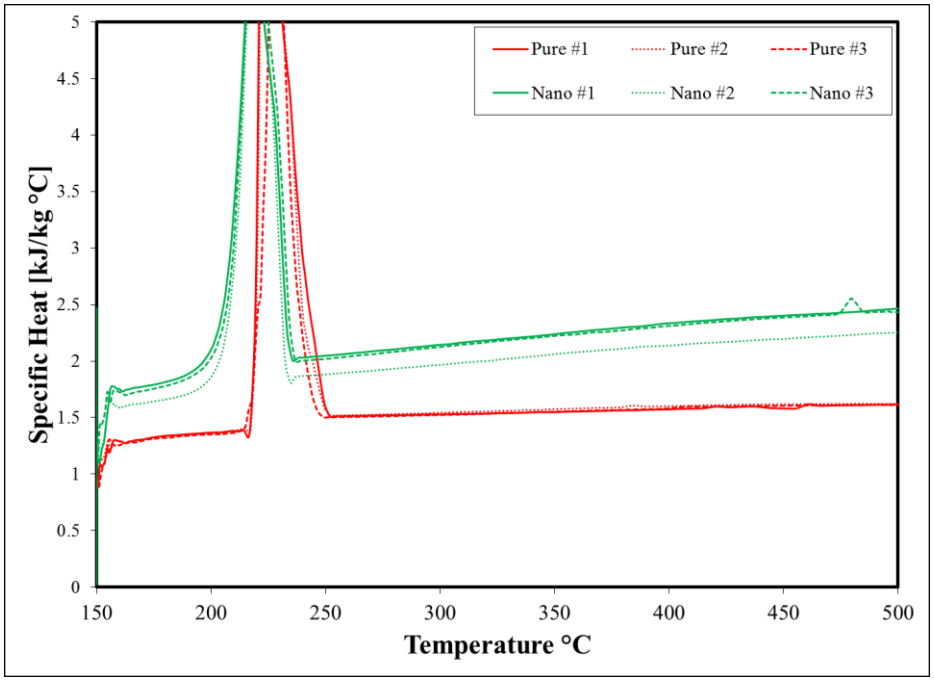

Figure 42 Specific heat capacity of the binary nitrate molten salt eutectic ($NaNO_3$-KNO_3) and nanofluid with MgO nanoparticle (1.06 % by weight ratio)

Table 3 Summary of the specific heat capacity of the binary nitrate molten salt eutectic and nanofluids (Al_2O_3 and MgO nanoparticle)

	Solar salt + $Al(NO_3)_3 \cdot 9H_2O$ 1.07 % Al_2O_3		Solar salt + $Mg(NO_3)_2 \cdot 6H_2O$ 1.06 % MgO		Pure salt	
Sample	C_p at 300 °C (kJ/kg °C)	Enhancement (%)	C_p at 300 °C (kJ/kg °C)	Enhancement (%)	C_p at 300 °C (kJ/kg °C)	Ref [98]
#1	2.13	40.1	2.14	40.8	1.53	1.495
#2	2.09	37.5	1.97	29.6	1.54	
#3	2.15	41.4	2.13	40.1	1.52	
Average	2.12	39.7	2.08	36.8	1.53	

The ternary nitrate molten salt eutectic ($NaNO_3$-KNO_3-$Ca(NO_3)_2 \cdot 4(H_2O)$) was used to measure specific heat and it was the base fluid as well as nanofluid with nanoparticles (Al_2O_3 and MgO). The concentration of Al_2O_3 is 1.32 % by weight ratio and MgO is 1.25 % by weight ratio from the thermal decomposition process. Pure samples and nanofluid samples were prepared in the different days and they were tested for the specific heat capacity in MDSC. As shown in figure 43, the ternary nitrate molten salt with Al_2O_3 nanoparticle shows the enhanced specific heat capacity compared to the pure eutectic salt. As shown in table 4, the average enhancement is 18.8 % and it shows 1.83 kJ/kg °C and the maximum enhancement is 20.1 % (1.85 kJ/kg °C) compared to the ternary nitrate molten salt eutectic. As shown in figure 44, the ternary nitrate molten salt with MgO nanoparticle shows the enhanced specific heat capacity compared to the pure eutectic salt. As shown in table 3, the maximum enhancement is 33.8 % (2.06 kJ/kg °C). The average of the specific heat capacity is 2.00 kJ/kg °C and it shows 29.8 % enhancement compared to the ternary nitrate molten salt eutectic.

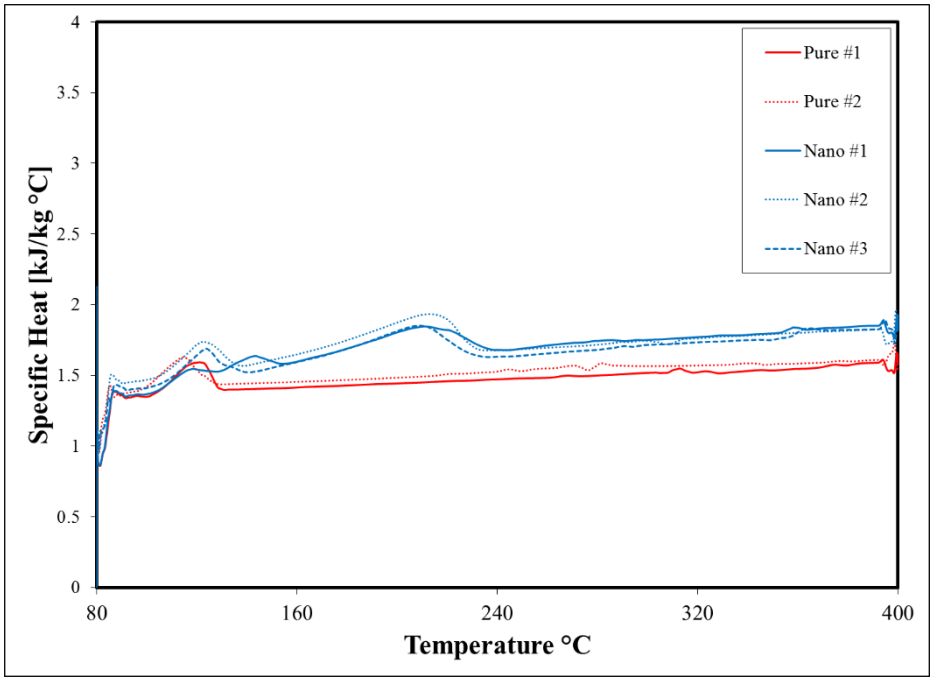

Figure 43 Specific heat capacity of the ternary nitrate molten salt eutectic ($NaNO_3$-KNO_3-$Ca(NO_3)_2 \cdot 4(H_2O)$) and nanofluid with Al_2O_3 nanoparticle (1.32 % by weight ratio)

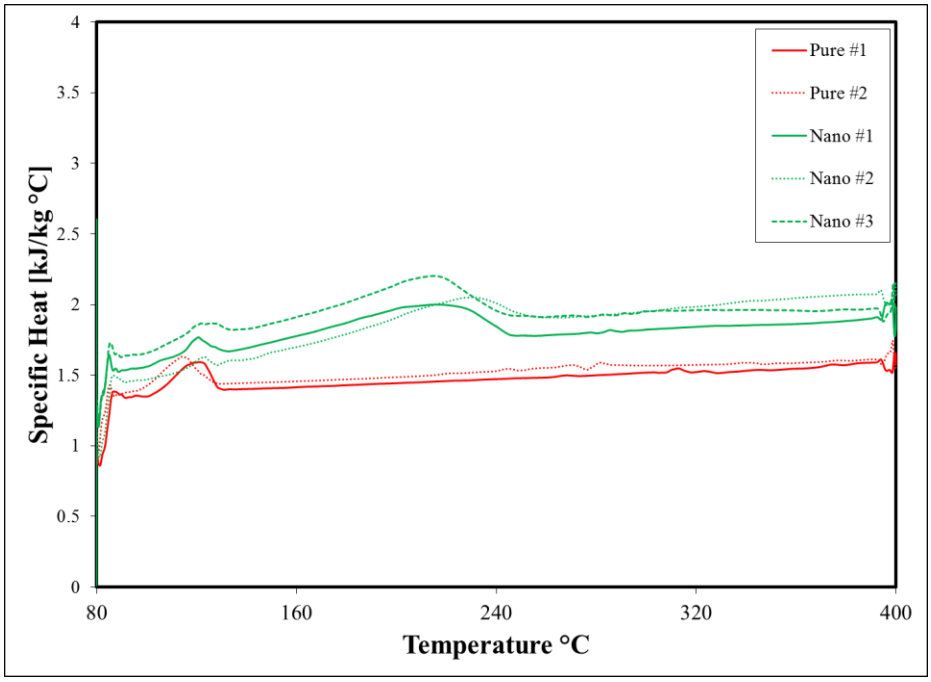

Figure 44 Specific heat capacity of the ternary nitrate molten salt eutectic ($NaNO_3$-KNO_3-$Ca(NO_3)_2 \cdot 4(H_2O)$) and nanofluid with MgO nanoparticle (1.25 % by weight ratio)

Table 4 Summary of the specific heat capacity of the ternary nitrate molten salt eutectic and nanofluids (Al_2O_3 and MgO nanoparticle)

	Ternary salt + $Al(NO_3)_3 \cdot 9H_2O$ 1.32 % Al_2O_3		Ternary salt + $Mg(NO_3)_2 \cdot 6H_2O$ 1.25 % MgO		Pure salt
Sample	C_p (kJ/kg °C)	Enhancement (%)	C_p (kJ/kg °C)	Enhancement (%)	C_p (kJ/kg °C)
#1	1.83	18.8	1.94	26.0	1.52
#2	1.85	20.1	1.99	29.2	1.55
#3	1.82	18.2	2.06	33.8	
Average	1.83	18.8	2.00	29.8	1.54

Measurement of Viscosity (v)

Experimental Setup

A discovery hybrid rheometer (HR-2, TA Instruments Inc.) was employed to measure viscosity of each sample (e.g., pure molten salt eutectic as well as nanofluid) as shown in figure 45. The amount of each sample was 1.29 g due to the size of the bottom and upper part as shown in figure 46. This amount is also related to density of each sample (nitrate based molten salt) because density will be changed at specific temperature (e.g., high temperature) during measurement. The results of the binary and ternary molten salt eutectic were in good agreement with the literature. According to the results of viscosity, the nanofluids shows the increased viscosity. Nanofluids that show the increased viscosity were evaluated by comparing the required pumping power to maintain the temperature difference between inlet and outlet of storage fluid with the figure of merit [71].

Figure 45 Discovery hybrid rheometer (HR-2, TA Instruments Inc.)

Figure 46 Bottom and upper part that are related to the loading sample

Measurement Results

To measure viscosity of the nanofluid, the binary nitrate molten salt eutectic (solar salt: $NaNO_3$-KNO_3 with 60:40 weight ratio) was used. It was the base fluid as well as nanofluids with Al_2O_3 and MgO nanoparticle from the thermal decomposition process. The temperature range was from 300 °C to 565 °C and viscosity was measured at each temperature. As shown in figure 47, it shows the results of viscosity of the binary nitrate molten salt eutectic ($NaNO_3$-KNO_3) as well as nanofluid with Al_2O_3 nanoparticle (1.07 % by weight ratio). Total 6 nanofluid samples were tested at seven different temperature points (300 °C, 350 °C, 400 °C, 450 °C, 500 °C, 550 °C, and 565 °C). The scale-up test (50 g sample) was performed to compare the results of viscosity of a large amount of the molten salt eutectic and nanofluid with the sample of the laboratory level. Six different nanofluid samples were tested at seven different temperature points (300 °C, 350 °C, 400 °C, 450 °C, 500 °C, 550 °C, and 565 °C). Six nanofluid samples show increased viscosity compared to the binary pure molten salt as shown in table 5. The results of the scale-up are similar to the results of the laboratory level sample. Figure 48 shows viscosity of the binary nitrate molten salt eutectic ($NaNO_3$-KNO_3) and nanofluid with MgO nanoparticle (1.06 % by weight ratio). Six nanofluid samples show increased viscosity compared to the binary pure molten salt, but the difference is not substantial as shown in table 6. The results of the scale-up are similar to the results of the laboratory level sample as well as the nanofluid with Al_2O_3 nanoparticle.

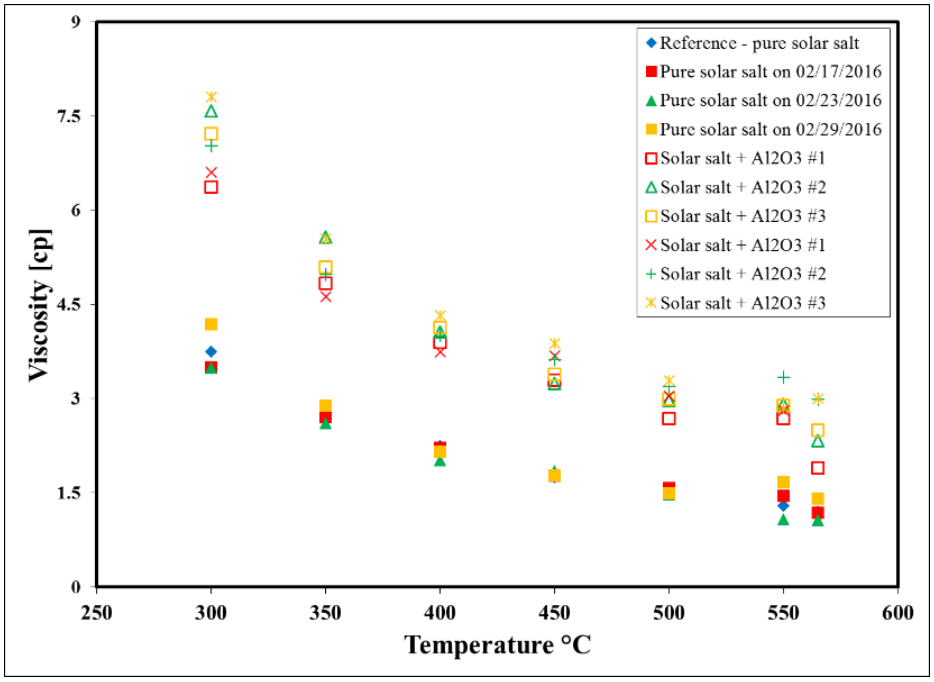

Figure 47 Viscosity of the binary nitrate molten salt eutectic ($NaNO_3$-KNO_3) and nanofluid with Al_2O_3 nanoparticle (1.07 % by weight ratio)

Table 5 Summary of viscosity of the binary nitrate molten salt eutectic ($NaNO_3$-KNO_3) and nanofluid with Al_2O_3 nanoparticle (1.07 % by weight ratio)

Temp (°C)	Ref [99] (cP)	P #1 (cP)	P #2 (cP)	P #3 (cP)	N #1 (cP)	N #2 (cP)	N #3 (cP)	NS #1 (cP)	NS #2 (cP)	NS #3 (cP)
300 °C	3.75	3.51	3.49	4.19	6.37	7.58	7.22	6.60	7.03	7.8
350 °C	2.75	2.70	2.61	2.89	4.84	5.57	5.10	4.63	4.98	5.55
400 °C	2.25	2.22	2.02	2.16	3.90	4.06	4.13	3.74	4.00	4.32
450 °C	1.75	1.77	1.84	1.78	3.29	3.24	3.39	3.68	3.62	3.88
500 °C	1.50	1.58	1.48	1.49	2.68	2.97	2.99	3.04	3.20	3.29
550 °C	1.30	1.45	1.07	1.67	2.68	2.91	2.89	2.81	3.34	2.84
565 °C	1.20	1.19	1.06	1.41	1.90	2.33	2.50		2.99	3.00

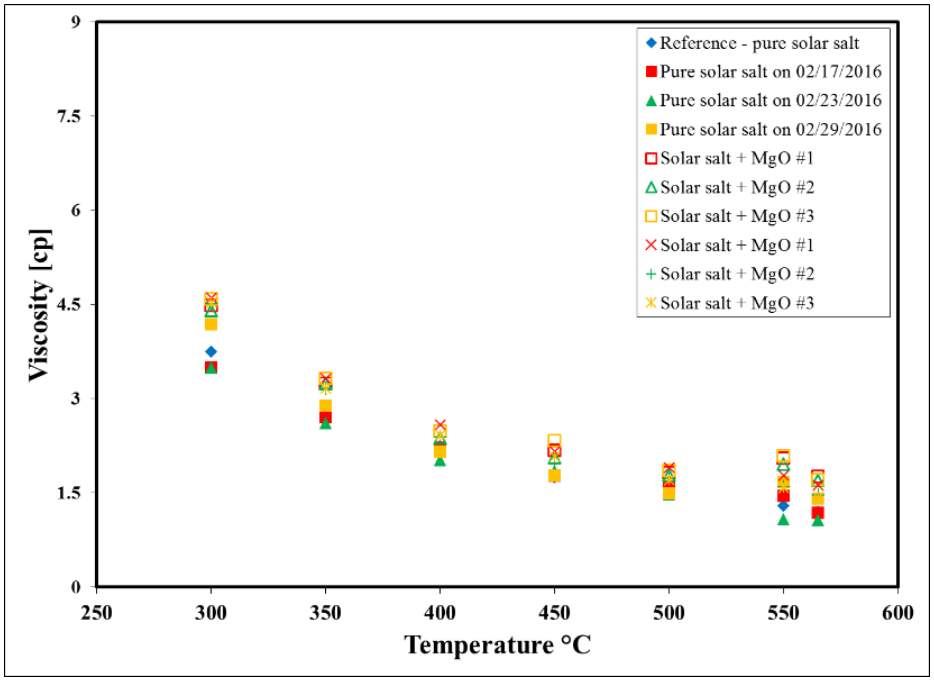

Figure 48 Viscosity of the binary nitrate molten salt eutectic ($NaNO_3$-KNO_3) and nanofluid with MgO nanoparticle (1.06 % by weight ratio)

Table 6 Summary of viscosity of the binary nitrate molten salt eutectic ($NaNO_3$-KNO_3) and nanofluid with MgO nanoparticle (1.06 % by weight ratio)

Temp (°C)	Ref [99] (cP)	P #1 (cP)	P #2 (cP)	P #3 (cP)	N #1 (cP)	N #2 (cP)	N #3 (cP)	NS #1 (cP)	NS #2 (cP)	NS #3 (cP)
300 °C	3.75	3.51	3.49	4.19	4.49	4.40	4.59	4.60	4.51	4.53
350 °C	2.75	2.70	2.61	2.89	3.24	3.24	3.33	3.32	3.17	3.16
400 °C	2.25	2.22	2.02	2.16	2.49	2.37	2.49	2.59	2.39	2.42
450 °C	1.75	1.77	1.84	1.78	2.18	2.06	2.33	2.16	1.97	2.08
500 °C	1.50	1.58	1.48	1.49	1.82	1.78	1.85	1.90	1.73	1.71
550 °C	1.30	1.45	1.07	1.67	2.05	1.96	2.09	1.78	1.60	1.58
565 °C	1.20	1.19	1.06	1.41	1.76	1.70	1.71	1.62	1.47	1.43

The ternary nitrate molten salt eutectic ($NaNO_3$-KNO_3-$Ca(NO_3)_2{\cdot}4(H_2O)$) was used for the measurement of viscosity at seven different temperature points (300 °C, 350 °C, 400 °C, 450 °C, 500 °C, 550 °C, and 565 °C). Two additives (Al_2O_3 and MgO nanoparticle) were used to measure viscosity of the ternary nitrate molten salt nanofluid. According to the literature [100], [101], they show the reference value of the ternary nitrate molten salt eutectic ($NaNO_3$-KNO_3-$Ca(NO_3)_2{\cdot}4(H_2O)$) with different compositions. Hitec XL ($NaNO_3$-KNO_3-$Ca(NO_3)_2{\cdot}4(H_2O)$; 7:45:28 by weight ratio) shows 6.27 cP-6.37 cP at 300 °C and $NaNO_3$-KNO_3-$Ca(NO_3)_2{\cdot}4(H_2O)$ (12:44:44 by weight ratio shows 10 cP at 300 °C. Figure 49 shows viscosity of the ternary nitrate molten salt eutectic ($NaNO_3$-KNO_3-$Ca(NO_3)_2{\cdot}4(H_2O)$) at 1000 s^{-1} shear rate. Three tested samples show 7.88 cP on average at 300 °C as shown in table 7. Figure 50 shows viscosity of the ternary nitrate molten salt eutectic ($NaNO_3$-KNO_3-$Ca(NO_3)_2{\cdot}4(H_2O)$) with Al_2O_3 nanoparticle (1.32 % by weight ratio) at 1000 s^{-1} shear rate and figure 51 shows viscosity of the ternary nitrate molten salt eutectic ($NaNO_3$-KNO_3-$Ca(NO_3)_2{\cdot}4(H_2O)$) with MgO nanoparticle (1.25 % by weight ratio) at 1000 s^{-1} shear rate. As shown in table 8 and 9, two nanofluid samples show increased viscosity compared to the ternary nitrate molten salt eutectic and it is substantial.

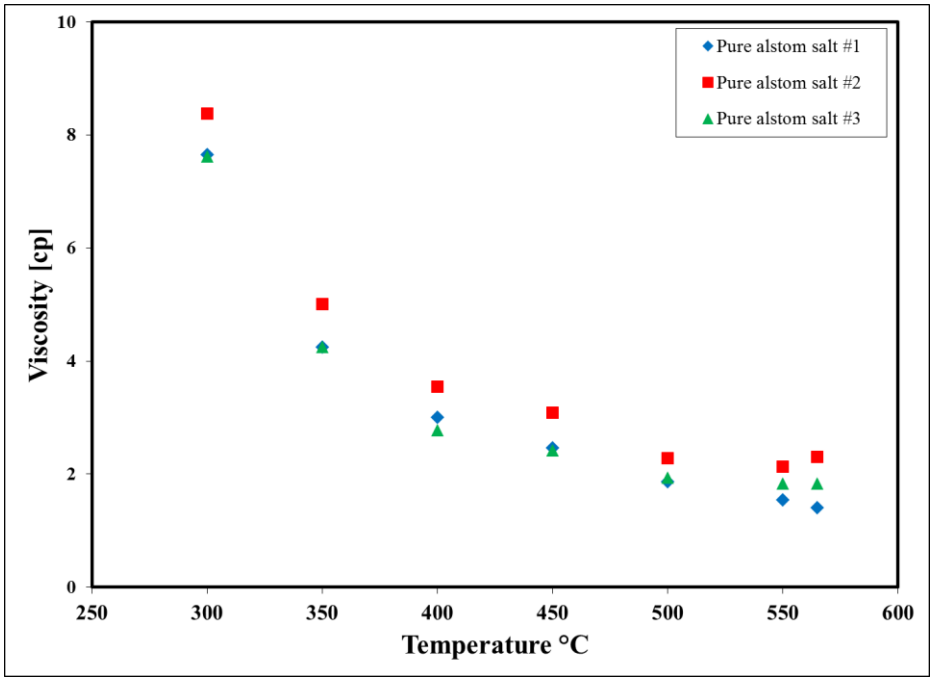

Figure 49 Viscosity of the ternary nitrate molten salt eutectic ($NaNO_3$-KNO_3-$Ca(NO_3)_2{\cdot}4(H_2O)$) at 1000 s^{-1} shear rate

Table 7 Summary of viscosity of the ternary nitrate molten salt eutectic ($NaNO_3$-KNO_3-$Ca(NO_3)_2{\cdot}4(H_2O)$) at 1000 s^{-1} shear rate

Temp (°C)	P #1 (cP)	P #2 (cP)	P #3 (cP)
300 °C	7.65	8.38	7.62
350 °C	4.25	5.01	4.25
400 °C	3.00	3.55	2.78
450 °C	2.46	3.09	2.42
500 °C	1.87	2.28	1.94
550 °C	1.54	2.13	1.83
565 °C	1.40	2.30	1.83

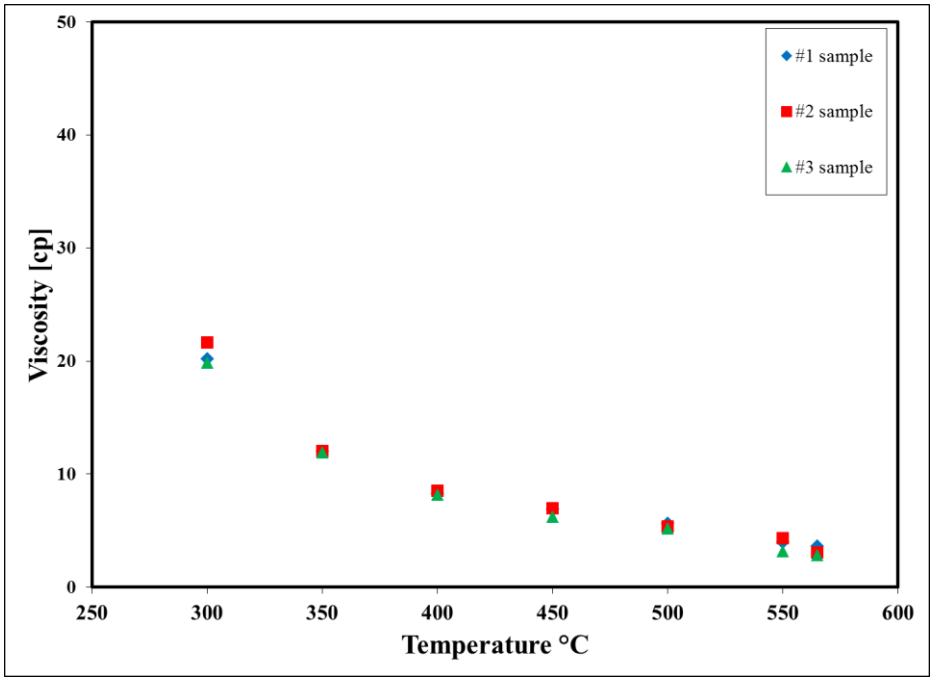

Figure 50 Viscosity of the ternary nitrate molten salt eutectic ($NaNO_3$-KNO_3-$Ca(NO_3)_2{\cdot}4(H_2O)$) with Al_2O_3 nanoparticle (1.32 % by weight ratio) at 1000 s^{-1} shear rate

Table 8 Summary of viscosity of the ternary nitrate molten salt eutectic ($NaNO_3$-KNO_3-$Ca(NO_3)_2{\cdot}4(H_2O)$) with Al_2O_3 nanoparticle (1.32 % by weight ratio) at 1000 s^{-1} shear rate

Temp (°C)	N #1 (cP)	N #2 (cP)	N #3 (cP)
300 °C	20.21	21.62	19.85
350 °C	12.03	12.04	11.90
400 °C	8.29	8.50	8.15
450 °C	6.94	6.97	6.24
500 °C	5.66	5.33	5.20
550 °C	3.96	4.33	3.20
565 °C	3.63	3.03	2.84

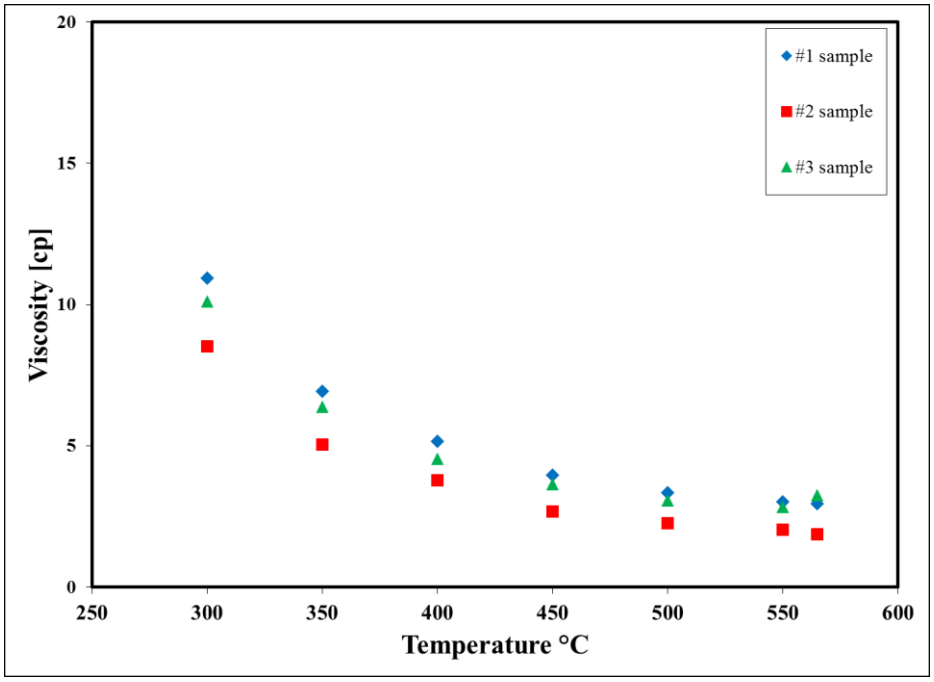

Figure 51 Viscosity of the ternary nitrate molten salt eutectic ($NaNO_3$-KNO_3-$Ca(NO_3)_2{\cdot}4(H_2O)$) with MgO nanoparticle (1.25 % by weight ratio) at 1000 s^{-1} shear rate

Table 9 Summary of viscosity of the ternary nitrate molten salt eutectic ($NaNO_3$-KNO_3-$Ca(NO_3)_2{\cdot}4(H_2O)$) with MgO nanoparticle (1.25 % by weight ratio) at 1000 s^{-1} shear rate

Temp (°C)	N #1 (cP)	N #2 (cP)	N #3 (cP)
300 °C	10.93	8.51	10.1
350 °C	6.92	5.04	6.37
400 °C	5.16	3.77	4.54
450 °C	3.97	2.68	3.64
500 °C	3.35	2.26	3.07
550 °C	3.02	2.02	2.84
565 °C	2.94	1.86	3.25

Figure of Merit (FOM1)

Thermal energy storage (TES) has the high heat capacity (e.g., high heat storage capability) and thus it can reduces cost of the structure and material. However, when viscosity of the heat transfer fluid (HTF) is increased in the thermal energy storage (TES), the total cost of concentrated solar power (CSP) systems is significantly increased due to the high pumping power. To estimate the required pumping power in CSP system, the evaluation of thermophysical properties of nanofluids is necessary for the system to maintain temperature difference between the inlet and outlet of the storage fluid. According to the figure of merit (FOM1) for the storage fluid point [71], the required pumping power of different fluids is evaluated and the density of the storage fluid is constant in this case as shown equation 4.

$$\mathrm{FOM1} = \frac{\rho^{2.0} {C_p}^{2.8}}{\mu^{0.2}} \qquad (4)$$

where ρ is density, C_p is the specific heat capacity, and μ is viscosity respectively. As shown in table 10, the enhancement of the specific heat capacity of the binary nitrate molten salt eutectic ($NaNO_3$-KNO_3) and nanofluid with Al_2O_3 and MgO nanoparticle is 39.7 % and 36.8 % on average at 300 °C respectively. The enhancement of the viscosity of this nanofluid with Al_2O_3 and MgO nanoparticle is 66.5-133.7 % and 24.8~36.7 % at 300 °C respectively. As shown in table 10, the performance of the binary nitrate molten salt eutectic with Al_2O_3 and MgO nanoparticle is enhanced by 115 %-130 % and 125 %-130 % respectively for the the storage fluid point from the figure of merit (FOM1). As shown in table 11, the enhancement of the specific heat capacity of the ternary nitrate molten salt eutectic ($NaNO_3$-KNO_3-$Ca(NO_3)_2{\cdot}4(H_2O)$) and nanofluid with Al_2O_3 and MgO nanoparticle is 18.8 % and 29.8 % on average respectively. The enhancement of the viscosity of this nanofluid with Al_2O_3 and MgO nanoparticle is 160.8 %-274.0 % and 24.9

%-33.2 % respectively. The performance of the ternary nitrate molten salt eutectic with Al_2O_3 and MgO nanoparticle is enhanced by 24 %-34 % and 96 %-99 % respectively for the storage fluid point from the figure of merit (FOM1) as shown in table 11.

Table 10 Figure of merit (FOM1) of the binary nitrate molten salt eutectic ($NaNO_3$-KNO_3) and its nanofluid with Al_2O_3 and MgO nanoparticle

%	Pure binary salt	With Al_2O_3 1.07 %	With MgO 1.06 %
C_p	0 %	39.7 %	36.8 %
μ	0 %	66.5-133.7 %	24.8-36.7 %
FOM1	1	2.15-2.30	2.25-2.30

Table 11 Figure of merit (FOM1) of the ternary nitrate molten salt eutectic ($NaNO_3$-KNO_3-$Ca(NO_3)_2{\cdot}4(H_2O)$) and nanofluid with Al_2O_3 and MgO nanoparticle

%	Pure ternary salt	With Al_2O_3 1.32 %	With MgO 1.25 %
C_p	0 %	18.8 %	29.8 %
μ	0 %	160.8-274.0 %	24.9-33.2 %
FOM1	1	1.24-1.34	1.96-1.99

Measurement of Thermal Conductivity (k)

Experimental Setup

According to the literature [102], [103], the laser flash method was used to measure thermal conductivity, but it is only valid at the solid phase. According to the previous studies [104], [105], the transient hot wire method was used to measure thermal conductivity of the molten salt as well as its eutectic (e.g., $NaNO_3$, KNO_3, Li_2CO_3-K_2CO_3, and Li_2CO_3-Na_2CO_3). This hot wire method is usually used for the measurement of thermal conductivity of the molten salt eutectic. However, when the nanofluid (e.g., molten salt nanofluid) is tested with thermal conductivity using the hot wire method, there will be possible problem with the nanometer-sized particle in the molten salt eutectic during measurement. The nanometer-sized particle of the molten salt nanofluid may stick to the hot wire and it forms the nanometer-sized fin that is related to increased rate of heat transfer in the hot wire. In general, a fin can enlarge heat transfer surface to enhance the rate of heat transfer and it is impossible to measure its accurate thermal conductivity due to this extended heat transfer area. Moreover, due to the high operation temperature of molten salt, the customized apparatus was developed to characterize thermal conductivity. Therefore, the customized concentric cylinder was used for the measurement of thermal conductivity of the molten salt eutectic as well as its nanofluid. The concentric cylinder includes four holes in the inner cylinder and four holes in the outer cylinder for the temperature measurement with the k-type thermocouple as shown in figure 52. In another hole in the cylinder, the insulated heating wire (nichrome) was inserted in the center of the cylinder to release heat to the radial direction. To minimize the temperature variations between the inside and outside cylinder, two radiation shields (4130 alloy steel) were installed along the tangential direction due to the heater location of the laboratory furnace as shown in figure 53. To measure thermal conductivity using

the concentric cylinder type, convective heat transfer along the vertical direction is the most important factor during measurement and thus it requires a detailed analysis of heat transfer (e.g., heat loss).

Figure 52 Customized cylinder includes four holes in the inner cylinder and four holes in the outer cylinder for the temperature measurement

Figure 53 Customized cylinder in a laboratory furnace with two radiation shields

As shown in figure 54, it shows the schematic of the system of the k measurement of the molten salt eutectic and its nanofluid. The customized measurement system includes the DAQ (data acquisition) system, LabVIEW, DC power supply (Keysight E3644A), and thermocouples (k-type), and a laboratory furnace. As shown in figure 55, the DAQ system consists of several components (from National Instruments) such as the general purpose terminal block (SCXI-1322), the isothermal terminal block (SCXI-1303), the isolated sensor input multiplexer (SCXI-1122), the thermocouple amplifier (SCXI-1102), the 4-slot chassis (SCXI-1000), the bracket/adapter assembly (SCXI-1349), the multifunction input/output device (NI PCIe-6321), and the shielded cable (SHC68-68-EPM).

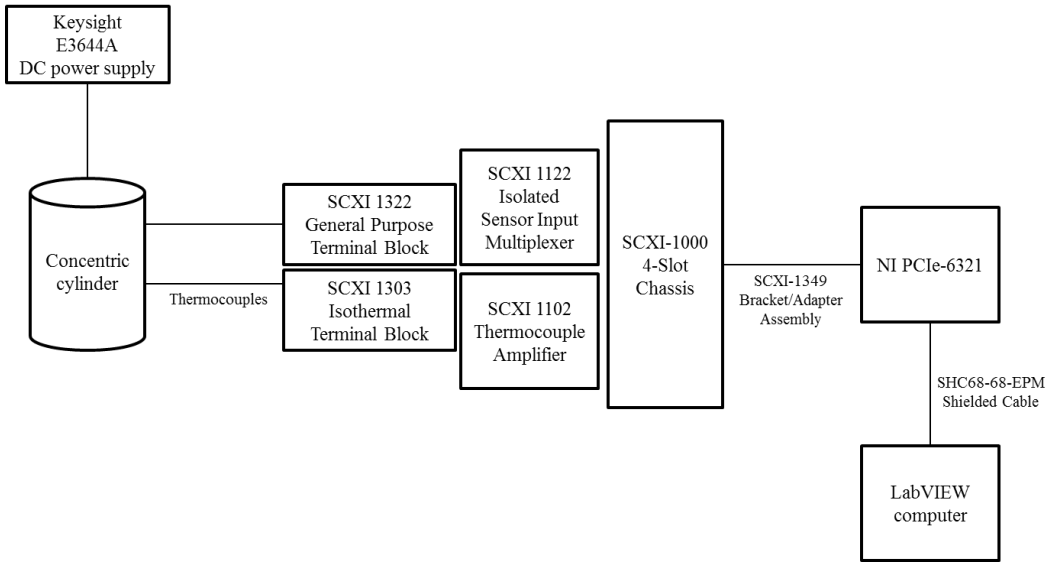

Figure 54 Schematic of the customized measurement system of thermal conductivity

As I mentioned earlier, all systems are customized and they have the number of possible error to measure thermal conductivity. Accurate measurement is the most important factor in measurement. Before the measurement of thermal conductivity, the calibration of the DAQ system was performed to optimize all systems that are related to

the data acquisition system. In other words, the system must be stable to measure accurate data. Calibrated DC power supply was used to improve the accuracy of the measurement. The calibration of each thermocouple (k-type) was performed to reduce errors. For the calibration of thermocouples, ice at 0 °C and hot water at 100 °C were prepared at the same time to measure the exact temperature of each state and then set the slope of temperature as shown in figure 56.

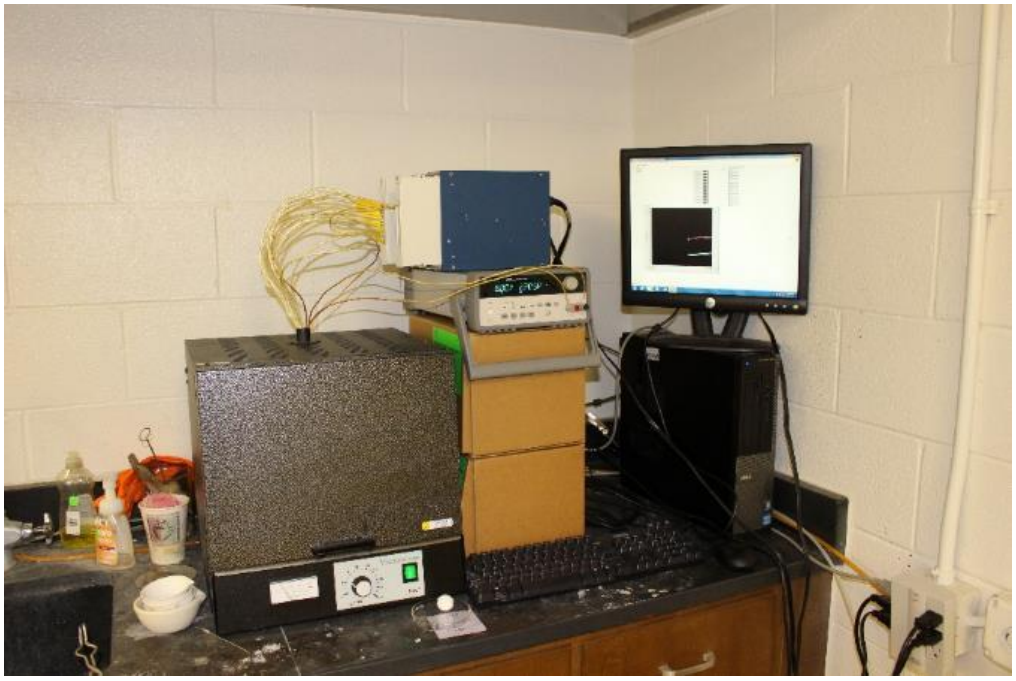

Figure 55 System of the measurement of thermal conductivity

Figure 56 Set-up of the calibration of each thermocouple with DAQ system

Measurement Results

According to the literature [106], thermal conductivity of the binary nitrate molten salt eutectic (e.g., solar salt: $NaNO_3$-KNO_3 with 60:40 weight ratio) shows 0.52 W/m °C at 300 °C. In this experimental set-up, the binary nitrate molten salt eutectic and its nanofluid with SiO_2 nanoparticle (10 nm) was used for the measurement of thermal conductivity at 300 °C. The amount of each sample was 14 g due to the size of the customized cylinder as well as density of each sample at specific temperature during measurement. Before the measurement, the preheating time for 4 hours was required to approach the steady state condition (isothermal condition) and it makes temperature of the cylinder to be homogeneous (300 °C). As shown equation 5, the equation was used to confirm that thermal conductivity of stainless steel affects thermal conductivity of each sample. Equation 5 includes thermal conductivity of stainless steel.

$$k_n = \frac{\ln\frac{r_3}{r_2}}{2\pi L(\frac{T_1 - T_2}{Q}) - \left(\frac{\ln\frac{r_2}{r_1} + \ln\frac{r_4}{r_3}}{k_s}\right)} \quad (5)$$

As shown in figure 57, 58 and 59, it shows the temperature difference of the binary nitrate molten salt eutectic at 300 °C. Four different thermocouples in the inner cylinder and another four in the outer cylinder were used to measure temperature at each point and temperature readings show a very small variation as shown in figure 57, 58, and 59. The temperature in the inner cylinder is higher than the temperature in the outer cylinder due to the heating wire in the center of the cylinder. As shown in table 12, it shows thermal conductivity of the binary nitrate molten salt eutectic at 300 °C. Thermal conductivity of the 1st sample is 0.63 W/m K, the 2nd sample shows 0.61 W/m K and the 3rd sample shows 0.59 W/m K. Thermal conductivity of three pure samples is higher than

the reference value and there is the possible reasons. According to the equation 5, Q (power) was used to release heat to the radial direction. As I mentioned earlier, the insulated heating wire was inserted in the center of the cylinder to release heat to the radial direction. However, heat was not transfer enough to the insulated heating wire due to the customized concentric cylinder. In other words, the length of the heating wire in the center of the cylinder was not enough to release heat uniformly to the radial direction to measure thermal conductivity.

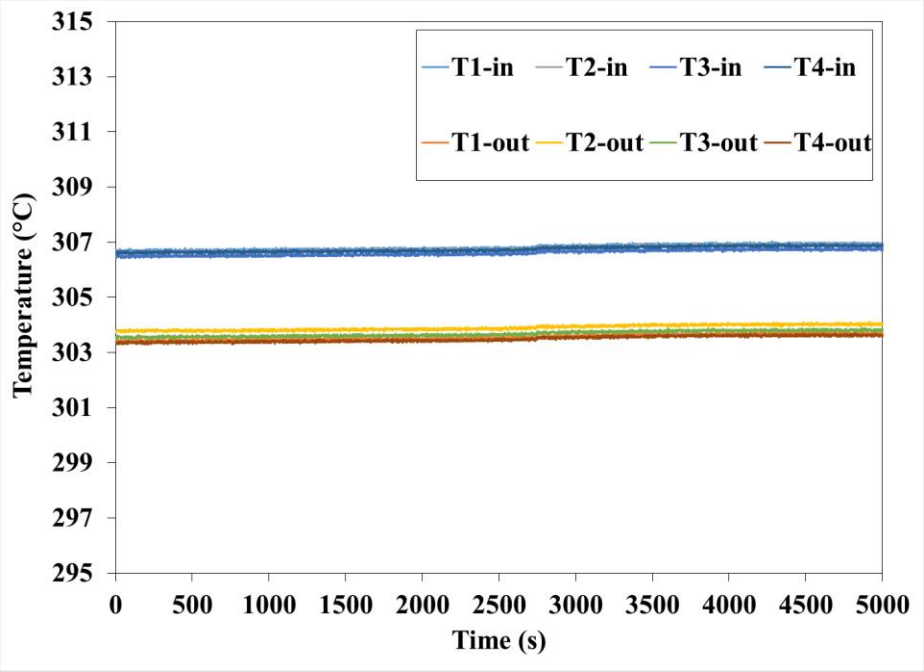

Figure 57 Temperature difference of the 1st sample of the binary nitrate molten salt eutectic ($NaNO_3$-KNO_3) at 300 °C

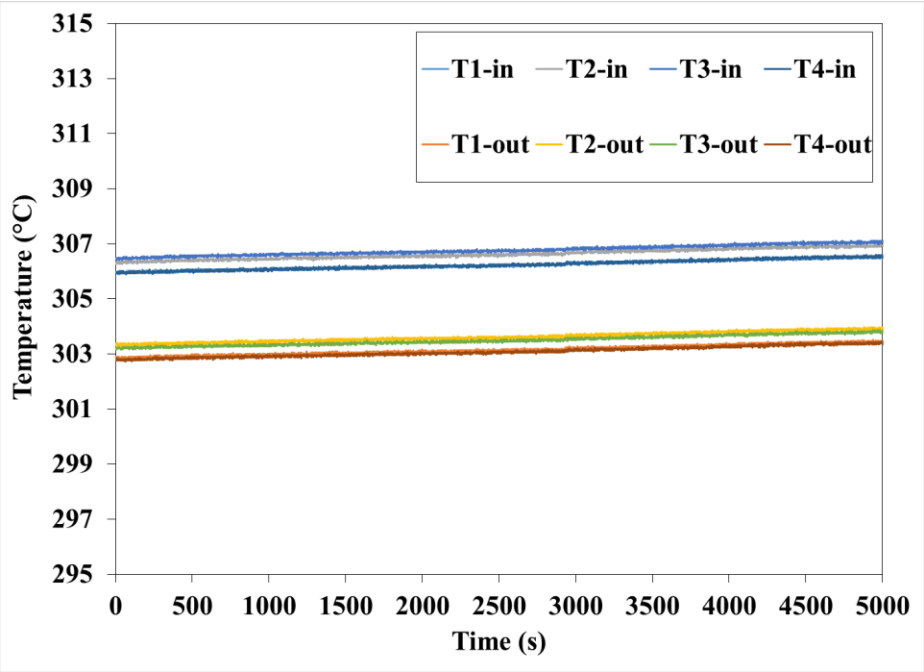

Figure 58 Temperature difference of the 2nd sample of the binary nitrate molten salt eutectic ($NaNO_3$-KNO_3) at 300 °C

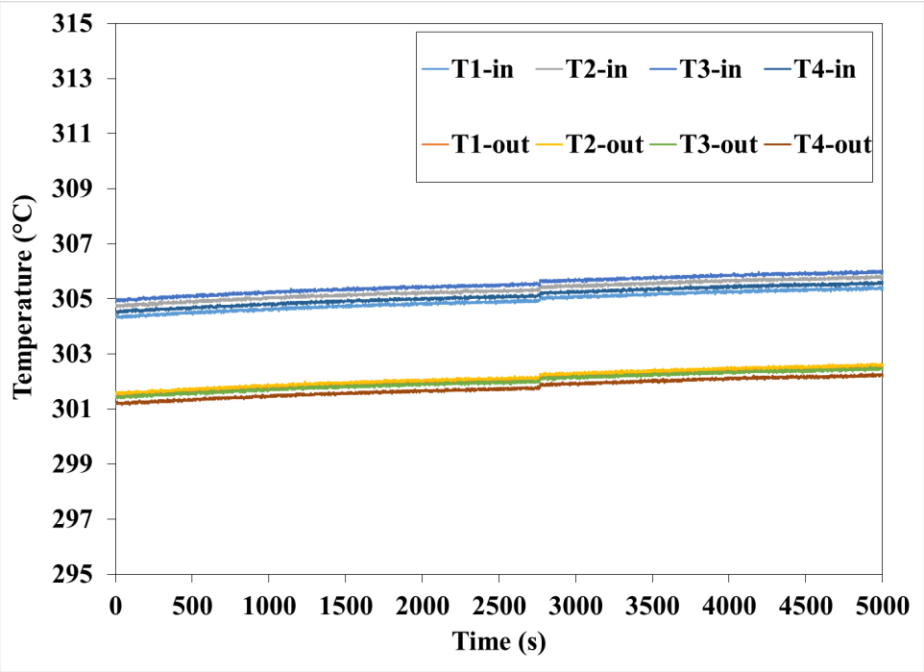

Figure 59 Temperature difference of the 3rd sample of the binary nitrate molten salt eutectic ($NaNO_3$-KNO_3) at 300 °C

Table 12 Summary of thermal conductivity of three samples of the binary nitrate molten salt eutectic at 300 °C (W/m °C)

Sample	k (W/m °C)	Ref. (W/m °C) [106]
#1	0.63	0.52
#2	0.61	
#3	0.59	
Average	0.61	-

As shown figure 60 and figure 61, it shows temperature difference of binary nitrate molten salt nanofluids at 300 °C respectively. In the inner cylinder and outer cylinder, they have four different thermocouples (k-type) to measure temperature at the different points during measurement. The temperature in the inner cylinder is higher than the temperature in the outer cylinder due to the heating wire in the center of the cylinder. Temperature readings show a very small variation and thus heat is uniformly distributed from the inner cylinder to outer cylinder during measurement. As shown in table 13, thermal conductivity of two nanofluid samples shows 0.75 W/m °C on average from equation 5. Thermal conductivity of this binary nitrate molten salt nanofluid with SiO_2 nanoparticle (10 nm size) were enhanced by 23 % on average compared to the binary molten salt eutectic.

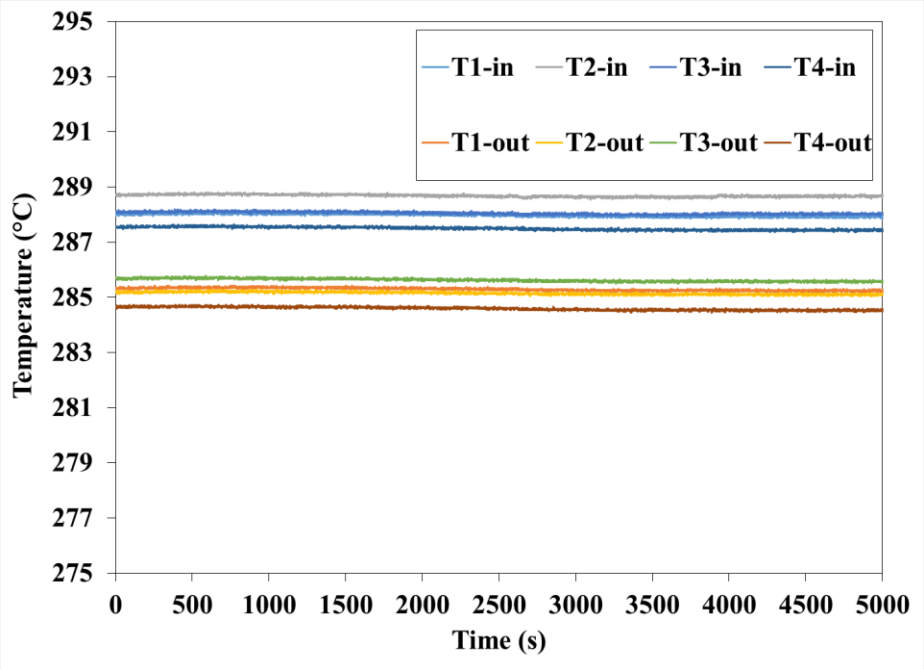

Figure 60 Temperature difference of the 1st sample of the binary nitrate molten salt nanofluid at 300 °C

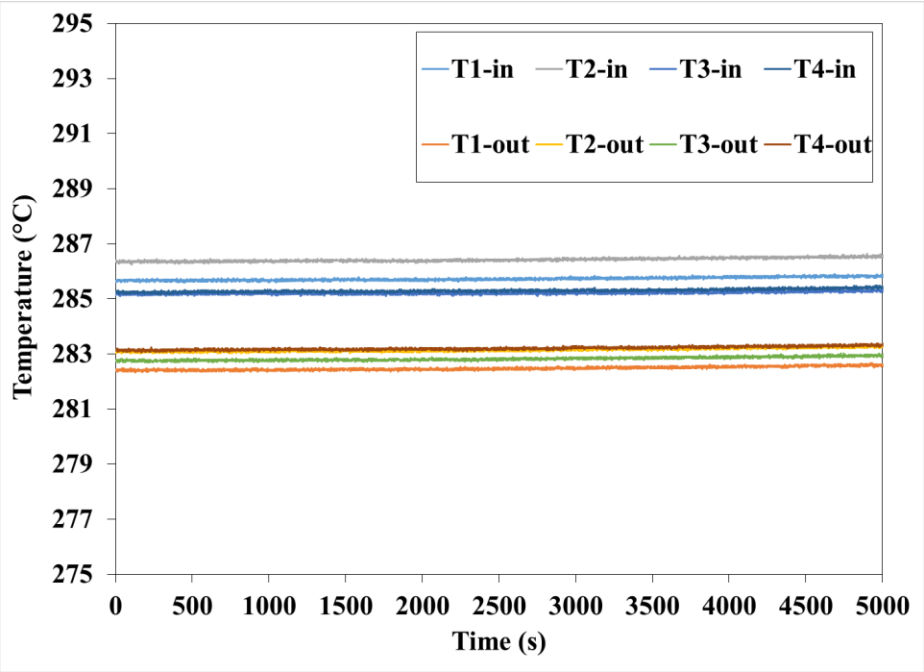

Figure 61 Temperature difference of the 2nd sample of the binary nitrate molten salt nanofluid at 300 °C

Table 13 Summary of thermal conductivity of two samples of the binary nitrate molten salt nanofluid at 300 °C (W/m °C)

Sample	k (W/m °C)	Pure (W/m °C)	Enhancement (%)	Ref. (W/m °C) [106]
#1	0.75	0.61	23 %	0.52
#2	0.75		23 %	
Average	0.75	-	23 %	-

Figure of Merit (FOM2)

According to the figure of merit (FOM1) for the storage fluid point [71], the required pumping power of different fluids is evaluated. This figure of merit analyzed performance of the system as thermal energy storage (e.g., storage fluid point). According to the figure of merit (FOM2) [49], performance of the system can be analyzed as heat transfer fluid (HTF). As I mentioned earlier, thermal energy storage (TES) system can reduce the cost of heat exchanger because it has the high thermal conductivity (e.g., high heat transfer capability). The density, specific heat, thermal conductivity, and viscosity of HTF are used to evaluate performance of the system as shown in equation 6. The density of the heat transfer fluid is constant in this case

$$\mathrm{FOM2} = \frac{\rho^{2.0} C_p{}^{1.6} k^{1.8}}{\mu^{1.4}} \qquad (6)$$

where ρ is density, C_p is the specific heat capacity, μ is viscosity, and k is thermal conductivity respectively.

Table 14 Figure of merit (FOM2) of the binary nitrate molten salt eutectic (NaNO3-KNO3) and its nanofluid with SiO_2 nanoparticle (10 nm)

%	Pure binary salt	With SiO_2 1.0 % (10 nm)
C_p	0 %	18 %
μ	0 %	24.8-36.7 %
k	0 %	23 %
FOM1	1	1.22-1.39

As shown in table 14, specific heat of the binary nitrate molten salt nanofluid ($NaNO_3$-KNO_3) with SiO_2 nanoparticle (10 nm) is enhanced by 18 %. The enhancement of viscosity of nanofluid with SiO_2 (10 nm) is 24.8-36.7 %. Thermal conductivity of nanofluid with SiO_2 (10 nm) is enhanced by 23 %. According to the figure of merit

(FOM2) as shown in equation 6, the performance of the binary molten salt eutectic ($NaNO_3$-KNO_3) with SiO_2 nanoparticle (10 nm) is enhanced by 22 %-29%.

Measurement of Validation

In this experimental set-up, the customized concentric cylinder was used to measure thermal conductivity of molten salt eutectic as well as its nanofluid. Because of the concentric cylinder, there is a gap to fill up a test sample (e.g., liquid phase) between the outer cylinder and inner cylinder. This gap is 0.3 cm and thus the thickness of the fluid layer is less than 0.3 cm. Convective heat transfer (e.g., heat loss) for the vertical direction is the important factor to measure accurate thermal conductivity data using the concentric cylinder. However, in the experimental tests, convective heat transfer for the vertical direction must be avoided because of liquid movement in the thickness of a gap between the outer and inner surface. According to previous research [107], there is the specific condition to consider convective heat transfer in the liquid movement with the concentric cylinder type. When GrPr > 1000, convection heat transfer is increased in the concentric cylinder. Gr is the Grashof number of the dimensionless parameter as shown in equation 7 and it is related to the ratio of the buoyancy to viscous force acting on a fluid. Pr is the Prandtl number and it is the dimensionless parameter as shown in equation 8 and it is related to the ratio of momentum diffusivity to thermal diffusivity.

$$\mathrm{Gr} = \frac{g\beta(T_s - T_\infty)L_c^3}{v^2} \qquad (7)$$

where g is gravitational acceleration, β (1/T) is coefficient of volume expansion, T_s is the temperature of the surface, T_∞ is the temperature of the fluid sufficiently far from the surface, L_c is the characteristic length of the geometry, and v (μ/ρ) is the kinematic viscosity of the fluid respectively.

$$\mathrm{Pr} = \frac{\mu C_p}{k} \qquad (8)$$

where μ is dynamic viscosity, C_p is specific heat, and k thermal conductivity respectively. From another previous study [108], the concentric cylinder type was used to measure

thermal conductivity and its thickness of the fluid layer between the outer cylinder and inner cylinder was 0.318 cm. It reported that the temperature difference between gaps was always less than 1 °C. In this case, GrPr ≤ 18 and there is not significant loss from convection arose between gaps (fluid layer). As I mentioned earlier, the thickness of the fluids layer of the customized concentric cylinder is 0.3 cm in this experimental set-up. GrPr (about 488) is definitely less than 1000 in the concentric cylinder in this measurement. Therefore, convective heat transfer for the vertical direction can be avoided to measure thermal conductivity using this the customized concentric cylinder type.

Material Characterization (SEM) Resutls

A scanning electron microscope (SEM: Hitachi S-3000N and S-5000H) was used for the material characterization of the molten salt nanofluid sample. The nanofluid sample with Al_2O_3 and MgO nanoparticle was tested in the MDSC to confirm the enhanced specific heat capacity before the material characterization (SEM). To confirm the fractal-like nanostructures in the binary nitrate molten salt eutectic after the thermal decomposition process, Al_2O_3 nanoparticle from the thermal decomposition process was used for the additive in the binary and ternary molten salt eutectic. As shown in figure 62, it shows SEM image of the fractal-like nanostructures of the binary nitrate molten salt eutectic ($NaNO_3$-KNO_3) with Al_2O_3 nanoparticle at 15000x magnification. As shown in figure 63, it shows SEM images of nanoparticles of the binary nitrate molten salt eutectic ($NaNO_3$-KNO_3) with Al_2O_3 nanoparticle at 1000x and 20000x magnification respectively. Nanometer-size particles were around salt mixtures and their size was relatively smaller than salt mixtures. The size of each nanometer-size particle was measured and they show approximately 60 nm-80 nm size particles.

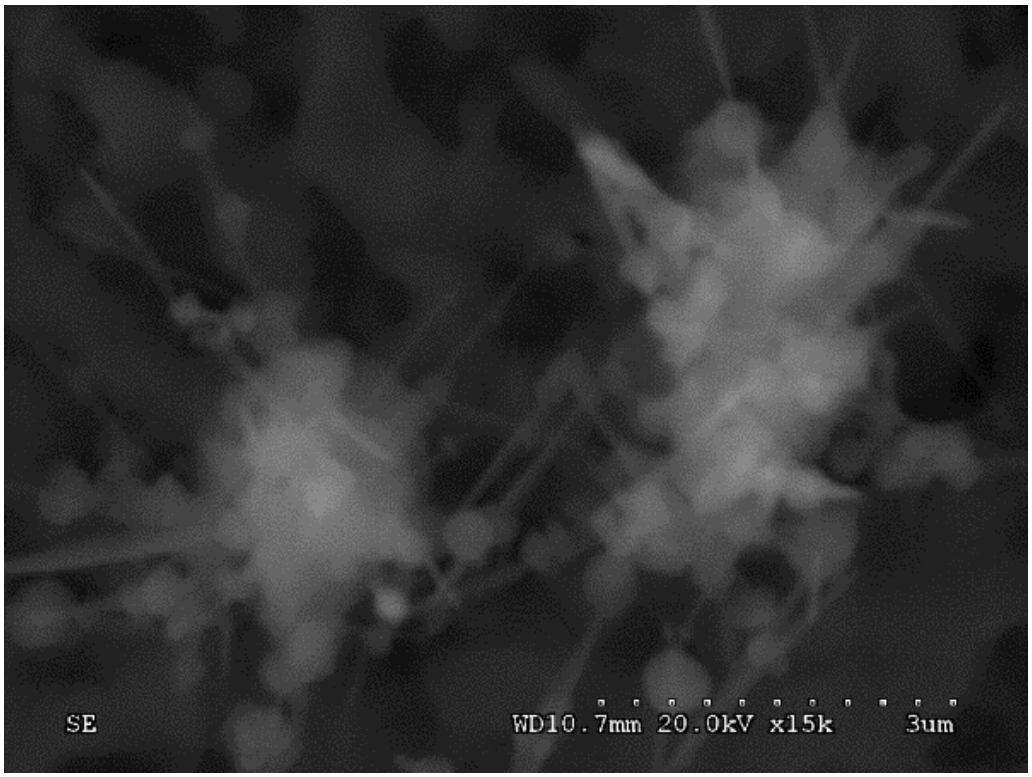

Figure 62 SEM image of the fractal-like nanostructures of the binary nitrate molten salt eutectic ($NaNO_3$-KNO_3) with Al_2O_3 nanoparticle at 15000x magnification

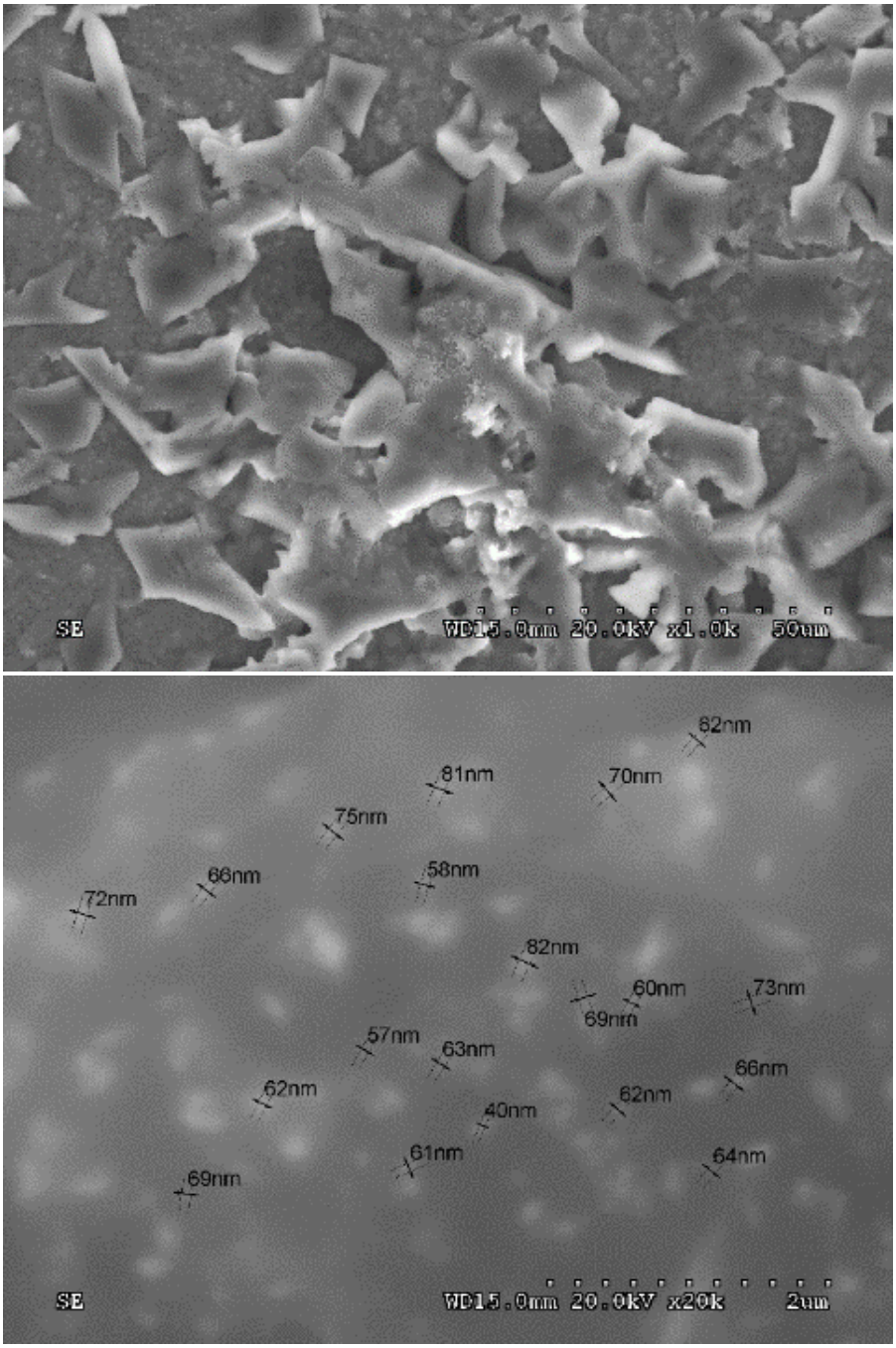

Figure 63 SEM images of nanoparticles of the binary nitrate molten salt eutectic ($NaNO_3$-KNO_3) with Al_2O_3 nanoparticle at 1000x (top) and 20000x (bottom) magnification

I investigated nanometer-size particles were in the ternary nitrate molten salt mixture ($NaNO_3$-KNO_3-$Ca(NO_3)_2 \cdot 4(H_2O)$ with Al_2O_3 nanoparticle. As shown in figure 64, it shows the SEM images of the ternary nitrate molten salt ($NaNO_3$-KNO_3-$Ca(NO_3)_2 \cdot 4(H_2O)$) and nanofluid with Al_2O_3 nanoparticle at x2000 and x10000 magnification respectively. A relatively small size of particle is of wide distribution around the salt compounds. As shown in figure 65, it shows the SEM images of nanoparticle (Al_2O_3) of the ternary nitrate molten salt eutectic ($NaNO_3$-KNO_3-$Ca(NO_3)_2 \cdot 4(H_2O)$) and nanofluid with Al_2O_3 nanoparticle at high magnification (100000x). Nanometer-size particles were around salt mixtures and their size was relatively smaller than salt mixtures. The size of each nanometer-size particle was measured and they show approximately 30 nm-60 nm size particles as shown in figure 65. Therefore, the thermal decomposition process with the molten salt eutectic is proved by the material characterization (SEM) and nanometer-size particle is verified by this SEM images as shown in figure 64 and 65.

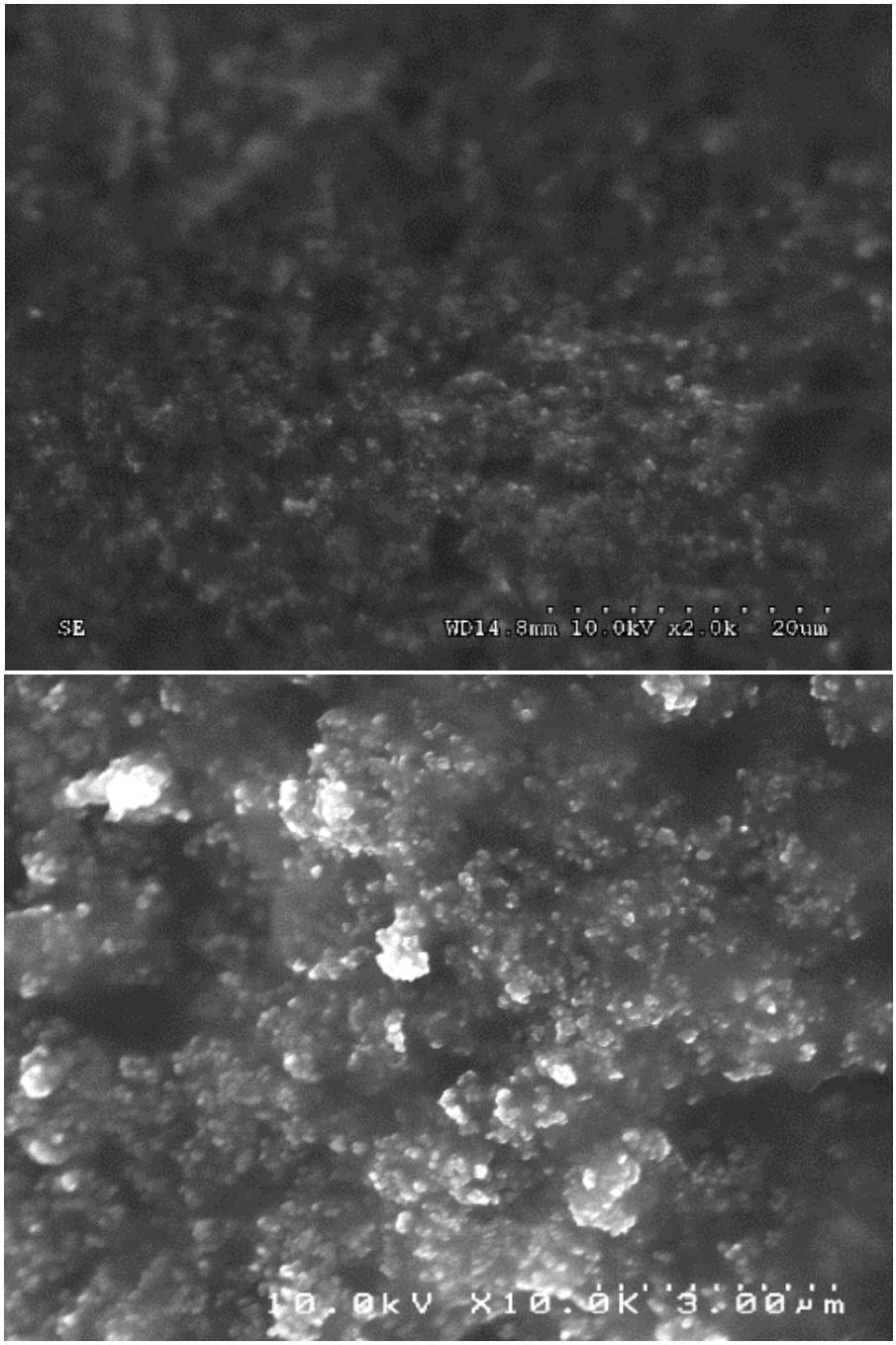

Figure 64 SEM image of the ternary nitrate molten salt eutectic ($NaNO_3$-KNO_3-$Ca(NO_3)_2{\cdot}4(H_2O)$) and nanofluid with Al_2O_3 nanoparticle at 2000x (top) and 10000x (bottom) magnification

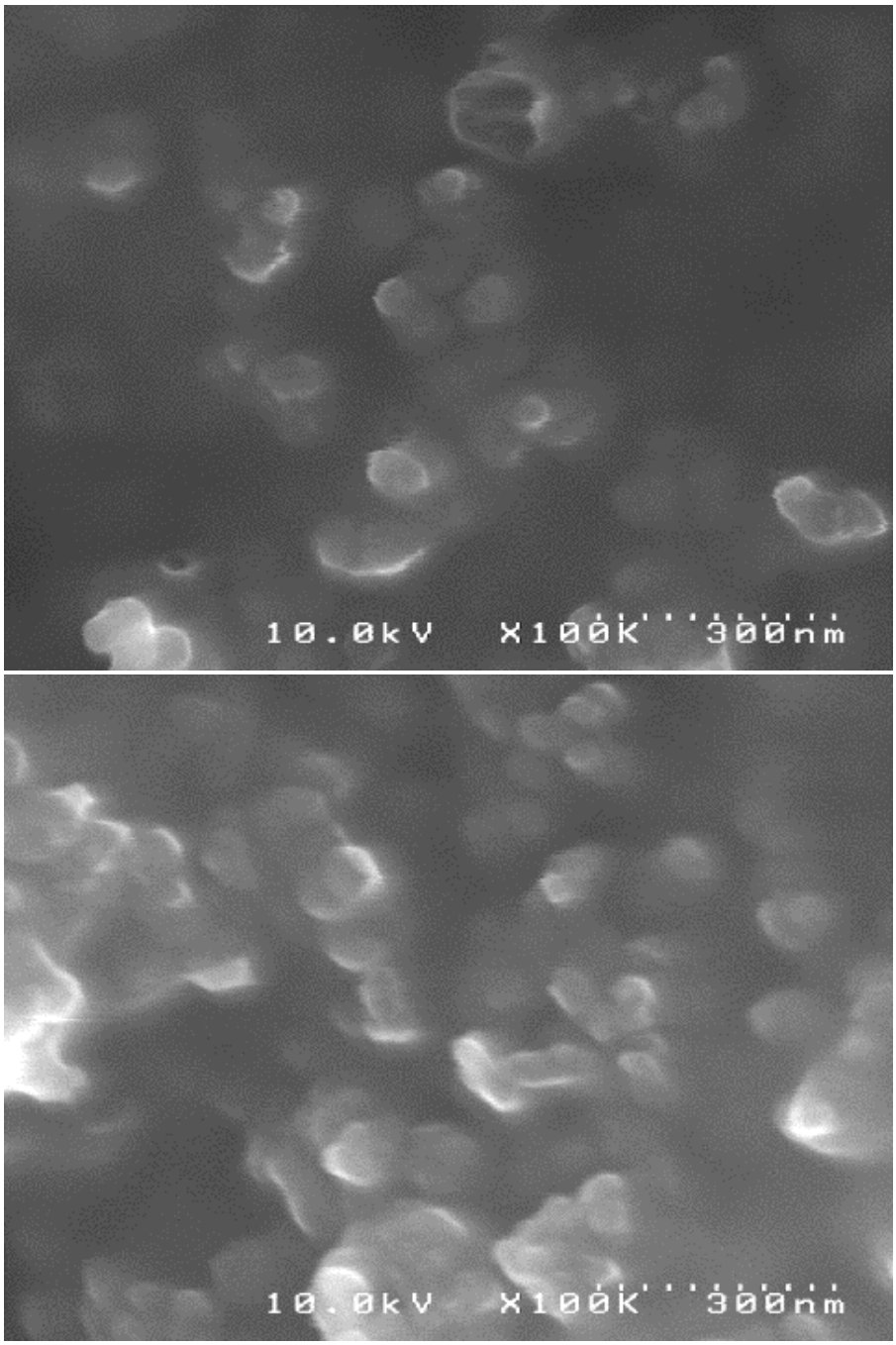

Figure 65 SEM images of nanoparticles of the ternary nitrate molten salt eutectic ($NaNO_3$-KNO_3-$Ca(NO_3)_2 \cdot 4(H_2O)$) and nanofluid with Al_2O_3 nanoparticle at 100000x magnification

Chapter 5

New Method (Molten Mixing Method) for Sample Preparation

In general, the well-mixed nanofluid may show high enhancement of specific heat due to improved dispersion of nanoparticles. There are different methods (e.g., mixing process) to make homogenous molten salt eutectic as well as its nanofluid. According to the literature [20], [21], dry mixing (e.g., without any solutions) was used to mix ternary nitrate salt with SiO_2 nanoparticle. After mixing, temperature was increased over its melting point with the heat source (hot plate) to make sure the liquid state and melt completely. The mixture was remained as solid state. However, it expects the poor nanoparticle dispersion in it nanofluid. According to the previous study [23], the solution method with distilled water was used to mix each chemical (nitrate-based salt) with SiO_2 nanoparticle. To mix carbonate-based salts with SiO_2 nanoparticle, distilled water was also used as the solution [19]. The ultra sonicator was used to disperse each chemical in the solution. The liquid mixture was evaporated at the heat source (hot plate). The mixture was remained as solid state. However, nanoparticles are likely to agglomerate during the evaporation of liquid (distilled water). Another new method is required for further increasing specific heat of them. Moreover, there is another important factor during the sample preparation procedure to enhance specific heat of the molten salt eutectic with the nanoparticle. According to the literature [19]-[21], each sample was put on the heat source (hot plate) at the specific temperature to prevent the effect of moisture to each chemical as well as a mixture before measurement. In other words, the mixture or each chemical which has absorbed moisture may show different chemical properties (e.g., melting point, composition, decomposition, and phase) compared to the pure chemical. During the evaporation of liquid, nanoparticles are likely to agglomerate due to the different solubility of each chemical (e.g., salt and SiO_2 nanoparticle) in nanofluid. In

general, nitrate-based salts, carbonate-based salts, and nanoparticle (e.g., SiO_2) show totally different solubility depending on the different temperature ranges. It has a decisive effect on the enhancement of its specific heat. Therefore, the new method (e.g., molten mixing method) is proposed to find optimized procedure of the sample preparation for further increasing specific heat of the molten salt nanofluid with nanoparticles (e.g, SiO_2).

Measurement of Specific Heat Capacity (C_p)

Sample Preparation

The binary molten salt eutectic and its nanofluid with SiO_2 nanoparticle (10 nm) was prepared to measure its specific heat. Before the mixing process, each single chemical ($NaNO_3$, KNO_3, and SiO_2 nanoparticle) was put on the hot plate at 100 °C for 5 minutes to prevent the effect of moisture to chemicals. When the preheating temperature is set up, the melting point of each chemical must be considered. After 5 minutes, each chemical is mixed together in the same glass vial and pour distilled water (10 ml) into a vial. Each chemical's solubility was considered before use distilled water. According to the literature [109], the specific amount of water is required to dissolve SiO_2 nanoparticle and this solubility is varied at different temperature of water. In this case, 10 ml of distilled water is required to dissolve 2 mg of SiO_2 nanoparticle at 60 °C**.** The ultra sonicator was used at 60 °C for 30 minutes to disperse each chemical, especially SiO_2 nanoparticle, into distilled water and it makes homogenous molten salt nanofluid. The laboratory furnace was used at 200 °C for 2 hours to evaporate distilled water and it makes completed dry sample. In other words, the effect of moisture to mixed molten salt was reduced during this evaporation process. The sample in liquid state was prepared to drop the sample into the pan in the laboratory furnace as shown in figure 66. According to the literature [19]-[21], [23], the phase of the molten salt must be changed from liquid to solid state during the loading process due to high melting point of the molten salt eutectic. However, in this case, the loading process from liquid state to solid state was removed by this molten mixing method and it can prevent possible errors (e.g., the effect of moisture and different final composition of the mixture) due to different phases during the sample preparation as well as different solubility during the evaporation of liquid.

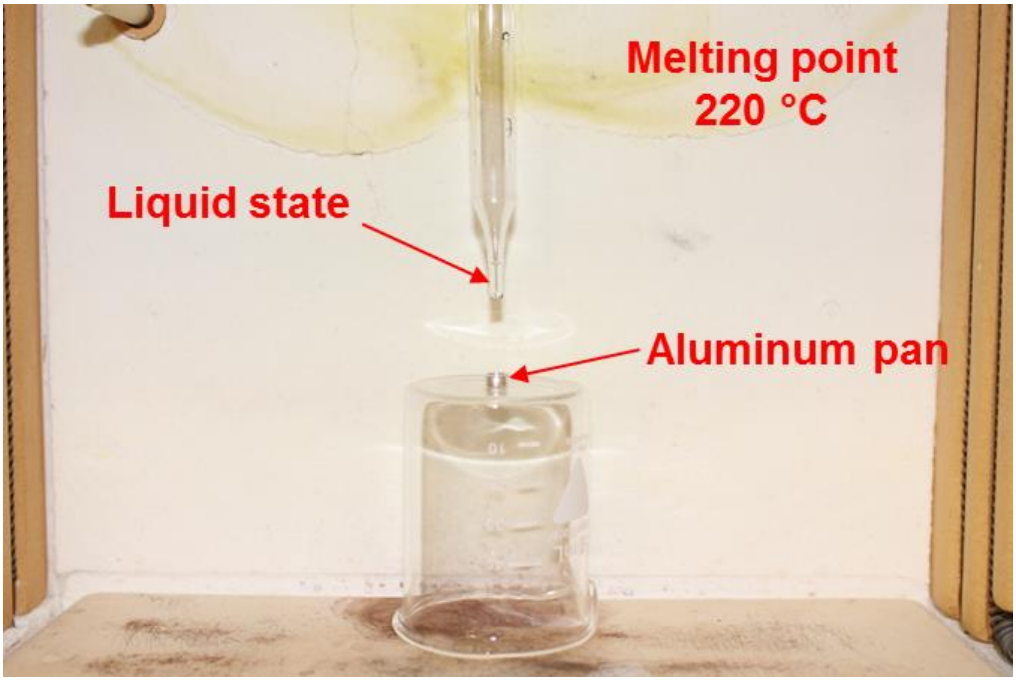

Figure 66 Molten mixing method (liquid to liquid) to drop the sample into the pan

Experimental Setup

As shown in figure 67, a modulated differential scanning calorimeter (MDSC; Q20, TA Instrument Inc.) was used to measure specific heat of the binary molten salt and its nanofluid at high temperature. There will be the possible errors (e.g., opened lid inside the MDSC) during measurement. Each sample was hermetically sealed in a Tzero hermetic pan and lid (TA Instruments Inc.) to prevent the loss of the amount of the sample during measurement at high temperature as shown in figure 68. For the protocol of measurement, temperature was increased up to 400 °C to melt a sample completely and it went back to 200 °C. The temperature range was from 200 °C to 300 °C to measure specific heat of the sample.

Figure 67 Modulated differential scanning calorimeter (MDSC; Q20, TA Instruments Inc.)

Figure 68 Tzero hermetic pan and lid (TA Instruments Inc.)

Measurement Results

According to the literature [57], [110], specific heat of the binary molten salt eutectic (e.g., $NaNO_3$-KNO_3) was reported different values from different researchers. It was from 1.45 kJ/kg °C to 1.55 kJ/kg °C at different temperature ranges. The dry mixing method was used to compare the new method (e.g., liquid to liquid) and specific heat of them was measured by MDSC. As shown in table 15, specific heat of the molten salt nanofluid with SiO_2 nanoparticle (e.g., 10 nm) shows 1.61 kJ/kg °C on average. Four different samples were used to measure specific heat of them and it shows only 2 % enhancement compared to its pure eutectic. According to the previous study [23], the solution method with distilled water was used for the sample preparation, but the loading process (e.g., liquid to solid) was used to move the amount of the sample into a pan. 10 nm of SiO_2 nanoparticle was used to make the molten salt nanofluid and its specific heat was measured by MDSC as shown in table 15. Five different samples were prepared and measured by MDSC and it shows 1.62 kJ/kg °C on average as well as 10 % enhancement. Twenty three sample were prepared by the solution method with distilled water. Each sample was dropped by liquid to liquid method into a pan to measure its specific heat. As shown in table 15, specific heat of those samples shows 1.88 kJ/kg °C on average and it has 18 % enhancement compared to the binary molten salt eutectic. The new method (e.g., liquid to liquid) shows the highest enhancement of specific heat compared to other methods. According to this new method, to further increasing specific heat, the preheating of each chemical is required to prevent the effect of moisture. Distilled water is needed as solution to mix each chemical and the sonication process is required to make homogenous sample. To drop the sample into a pan, the same phase (e.g., liquid state) of the sample is required to prevent the effect of moisture to mixed

sample. Therefore, the new method optimized procedure of the sample preparation for further increasing specific heat of the molten salt nanofluid with nanoparticles (SiO_2).

Table 15 Comparison of specific heat of the binary molten salt eutectic and its nanofluid in three different methods for the sample preparation

Method	C_p on average (kJ/kg °C)			Enhancement
	Nanofluid (SiO_2-10nm)	Pure eutectic	Ref [57], [110]	
Dry mixing	1.61	1.58	1.45-1.55	2 %
Solution [23]	1.62	1.47		10 %
Solution with Liquid to Liquid	1.88	1.60		18 %

Chapter 6

Computational Approach: Molecular Dynamics (MD) simulation

Basic Concept of Molecular Dynamics (MD) Simulation

According to the literature [111], [112], the periodic boundary condition was used for the simulation as shown in figure 69. In general, the whole system is required to calculate each property in the simulation, but it requires huge computational cost and time. To minimize possible errors of the simulation, divided small simulation box is required, but atoms interact at the edge of the discrete system. In other words, incorrect the formation of each molecule may have an effect on the accuracy of the calculation. Therefore, the periodic boundary condition is required to avoid this negative effect in the system as shown in figure 69. For the bonded interaction (e.g., intramolecular interaction), different types of bonded interactions were considered for all simulation system as shown in figure 60 [111], [112]. For example, bond-bond, angle-angle, bond-angle, end-bond-torsion, middle-bond-torsion, angle-torsion, and angle-angle-torsion intramolecular interactions were used to calculate the value of each property between atoms in the simulation. According to the previous studies [111], [112], the intermolecular interaction (e.g., Leonard-Jones potential) is considered to compute the value of each property between two atoms (molecules) for all simulation systems. To reduce computational cost and time, the cut off radius is used between two atoms which are separated by large distances as shown in figure 70.

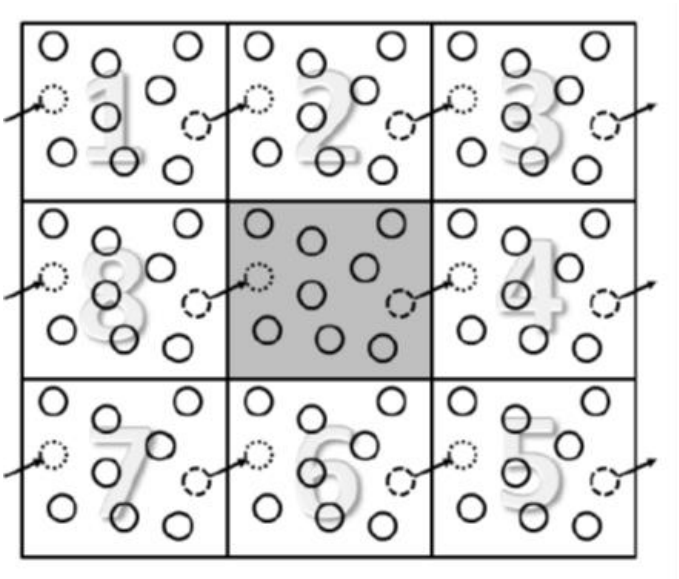

Figure 69 Periodic boundary condition [111], [112]

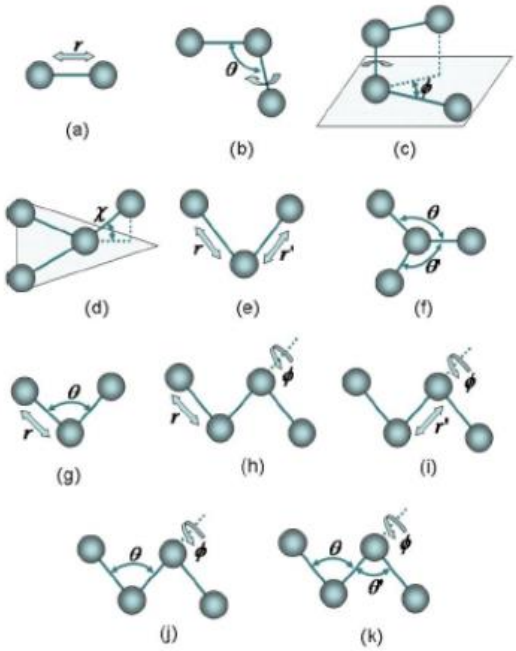

Figure 70 different types of bonded interactions (intramolecular interaction) between atoms [111], [112]

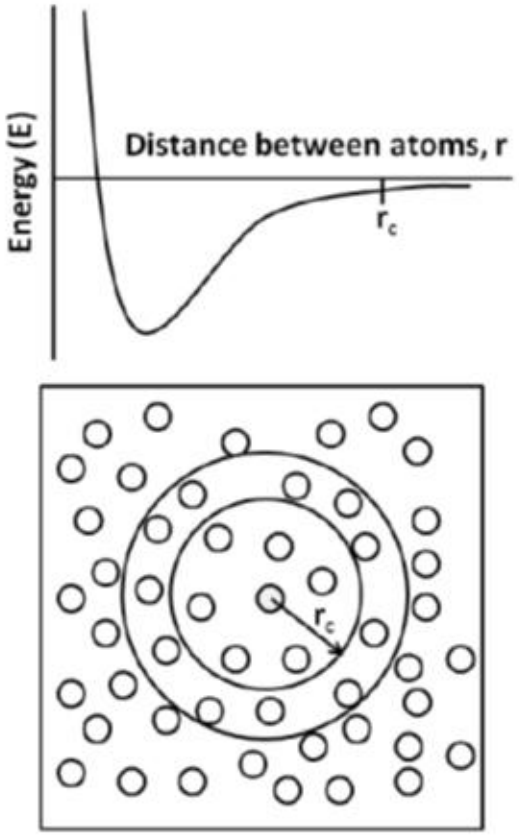

Figure 71 Non-bonded interactions (intermolecular interaction) between atoms [111], [112]

Procedure to Calculate Thermophysical Properties in Molecular Dynamics (MD) Simulation

Here is the procedure (flow chart) explain how to compute thermophysical properties in Molecular Dynamics (MD) simulation as shown in figure 72. The simulation domain box is required to set up the initial step before the actual computation starts. The size of the simulation domain box is varied depending on the size of the system (e.g., the number of atoms). It means that total number of atoms or molecules is varied according to the size of the simulation domain box. The computation time and cost depend on the size of the each simulation domain box. After the simulation domain box is set up, the minimization step is required to reduce energy in the system because each atom (e.g., molecules) is set up by intention. In other words, the total energy level of the initial step after all atoms are set up is higher than the actual system. The next step is the equilibration of the system as the micro-canonical ensemble (NVE). The NVE step means that the number of atoms, volume, and energy of the system are constant, but the system's temperature changes. In other words, The NVE step is not the actual condition for the simulation, but it is required to confirm that the system (e.g., the simulation domain box) is stable or not. When its temperature increased gradually, the density of the system can be calculated under this condition (NVE). After checking the stable system, the next step is to bring the system to base temperature running equilibration as the isothermal-isobaric ensemble (NPT). The NPT means that the number of atoms, pressure, and temperature of the system are constant, but the system's volume changes. In other words, the density of the system is varied depending on its temperature in the NPT condition and it is under the actual condition for the simulation. The calculation of density is calculated by the NPT condition. The next step is to raise the temperature of the system to a desired value by velocity (temperature) scaling and the value of temperature,

density, and total energy could be determined. If the temperature, density, and total energy have converged, the computational step must be terminated. If each value does not converge, the previous step (e.g., minimization, equilibration as the NVE or NPT) is required to compute again. To calculate specific heat, the total energy (e.g., potential energy and kinetic energy) was computed at different temperature and then it created the slope to calculate specific heat of the pure eutectic as well as its nanofluids [113].

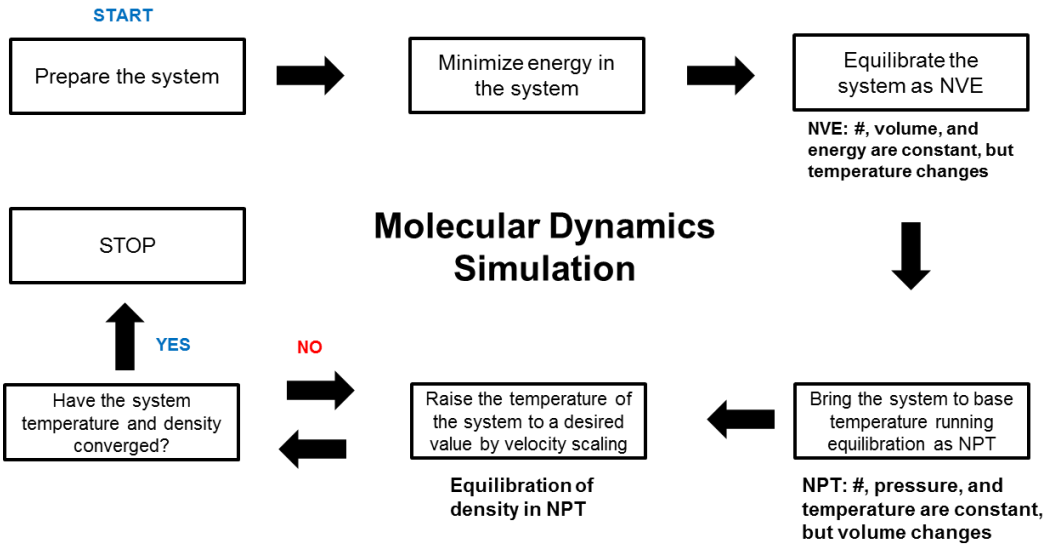

Figure 72 Flow chart of Molecular Dynamics (MD) simulation

Simulation Setup

Lennard-Jones (LJ) Potential

In this simulation study, LAMMPS (Large-scale Atomic/Molecular Massively Parallel Simulator) by Sandia National Laboratory was used to compute the thermophysical properties (e.g., density and specific heat capacity) of the binary molten salt eutectic ($NaNO_3$-KNO_3) and its nanofluid. The Buckingham potential with the long-range Coulombic interactions was used for the simulation of a molten salt nanofluid from the previous research [72], [73]. However, the Lennard-Jones (LJ) potential is mainly used for a simulation of the molten salt system due to lower computational costs [113] and it makes all systems stable during long computational steps. According to the previous research [114], the Lennard-Jones (LJ) potential was used to calculate the intermolecular atomic motion between two non-bonded atoms in the the binary molten salt ($NaNO_3$-KNO_3). The long-range Coulombic force was also used to compute the intramolecular atomic motion in all simulations and thus the Lennard-Jones (LJ) potential with long-range Coulombic force was used to compute density and specific heat of the binary molten salt and it nanofluid as shown in equation 9.

$$\mathrm{E} = \frac{\mathrm{C q_i q_j}}{\mathrm{r}} + 4\varepsilon\left[\left(\frac{\sigma}{\mathrm{r}}\right)^{12} - \left(\frac{\sigma}{\mathrm{r}}\right)^{6}\right] \qquad (9)$$

where E is the potential energy between two atoms, C is an energy conversion constant, q is the charge of two atoms (i and j), r is the distance between two atoms, ε is the depth of the potential well, and σ is the finite distance when the inter-particle potential is zero. For the long-range Coulombic interactions, a standard Ewald summation was used in the simulation system and it was with an accuracy of 10^{-4} [115]. This setup of the long-range Coulombic interactions was unlike the particle-particle particle-mesh (PPPM) in the literature [72]. The computational time step was 0.5fs for each step to obtain the stable value in all systems and the Polak-Ribiere version of the conjugate gradient (CG) was

used for a minimization algorithm in all simulation systems [116]. The Berthlot mixing rule was used between different atoms to calculate the interatomic parameter of the Lennard-Jones (LJ) potential [117]. For the intramolecular atomic motion (e.g., bonded interaction), bond potential force (harmonic style), angle potential force (harmonic style), and torsional potential force (cvff style) were used for all simulation systems. Each simulation was performed in a system trajectory consistent with the micro-canonical ensemble (NVE) and time integration on Nose-Hoover style non-Hamiltonian equations of motion are designed to generate the isothermal-isobaric ensemble (NPT) [115]. Intermolecular and intramolecular parameters of the Lennard-Jones (LJ) potential were used to compute between different atoms during all simulation steps. To calculate specific heat of the molten salt eutectic and its nanofluid, the total energy (potential energy and kinetic energy) was computed at the different temperature range between 250 °C (523 K) and 420 °C (693 K). After that, it created the slope (total energy vs. temperature) to calculate specific heat of the pure eutectic as well as its nanofluid. To compute the number of atoms (molecules) of the MD simulation system, the massive supercomputing power and high speed supercomputer systems are required to reduce the huge computational cost and time. There are two supercomputing systems to calculate thermophyscial properties (e.g., density and specific heat) of the molten salt eutectic and its nanofluid. Texas Advanced Computing Center (TACC) was used to compute each simulation and this computing system consists of a 6,400+ node cluster of Dell PowerEdge server nodes featuring Intel Xeon E5 Sandy Bridge host processors and the Intel Knights Corner (KNC) coprocessor. The High Performance Computing (HPC) at the University of Texas at Arlington was also used to calculate each simulation step in the different simulation systems and it consists of computational nodes utilize Intel Xeon processors with Red Hat Enterprise Linux as an operating environment.

Design of Different Simulation Domains (Different Mass Fraction)

The different simulation domain boxes were built for this simulation study using Material Studio (version 4.4, BIOVIA, San Diego, CA). Here is the step to build the different simulation domains in Material Studio. The size of the simulation box is setup and then the number of atom (molecules) of each mixture (e.g., $NaNO_3$, KNO_3, and $NaNO_3$ nanostructure rod) are built in the simulation domain box. After the computation is over, the visualization step is required to look at the position of each atom (molecule) or the formation of the each structure that are stable or not. The OVITO (The Open Visualization Tool) program was used to visualize each simulation domain with $NaNO_3$ nanostructure rods in the simulation [118]. First, the total 995 atoms (Na: 133, K: 66, N: 199, and O: 597 atoms) were built for the binary molten salt eutectic (e.g., $NaNO_3$-KNO_3=60:40 by weight ratio) to compute its thermophysical properties (e.g., density and specific heat) as shown in figure 73. The size of the box of the simulation domain is 27.5 Å x 27.5 Å x 27.5 Å (2.75 nm x 2.75 nm x 2.75 nm) for each simulation. For the binary molten salt nanofluid, the different size and shape of nanostructures ($NaNO_3$ rod) were used to verify the effect of the surface atoms on enhanced specific heat over the interior atoms in the nanostructure ($NaNO_3$ rod). In other words, each $NaNO_3$ nanostructure rod was inserted in the same binary molten salt eutectic with 995 atoms. Because of the huge computational cost and time in the simulation, nanostrucutres' size and shape are not same as the nanostructure at the actual experimental conditions. It means that the periodic boundary condition (simulation domain box) was used for the simulation. However, the results of each computation is reasonable to understand between the effect of the surface atoms and interior atoms as well as its enhanced specific heat of nanostructure in the molten salt nanofluid. As shown in figure 74-77, one, two, three, and four $NaNO_3$ nanostructure rods (same shape) were inserted into the binary molten salt

eutectic (e.g., pure system: 995 atoms) to confirm the effect of the surface on enhanced specific heat in the nanostructure. The mass fraction of the one single $NaNO_3$ nanostructure (Na: 7, N: 7, and O: 21 atoms) is 3.2 % and this single nanostructure rod was used to increase the number of rods (one, two, three, and four rods) at the different simulation domain box as shown in figure 74-77. As I mentioned earlier, although different number of the $NaNO_3$ nanostructure rod was used, the size and shape of this single $NaNO_3$ nanostructure rod is the same for each simulation domain box. Each mass fraction of the total nanostructure rod is gradually increase with a number of the single $NaNO_3$ nanostructure rod such as 3.2 % (Na: 7, N: 7, and O: 21 atoms), two $NaNO_3$ nanostructure rods with 6.2 % (Na: 14, N: 14, and O: 42 atoms), three $NaNO_3$ nanostructure rods with 9.0 % (Na: 21, N: 21, and O: 63 atoms), and four $NaNO_3$ nanostructure rods with 11.7 % (Na: 28, N: 28, and O: 84 atoms) respectively as shown in figure 73-76 (top view and front view of the simulation domain box were given). According to the table 16, the surface area of the $NaNO_3$ nanostructure rod when the number of the rod is increased. The surface area of the one single $NaNO_3$ nanostructure rod (3.2 %) is 1.48 nm^2. Two $NaNO_3$ nanostructure rod (6.2 %) is 2.96 nm^2, three $NaNO_3$ nanostructure rod (9.0 %) is 4.44 nm^2, and four $NaNO_3$ nanostructure rod (11.7 %) is 5.92 nm^2 respectively. As shown in figure 78, the SiO_2 nanoparticle was inserted into the binary molten salt eutectic to confirm the effect of the surface energy between the binary molten salt eutectic and nanoparticle. The one single SiO_2 nanoparticle (Si: 6 and O: 12 atoms) was used in the binary molten salt eutectic and it total mass fraction is 2.0 %.

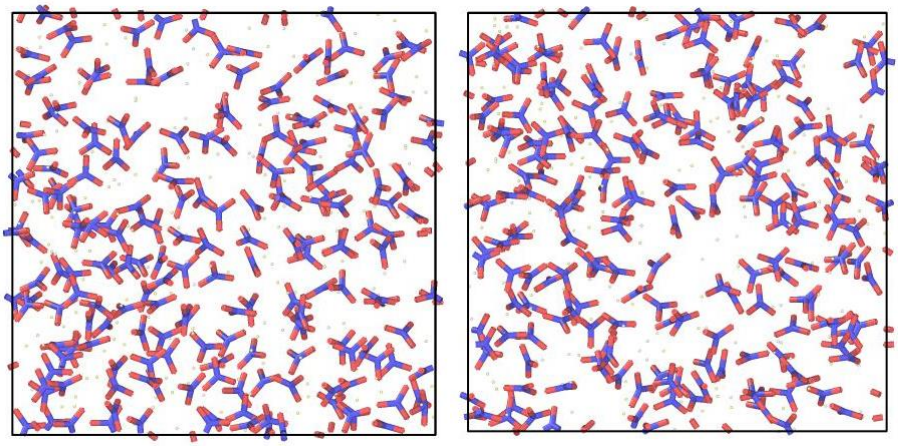

Figure 73 Simulation domain of the binary molten salt eutectic: $NaNO_3$ and KNO_3 (top view-left and front view-right)

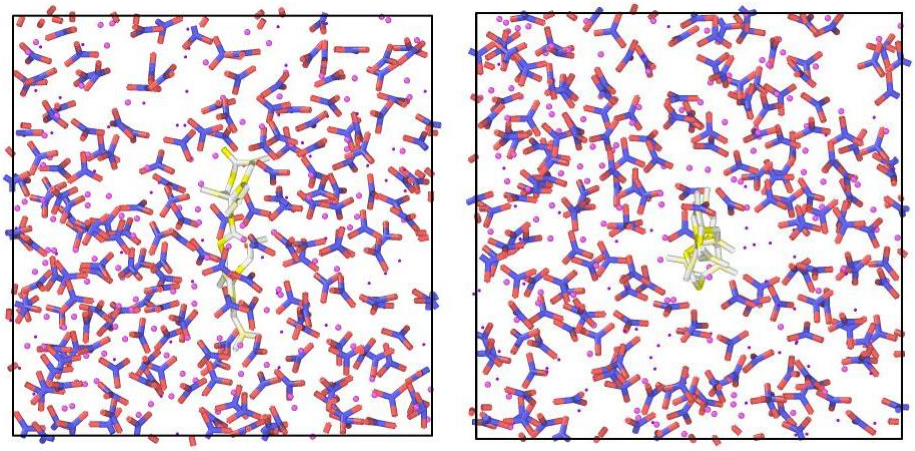

Figure 74 Simulation domain of the binary molten salt nanofluid mixed with one $NaNO_3$ rods: 3.2 % (top view-left and front view-right)

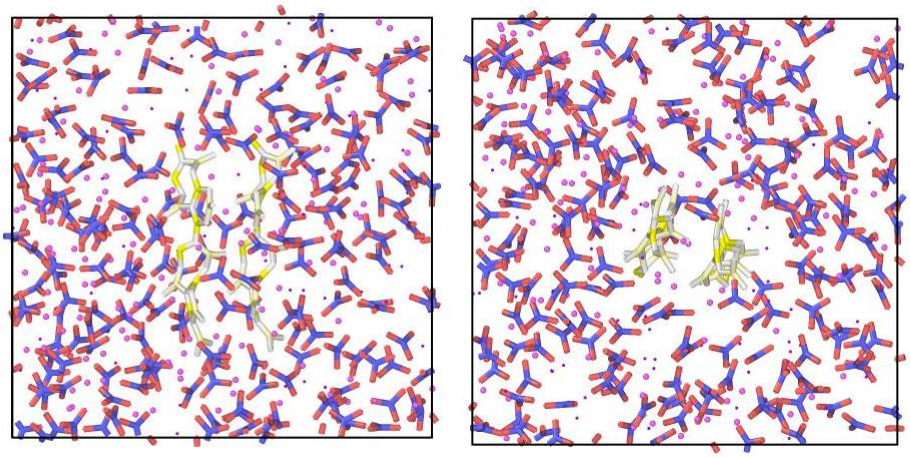

Figure 75 Simulation domain of the binary molten salt nanofluid mixed with two $NaNO_3$ rods: 6.2 % (top view-left and front view-right)

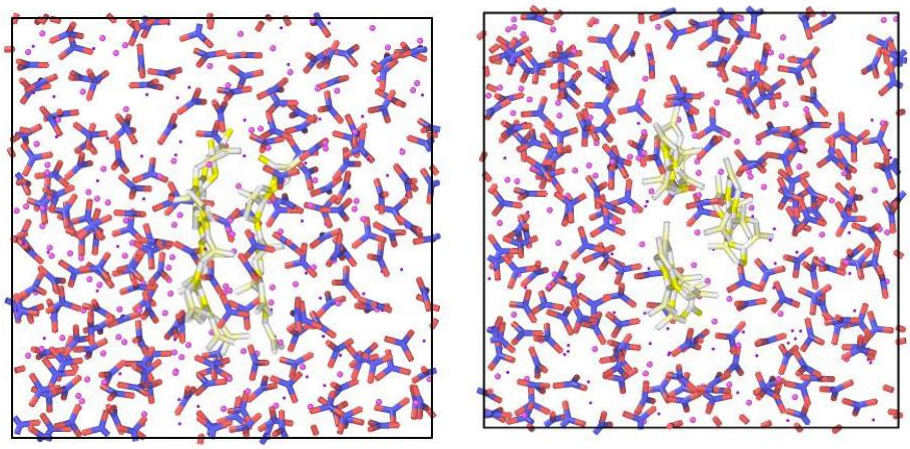

Figure 76 Simulation domain of the binary molten salt nanofluid mixed with three $NaNO_3$ rods with: 9.0 % (top view-left and front view-right)

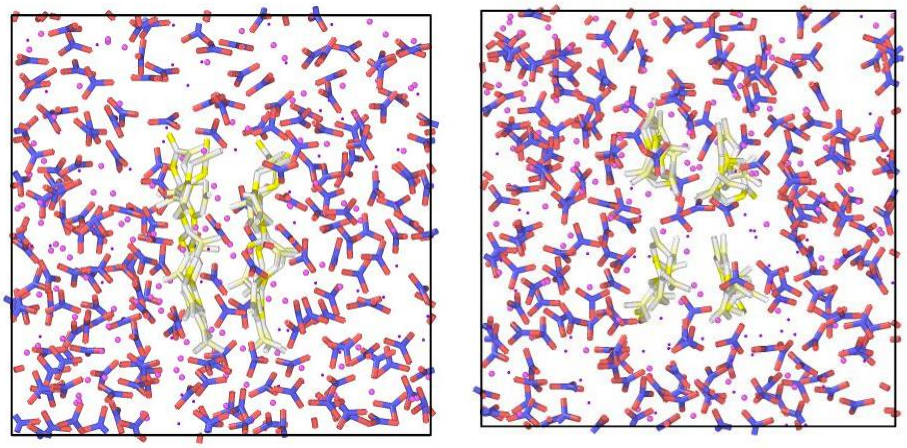

Figure 77 Simulation domain of the binary molten salt nanofluid mixed with four $NaNO_3$ rods: 11.7 % (top view-left and front view-right)

Table 16 Surface area of $NaNO_3$ nanostructure rod (3.2 %)

Rod	Mass fraction (%)	Surface area (nm^2)	One $NaNO_3$ rod (3.2 %)	
			Diameter (nm)	Length (nm)
One $NaNO_3$ rod	3.2	1.48	0.30	1.57
Two $NaNO_3$ rods	6.2	2.96		
Three $NaNO_3$ rods	9.0	4.44		
Four $NaNO_3$ rods	11.7	5.92		

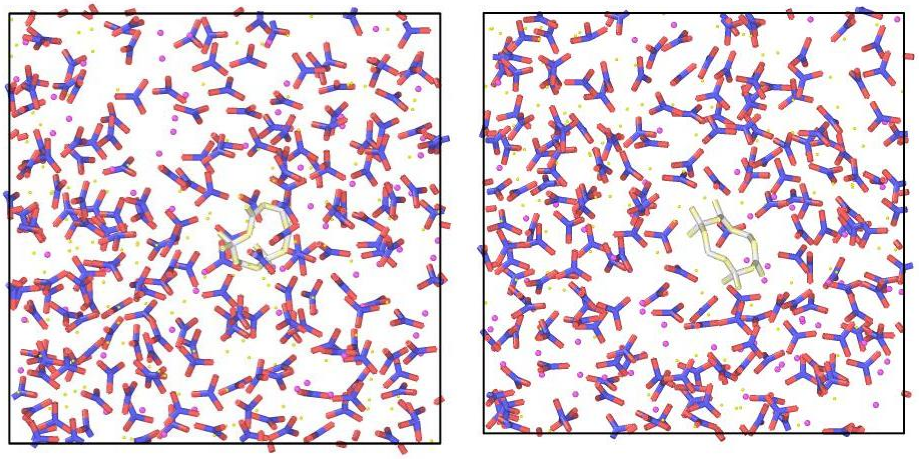

Figure 78 Simulation domains of the binary molten salt nanofluid mixed with SiO_2 nanoparticle (top view: left and front view: right)

Design of Different Simulation Domains (Same Mass Fraction: 6.0 %, 9.0 %, and 12.0 %)

As shown in figure 79-81, the different $NaNO_3$ nanostructures (different size, shape, and interface) rods were inserted into the binary molten salt eutectic to confirm the effect of the surface on the nanofluid at the same mass fraction. In other words, the contribution of the effect of the surface atoms is related to the enhanced thermophysical properties (e.g., specific heat) of nanolfuid and thus the different size of $NaNO_3$ rod (different surface energy) was used at the same mass fraction. As shown in figure 79, the one single $NaNO_3$ nanostructure rod (Na: 14, N: 14, and O: 42 atoms) was used and this mass fraction is 6.0 %. Two $NaNO_3$ nanostructure rods were used to compare the effect of the surface atoms and its total mass fraction of nanostructures is 6.0 % with two $NaNO_3$ nanostructure rods. The mass fraction of the one $NaNO_3$ nanostructure rod is 3.2 % (Na: 7, N: 7, and O: 21 atoms). According to the table 17, the surface area of the $NaNO_3$ nanostructure rod is increased when the number of the rod is increased at the same mass fraction (6.0 %). The surface are of the one single $NaNO_3$ nanostructure rod is 1.67 nm^2. Two $NaNO_3$ nanostructure rod is 2.96 nm^2. As shown in figure 80, the total mass fraction of $NaNO_3$ nanostructure was fixed at 9.0 % for each simulation box. The one single $NaNO_3$ nanostructure rod (Na: 21, N: 21, and O: 63 atoms) was used and its mass fraction is 9.0 %. Two $NaNO_3$ nanostructure rods were used and the mass fraction of the one single $NaNO_3$ nanostructure is 4.9 % (Na: 11, N: 11, and O: 33 atoms) in this condition. Three $NaNO_3$ nanostructure rods was used and the mass fraction of the single $NaNO_3$ nanostructure rod is 3.2 % (Na: 7, N: 7, and O: 21 atoms) in this case. According to the table 18, the surface area of the NaNO3 nanostructure rod when the number of the rod is increased at the same mass fraction (9.0 %). The surface area of the one single $NaNO_3$ nanostructure rod is 2.19 nm^2. Two $NaNO_3$ nanostructure rod is 3.17 nm^2, three $NaNO_3$ nanostructure rod is 4.44 nm^2. As shown in figure 81, the total mass fraction of

$NaNO_3$ nanostructure was fixed at 12.0 % for each simulation box. The one single $NaNO_3$ nanostructure rod (Na: 21, N: 21, and O: 63 atoms) was used and its mass fraction is 11.7 %, two $NaNO_3$ nanostructure rods were inserted and each rod's mass fraction is 6.2 % (Na: 14, N: 14, and O: 42 atoms). Three $NaNO_3$ nanostructure rods were inserted and each rod's mass fraction is 4.1 % (Na: 9, N: 9, and O: 27 atoms). Four $NaNO_3$ nanostructure rods were used the mass fraction the on single $NaNO_3$ nanostructure is 3.2 % (Na: 7, N: 7, and O: 21 atoms). According to the table 19, the surface area of the NaNO3 nanostructure rod when the number of the rod is increased at the same mass fraction (12.0 %). The surface are of the one single $NaNO_3$ nanostructure rod is 3.64 nm^2. Two $NaNO_3$ nanostructure rod is 4.25 nm^2, three $NaNO_3$ nanostructure rod is 4.50 nm^2, and four $NaNO_3$ nanostructure rod is 5.92 nm^2.

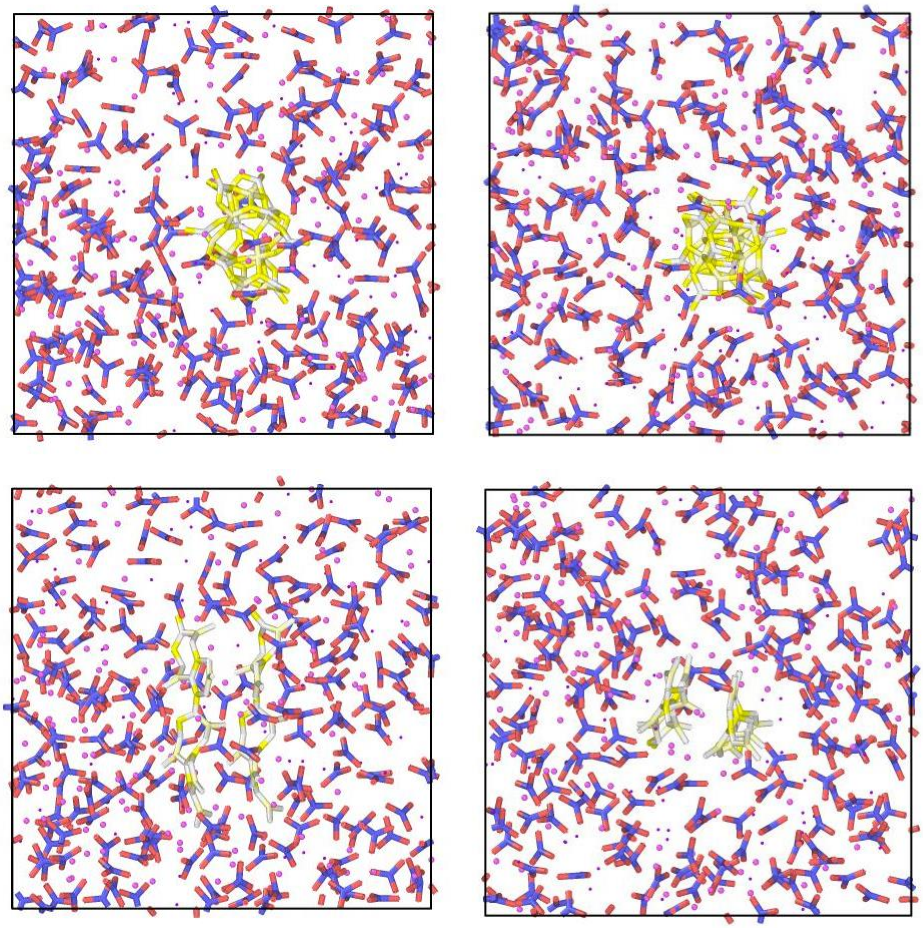

Figure 79 Simulation domains of the binary molten salt nanofluid mixed with different $NaNO_3$ rods (one rod: top and two rods: bottom) at 6.0 % (top view: left and front view: right)

Table 17 Surface area of $NaNO_3$ nanostructure rod (6.0 %)

Rod	Surface area (nm^2)	One $NaNO_3$ rod	
		Diameter (nm)	Length (nm)
One $NaNO_3$ rod	1.67	0.50	1.10
Two $NaNO_3$ rods	2.96	0.30	1.57

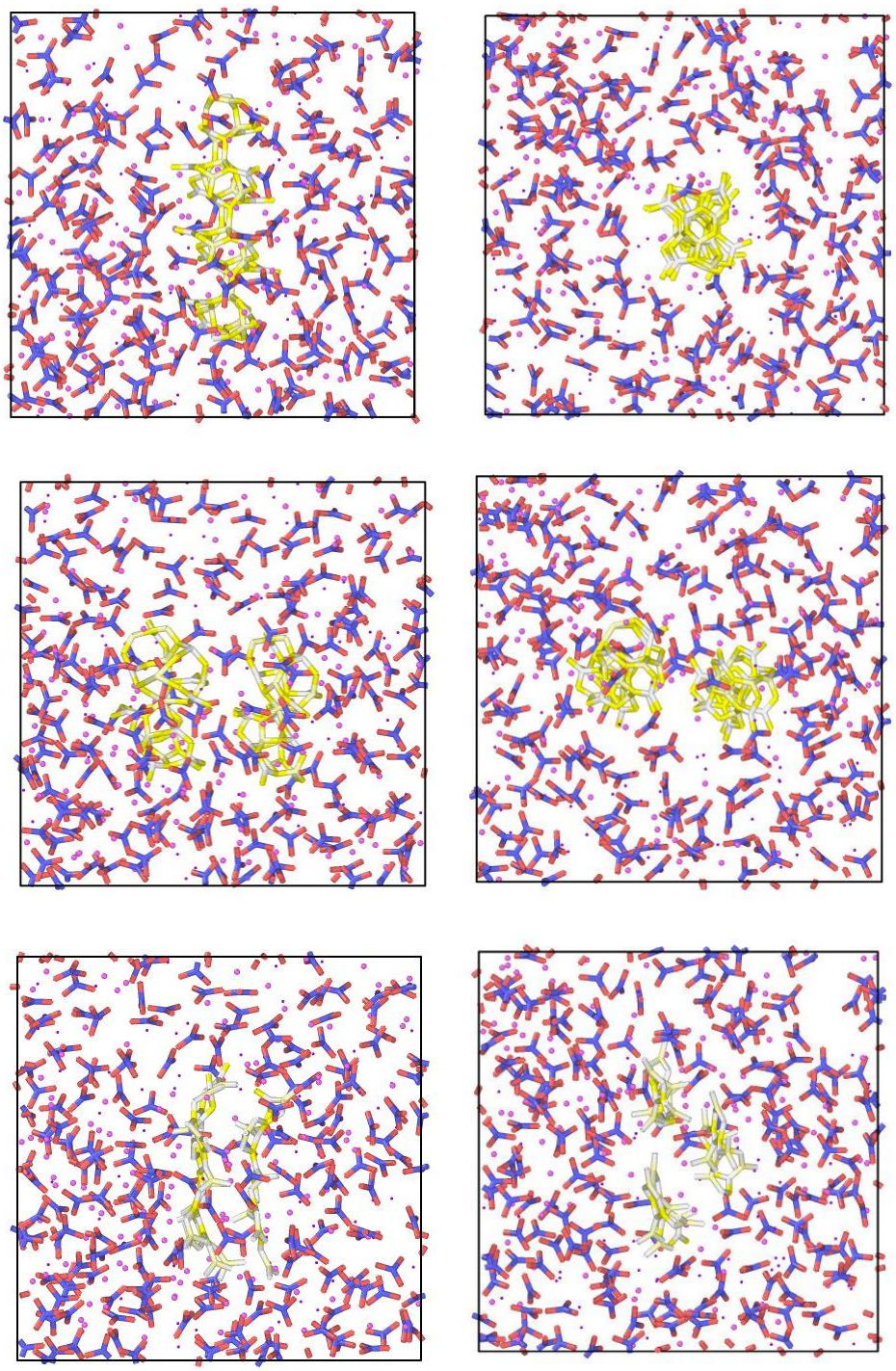

Figure 80 Simulation domains of the binary molten salt nanofluid mixed with different $NaNO_3$ rods (one rod: top, two rods: middle, three rods: bottom) at 9.0 % (top view: left and front view: right)

Table 18 Surface area of $NaNO_3$ nanostructure rod (9.0 %)

Rod	Surface area (nm^2)	One $NaNO_3$ rod	
		Diameter (nm)	Length (nm)
One $NaNO_3$ rod	2.19	0.30	2.32
Two $NaNO_3$ rods	3.17	0.40	1.26
Three $NaNO_3$ rods	4.44	0.30	1.57

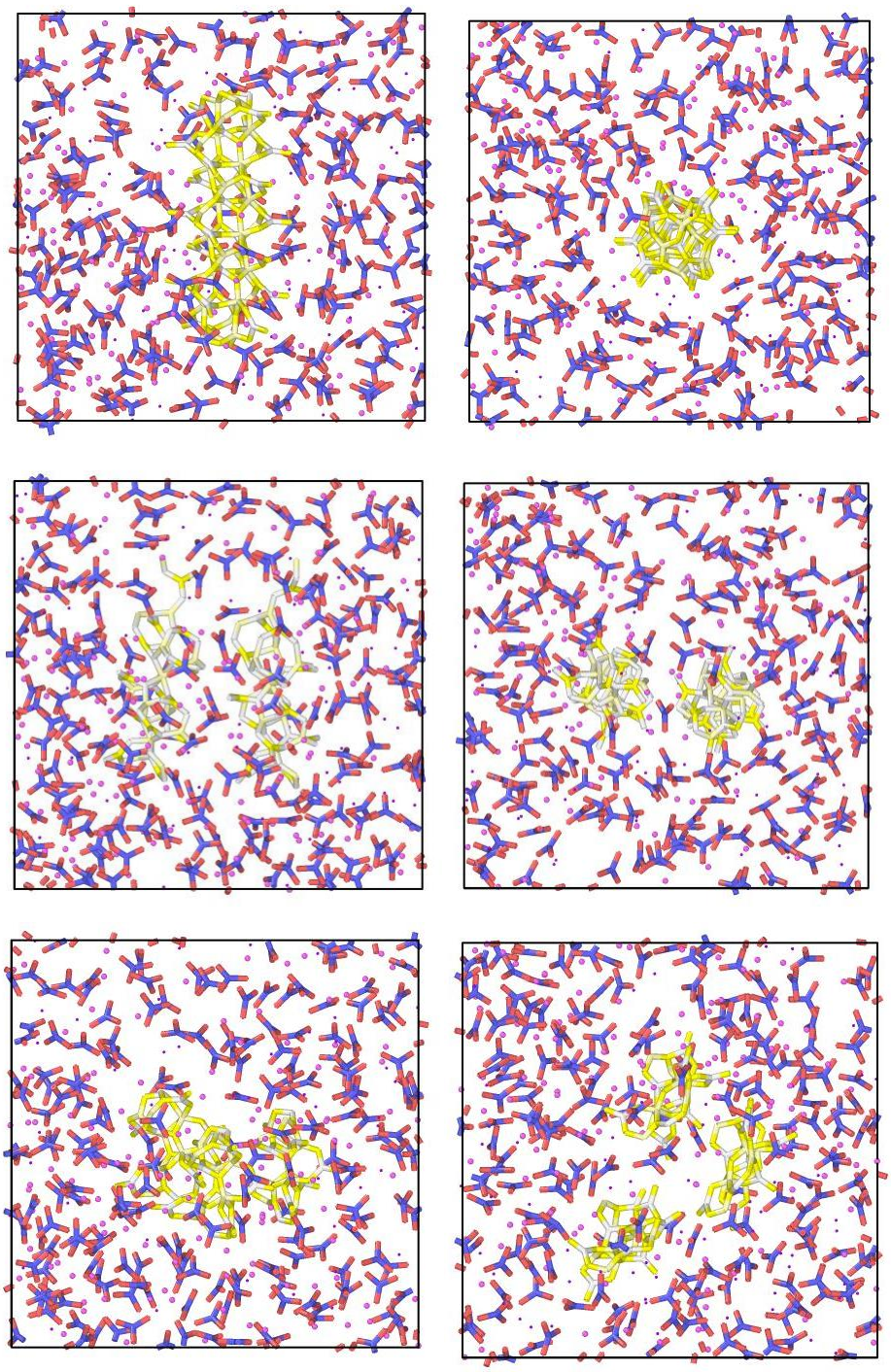

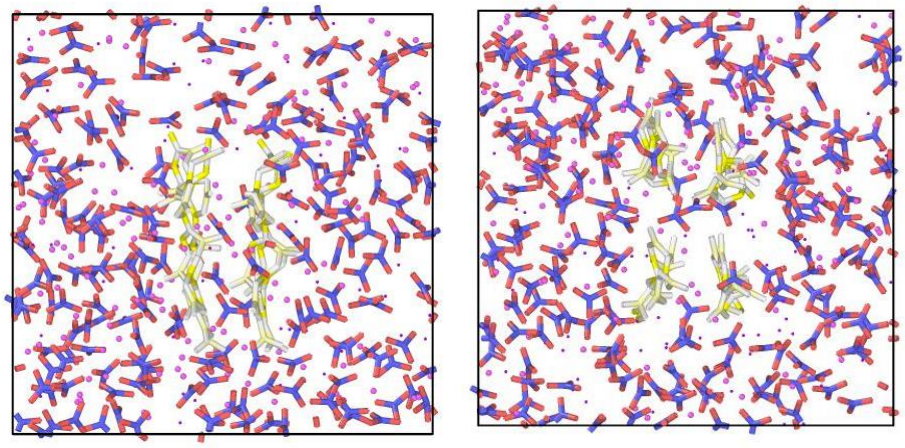

Figure 81 Simulation domains of the binary molten salt nanofluid mixed with different $NaNO_3$ rods (one rod: 1st line, two rods: 2nd line, three rods: 3rd line, and four rods: 4th line) at 12.0 % (top view: left and front view: right)

Table 19 Surface area of $NaNO_3$ nanostructure rod (12.0 %)

Rod	Surface area (nm^2)	One $NaNO_3$ rod	
		Diameter (nm)	Length (nm)
One $NaNO_3$ rod	3.64	0.50	2.32
Two $NaNO_3$ rods	4.25	0.40	1.69
Three $NaNO_3$ rods	4.50	0.45	1.10
Four $NaNO_3$ rods	5.92	0.30	1.57

Simulation Results

As shown in figure 82 and table 20, the density of the binary molten salt eutectic was calculated by 2000000 run in the NPT (e.g., isothermal-isobaric ensemble). The results of density converges during the simulation (2000000 run). There is no a great fluctuation (convergence) over the computation time and thus the system is stable. The temperature range of all simulation was between 250 °C (523 K) and 420 °C (693 K). As shown in table 20, the density of the binary molten salt eutectic is 1.84 g/cm^3 at 420 °C (693 K). According to the literature [5], the density of the single chemical, $NaNO_3$ and KNO_3, was given and $NaNO_3$ is 1.80 g/cm^3 and KNO_3 is 1.81 g/cm^3 at 420 °C (693 K) respectively. It also shows that the density of the binary molten salt eutectic ($NaNO_3$-KNO_3=60:40 by weight ratio) is 1.82 g/cm^3 at 420 °C (693 K) and thus the results of density simulation made a good agreement. As I mentioned earlier, the step of the computation of density is required to confirm that the system (e.g., the simulation domain box) is stable or not. After checking the stable system, the next step is to bring the system to base temperature running equilibration as the isothermal-isobaric ensemble (NPT) to calculate thermophysical properties (e.g., specific heat). If the system is not stable, it may show a great fluctuation of the density value over the calculation time. It also shows the different value of density compared to the reference over the calculation time under this condition and it does not converge at all. The result of the density of the binary molten salt eutectic shows not only the reasonable value compared to the reference [5] but also stable curve (converge) over the computation time (2000000 run). In other words, this system is stable enough to calculate specific heat at the isothermal-isobaric ensemble (NPT) at the different temperature range between 250 °C (523 K) and 420 °C (693 K).

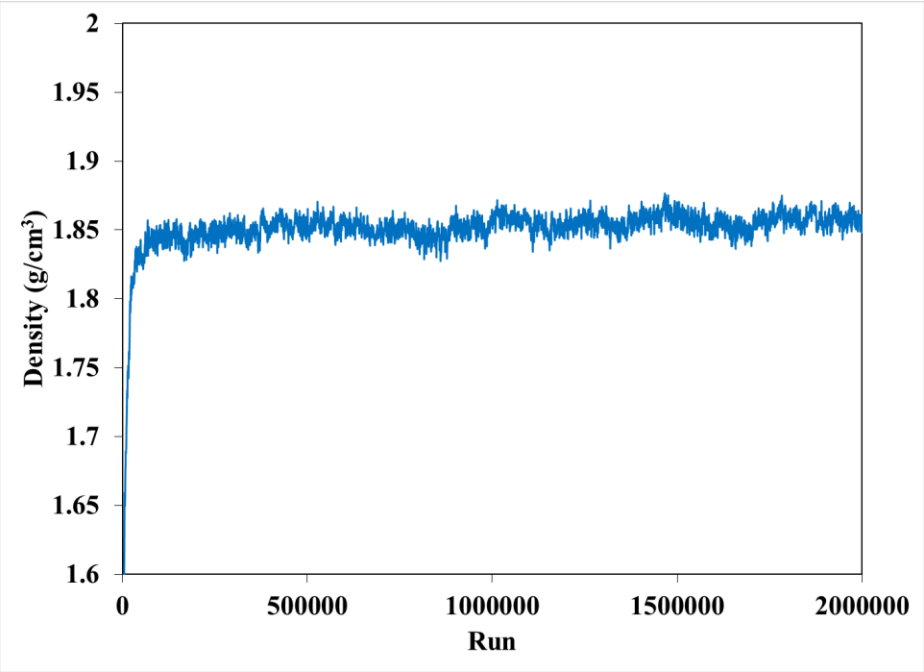

Figure 82 Density plot of the binary nitrate molten salt eutectic ($NaNO_3$-KNO_3) at 693 K

Table 20 Density of the binary molten salt eutectic at 693K

Sample	Density (g/cm^3) at the final step (2000000) at 693 K (420 °C)	
	Simulation	Ref [5]
Molten salt eutectic	1.848	1.82

For the specific heat calculation, the total energy (e.g., potential and kinetic energy) of the binary molten salt eutectic was computed by the NPT (isothermal-isobaric ensemble) at different temperature ranges between 250 °C (523 K) and 420 °C (693 K). The slope (total energy vs. temperature) was created to calculate specific heat of the pure eutectic. As shown in figure 83 and table 21, the specific heat of the pure eutectic salt is 1.5756 kJ/kg °C. According to the literature [57], it shows that specific heat of the binary molten salt eutectic (e.g., NaNO3-KNO3: 60:40 by weight ratio) is 1.48 J/g K between 250 °C (523 K) and 420 °C (693 K). According to other studies [57], [110], the

different values of specific heat of the binary molten salt eutectic (e.g., $NaNO_3$-KNO_3) was reported by different researchers and this value shows from 1.45 kJ/kg °C to 1.55 kJ/kg °C at different temperature ranges. Therefore, the simulation results of the binary molten salt eutectic made a good agreement.

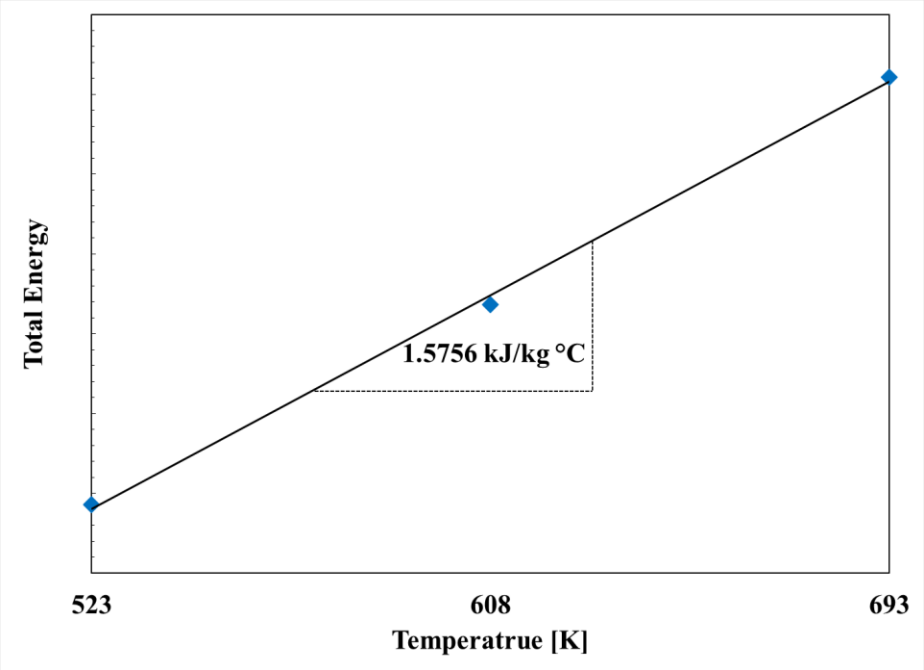

Figure 83 Slope of total energy and temperature of the binary molten salt eutectic between 250 °C (523 K) and 420 °C (693 K)

Table 21 Specific heat of the binary molten salt eutectic between 250 °C (523 K) and 420 °C (693 K)

Sample	250 °C (523 K) to 420 °C (693 K)	
	Cp (kJ/kg °C)	Cp (J/g K)
	Simulation	Ref [57]
Molten salt eutectic	1.5756	1.48

The results of the simulation can be used to explain how the surface atoms have an effect on the effective specific heat over the interior atoms in the nanostructure. In this simulation, one, two, three, and four $NaNO_3$ nanostructure rods were used to verify the effect of surface atoms on the nanostructure in the binary molten salt nanofluid. The same size, shape, and interface of the $NaNO_3$ nanostructure rod were used to compare each simulation. The density of the molten salt nanofluid with the number of $NaNO_3$ nanostructure rods was calculated by 2000000 run in the NPT (e.g., isothermal-isobaric ensemble). The results of density converges during the simulation (2000000 run). In other words, there is no a great fluctuation over the computation time and thus this system is stable enough to calculate thermophysical properties (e.g., specific heat). The temperature range of all simulation was between 250 °C (523 K) and 420 °C (693 K). The contribution of the surface energy (different surface) of the nanostructure is related to enhanced specific heat of nanofluids. $NaNO_3$-KNO_3 molten salt eutectic mixed with one, two, three, and four $NaNO_3$ nanostructure rods were used to verify the surface energy on the nanostructure. The one single $NaNO_3$ nanostructure rod (3.2 %) was used to increase the number of rods for each simulation in the binary molten salt nanofluid ($NaNO_3$-KNO_3=60:40 by weight ratio). The total mass fraction of each case is 3.2 %, 6.2 %, 9.0 %, and 11.7 % respectively when the number of the $NaNO_3$ nanostructure rod is increased. According to the literature [5], the density of the single chemical (e.g., $NaNO_3$ and KNO_3) was given and $NaNO_3$ is 1.80 g/cm^3 and KNO_3 is 1.81 g/cm^3 at 420 °C (693 K) respectively. As shown in figure 84 and table 22, the results show the density of each simulation domain. There is no a great fluctuation during the long computation time and thus the system is stable (convergence). Its density is 1.860 g/cm^3, 1.876 g/cm^3, 1.877 g/cm^3, and 1.863 g/cm^3 at the final step (2000000 run) at 693 K (420 °C) respectively when the number of the $NaNO_3$ nanostructure rod is increased. In other words, the

density of the system is increased when the number of the $NaNO_3$ nanostructure is increased. When four $NaNO_3$ nanostructure rods were in the system, the density of the system was not increased because the density value from the final step (2000000 run) was only considered.

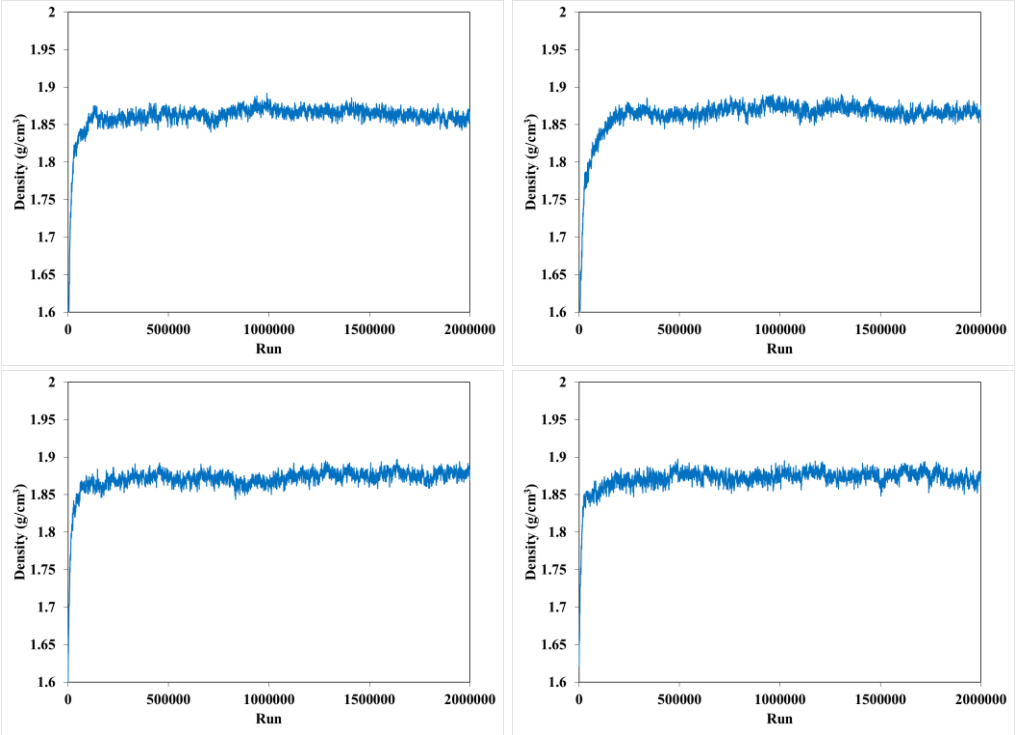

Figure 84 Density plot of the binary molten salt nanofluid mixed with $NaNO_3$ rods (one rod: top left, two rods: top right, three rods: bottom left, and four rods: bottom right) at 693 K

Table 22 Comparison of density the binary molten salt nanofluid mixed with $NaNO_3$ rods (one rod, two rods, three rods, and four rods) at 693 K

Number of rod	Mass fraction (%)	at the final step (2000000) at 693 K (420 °C)	
		Density (g/cm^3)	Molten salt eutectic Density (g/cm^3)
One $NaNO_3$ rod	3.2	1.860	1.848
Two $NaNO_3$ rods	6.2	1.876	
Three $NaNO_3$ rods	9.0	1.877	
Four $NaNO_3$ rods	11.7	1.863	

The total energy (e.g., potential energy and kinetic energy) of the binary molten salt nanofluid with the number of $NaNO_3$ nanostructure rods was calculated by NPT (the isothermal-isobaric ensemble) at different temperature ranges between 250 °C (523 K) and 420 °C (693 K). The specific heat of nanofluid can be computed by the total energy and the temperature range. The slope (total energy vs. temperature) was created to calculate the specific heat of the binary molten salt nanofluid. As shown in figure 85 and table 23, specific heat of the binary molten salt nanofluid mixed with $NaNO_3$ nanostructure rods was increased when the number of the $NaNO_3$ nanostructure rod was increased. It shows 1.6175 kJ/kg °C with one $NaNO_3$ nanostructure rod, 1.6469 kJ/kg °C with two $NaNO_3$ nanostructure rods, 1.6940 kJ/kg °C with three $NaNO_3$ nanostructure rods, and 1.7328 kJ/kg °C with four $NaNO_3$ nanostructure rods respectively. According to the table 23, the surface area of the NaNO3 nanostructure rod is increased, when the number of the $NaNO_3$ nanostructure rod is increased. The one single $NaNO_3$ nanostructure rod is 1.48 nm^2, two $NaNO_3$ nanostructure rods is 2.96 nm^2, three NaNO3 nanostructure rods is 4.44 nm^2, and four $NaNO_3$ nanostructure rod is 5.91 nm^2 respectively. This enlarged surface area is responsible for the enhanced specific heat of nanofluids. The binary molten salt mixed with four $NaNO_3$ nanostructure rods shows the highest enhanced specific heat compared to other cases (e.g., one, two, and three rods) due to the enlarged surface area over the interior atoms in the nanostructure. In other words, the surface area is increased when the number of the nanostructure rod (same shape) is inserted. Although enhanced specific heat was shown when the number of the $NaNO_3$ structure was increased in the molten salt eutectic, this increased specific heat is less than the experimental results of specific heat (~2.0 kJ/kg °C) from the previous chapter in this research. Only one, two, three, and four $NaNO_3$ nanostructure rods were used to calculate the enhanced specific heat of nanofluid. It is hard to mimic complicated

nanostructures observed from the actual experiment. According to this results of the simulation, it confirms that the effect of the surface atoms of $NaNO_3$ nanostructure is responsible for the enhanced specific heat of the binary molten salt nanofluids. Its specific heat can be increased when the number of the surface atoms of $NaNO_3$ nanostructure is increased. In other words, there is a close correspondence between the contribution of the effect of the surface atoms of the $NaNO_3$ nanostructure and enhanced specific heat of the binary molten salt nanofluid.

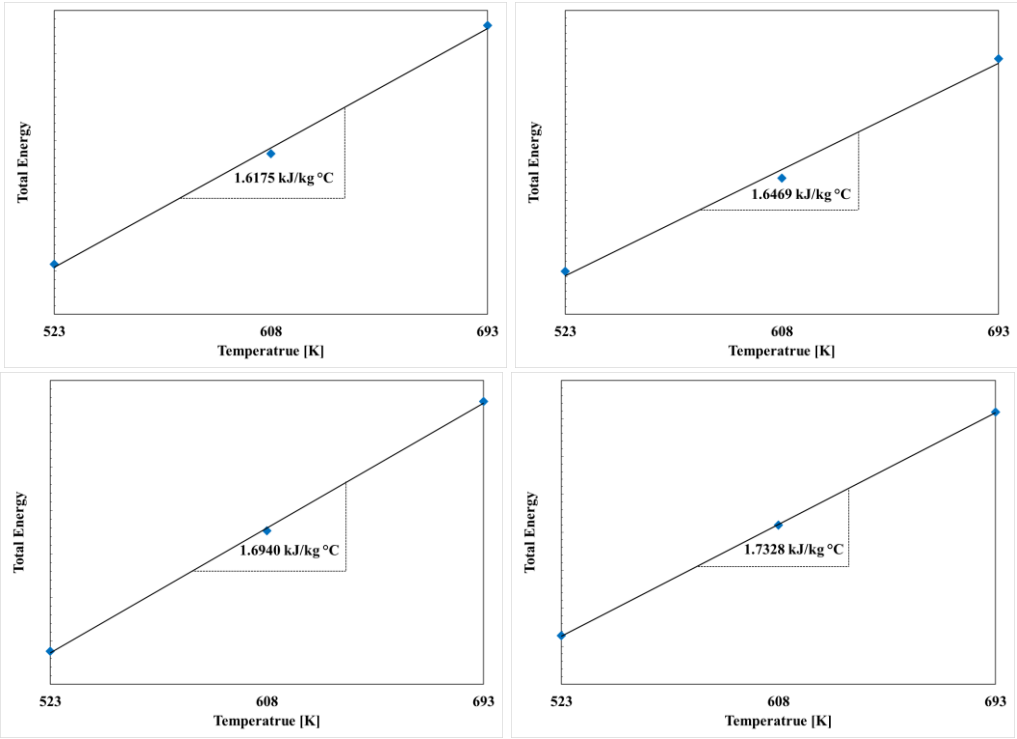

Figure 85 Slope of total energy and temperature of the binary molten salt nanofluid mixed with $NaNO_3$ rods (one rod: top left, two rods: top right, three rods: bottom left, and four rods: bottom right) between 250 °C (523 K) and 420 °C (693 K)

Table 23 Comparison of specific heat of the binary molten salt nanofluid mixed with the number of $NaNO_3$ rods (one rod, two rods, three rods, and four rods)

Number of rod	Mass fraction (%)	Surface area (nm^2)	250 °C (523 K) to 420 °C (693 K)	
			Cp (kJ/kg °C)	Molten salt eutectic Cp (kJ/kg °C)
One $NaNO_3$ rod	3.2	1.48	1.6175	1.5756
Two $NaNO_3$ rods	6.2	2.96	1.6469	
Three $NaNO_3$ rods	9.0	4.44	1.6940	
Four $NaNO_3$ rods	11.7	5.91	1.7328	

The different size of $NaNO_3$ nanostructure rods (one rod and two rods) were used at the same volume fraction (6.0 %). The mass fraction was fixed at 6.0 %. The effect of surface atoms can be explained why it has an effect on the effective specific heat on the nanostructure (over the interior atoms) at the same mass fraction. First, the density of the molten salt nanofluid with the different size of $NaNO_3$ nanostructure rods (one rod and two rods) at the same mass fraction was calculated by 2000000 run in NPT (e.g., isothermal-isobaric ensemble). The results of density converges during the simulation (2000000 run) it means that this system is stable to compute thermophysical properties (e.g., specific heat) at the NPT. The temperature range of all simulation was between 250 °C (523 K) and 420 °C (693 K). The contribution of the surface energy of the nanostructure at the same mass fraction is related to enhanced specific heat of the binary molten salt nanofluid. $NaNO_3$-KNO_3 molten salt eutectic mixed with one and two $NaNO_3$ nanostructure rods at the same mass fraction (6.0 %) to explain the effect of the surface atoms on the nanostructure. The one single $NaNO_3$ nanostructure rod was used and this mass fraction is about 6.0 %. Two $NaNO_3$ nanostructure rods was used to compare the effect of the surface atoms. The total mass fraction of nanostructures is about 6.0 % with two $NaNO_3$ nanostructure rods (one rod: 3.2 %). The density of the single chemical, $NaNO_3$ and KNO_3, was given and $NaNO_3$ is 1.80 g/cm^3 and KNO_3 is 1.81 g/cm^3 at 420 °C (693 K) respectively according to the literature [5]. As shown in figure 86 and table 24, the results shows the density of each simulation domain. There is no a great fluctuation (convergence) over the computation time and thus the system is stable enough. Its density is 1.892 g/cm^3 and 1.876 g/cm^3 at the final step (2000000 run) at 693 K (420 °C) respectively. It means that the density of the total system with the one single $NaNO_3$ nanostructure rod (larger size) is larger than two $NaNO_3$ nanostructure (smaller size) rods at the same mass fraction.

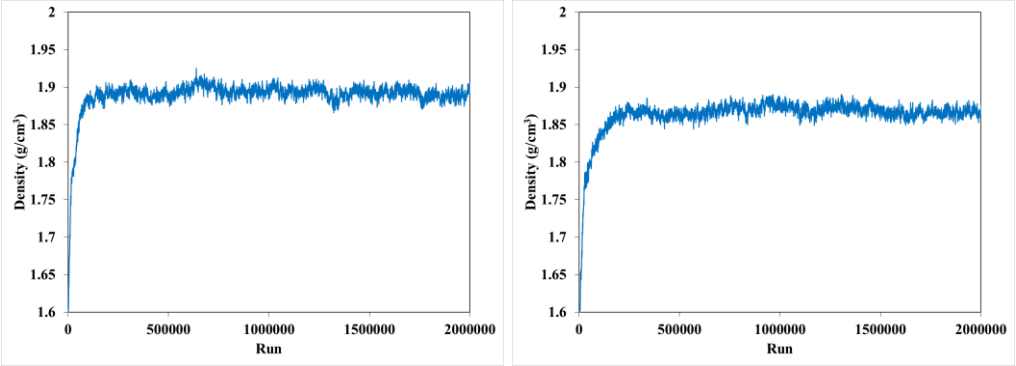

Figure 86 Density plot of the binary molten salt nanofluid mixed with $NaNO_3$ rods (one rod: left and two rods: right) at 693 K

Table 24 Comparison of density the binary molten salt nanofluid mixed with $NaNO_3$ rods (one rod and two rods) at the same mass fraction (6.0 %) at 693 K

Number of rod	Mass fraction (%)	at the final step (2000000) at 693 K (420 °C)	
		Density (g/cm^3)	Molten salt eutectic Density (g/cm^3)
One $NaNO_3$ rod	6.0	1.892	1.848
Two $NaNO_3$ rods	6.0	1.876	

For thermophysical properties (e.g., specific heat), the total energy (e.g., potential energy and kinetic energy) of the nanofluid with the different size of $NaNO_3$ nanostructure rods (one rod and two rods) at the same mass fraction (6.0 %) was calculated by NPT (the isothermal-isobaric ensemble) at different temperature ranges between 250 °C (523 K) and 420 °C (693 K). As shown in figure 87 and table 25, the specific heat of the binary molten salt nanofluid mixed with $NaNO_3$ nanostructure rods was increased when the number of the $NaNO_3$ nanostructure rod was increased at the same volume. It shows 1.6085 kJ/kg °C with one single $NaNO_3$ nanostructure rod and 1.6469 kJ/kg °C with two $NaNO_3$ nanostructure rods respectively. The binary molten salt mixed with two $NaNO_3$ nanostructure rods shows the highest enhanced specific heat compared to the one single $NaNO_3$ nanostructure rod due to the enlarged surface area over the interior atoms in the nanostructure. According to the table 25, the surface area of the $NaNO_3$ nanostructure was also calculated to verify its effect when the number of the $NaNO_3$ nanostructure rod is increased at the same mass fraction. It shows the one single $NaNO_3$ nanostructure rod is 1.67 nm^2 and two $NaNO_3$ nanostructure rods is 2.96 nm^2. It means that the surface area is increased when the number of the $NaNO_3$ nanostructure rod is increased and its enlarged surface area contributes the enhanced specific heat of nanofluid. Although enhanced specific heat was shown when the number of the $NaNO_3$ structure was increased in the molten salt eutectic, this increased specific heat is less than the experimental specific heat (~2.0 kJ/kg °C) from the previous chapter in this research. It is hard to mimic complicated nanostructures observed from the actual experimental results. In this simulation, the one and two $NaNO_3$ nanostructure rods were only used to calculate enhanced specific heat of nanofluid. According to this results of the simulation, it confirms that the effect of the surface atoms of $NaNO_3$ nanostructure is responsible for the enhanced specific heat of molten salt nanofluids at the same mass

fraction. Its specific heat can be increased when the number of the surface atoms of $NaNO_3$ nanostructure is increased at the same mass fraction. It means that the surface area of nanostructure is increased when the number of the $NaNO_3$ nanostructure rods is increased at the same mass fraction. In other words, there is a close correspondence between the contribution of the effect of the surface atoms of $NaNO_3$ nanostructure and enhanced specific heat of nanofluid at the same mass fraction.

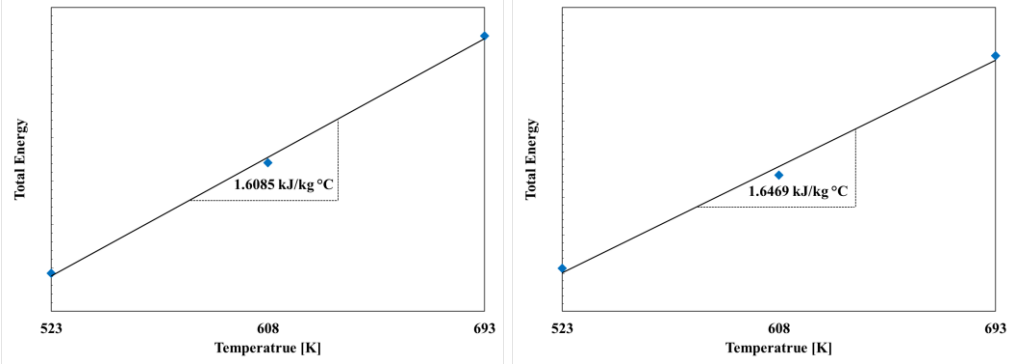

Figure 87 Slope of total energy and temperature of the binary molten salt nanofluid mixed with $NaNO_3$ rods (one rod: left and two rods: right) between 250 °C (523 K) and 420 °C (693 K)

Table 25 Comparison of specific heat of the binary molten salt nanofluid mixed with $NaNO_3$ rods (one rod and two rods) at the same mass fraction (6.0 %)

Number of rod	Mass fraction (%)	Surface area (nm^2)	250 °C (523 K) to 420 °C (693 K)	
			Cp (kJ/kg °C)	Molten salt eutectic Cp (kJ/kg °C)
One $NaNO_3$ rod	6.0	1.67	1.6085	1.5756
Two $NaNO_3$ rods	6.0	2.96	1.6469	

In this simulation, the different size and shape of $NaNO_3$ nanostructure rods were used at the same mass fraction (9.0 %). The results of this case can explain the effect of surface atoms which is related to the effective specific heat of nanostructures over the interior atoms. The density of the molten salt nanofluid with the different size and shape of $NaNO_3$ nanostructure rods at the same mass fraction was calculated by 2000000 run in the NPT (e.g., isothermal-isobaric ensemble). The results of density converges during the simulation (2000000 run). There is no fluctuation and this system is stable enough to calculate another thermophsical properties (e.g., specific heat). The temperature range of all simulation was between 250 °C (523 K) and 420 °C (693 K). From the results of this simulation, the contribution of the surface energy of the nanostructure at the same mass fraction will be related to enhanced specific heat of nanofluid. $NaNO_3$-KNO_3 molten salt eutectic mixed with one, two, and three $NaNO_3$ nanostructure rods at the same mass fraction (9.0 %) to verify the effect of the surface atoms on the nanostructure. The one single $NaNO_3$ nanostructure rod was used and this mass fraction is fixed at 9.0 %. Two $NaNO_3$ nanostructure rods were used to compare the effect of the surface atoms on the nanostructure. Its total mass fraction of nanostructures is about 9.0 % with two $NaNO_3$ nanostructure rods (one rod: 4.9 %). Three $NaNO_3$ nanostructure rods were inserted in the domain box and its total mass fraction of nanostructure is 9.0% with three $NaNO_3$ nanostructure rods (one rod: 3.2 %). According to the literature [5], density of the single chemical, $NaNO_3$ and KNO_3, was given and $NaNO_3$ is 1.80 g/cm^3 and KNO_3 is 1.81 g/cm^3 at 420 °C (693 K) respectively. As shown in figure 88 and table 26, the results shows the density of each simulation domain box. There is no a great fluctuation over the computation time and thus the system is stable (convergence). Its density is 1.8924 g/cm^3, 1.891 g/cm^3, and 1.877 g/cm^3 at the final step (2000000 run) at 693 K (420 °C) respectively. It means that the density of the total system with the one single $NaNO_3$

nanostructure rod is larger than two and three $NaNO_3$ nanostructure rods at the same mass fraction.

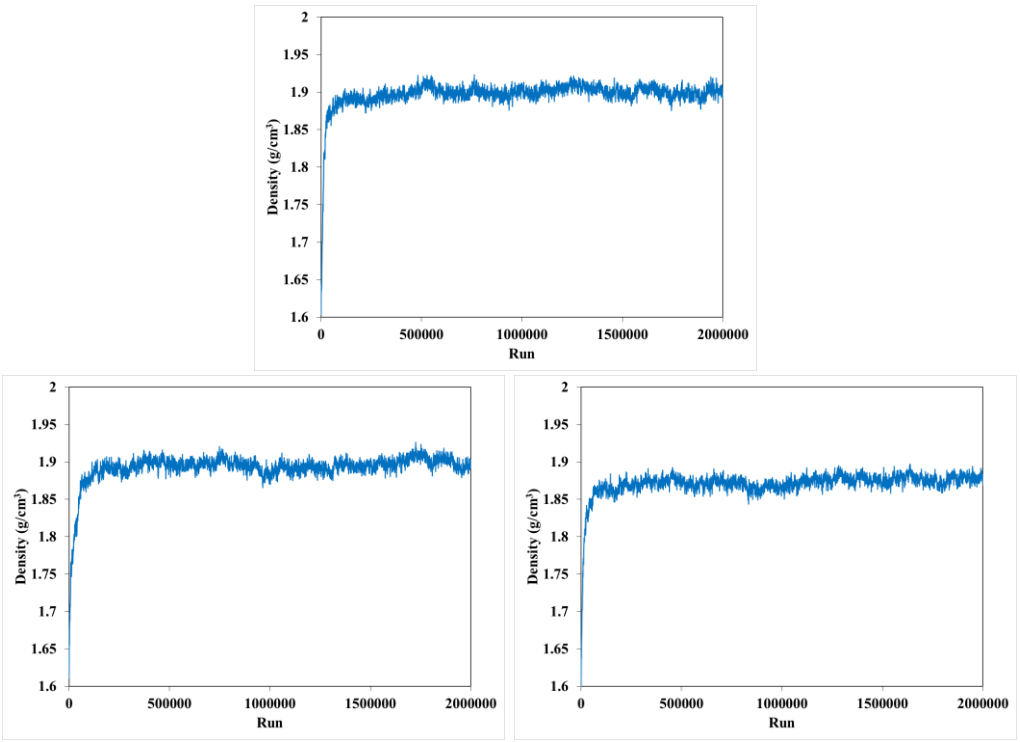

Figure 88 Density plot of the binary molten salt nanofluid mixed with $NaNO_3$ rods (one rod: top, two rods: bottom left, and three rods: bottom right) at the same mass fraction (9.0 %) at 693 K

Table 26 Comparison of density the binary molten salt nanofluid mixed with $NaNO_3$ rods (one rod, two rods, and three rods) at 693 K

Number of rod	Mass fraction (%)	at the final step (2000000) at 693 K (420 °C)	
		Density (g/cm^3)	Molten salt eutectic Density (g/cm^3)
One $NaNO_3$ rod	9.0	1.894	1.848
Two $NaNO_3$ rods	9.0	1.891	
Three $NaNO_3$ rods	9.0	1.877	

The total energy (e.g., potential energy and kinetic energy) of the binary molten salt nanofluid was used to calculate its specific heat with the different size and shape of $NaNO_3$ nanostructure rods at the same mass fraction (9.0 %). It was calculated by the NPT (the isothermal-isobaric ensemble) at different temperature ranges between 250 °C (523 K) and 420 °C (693 K). As shown in figure 89 and table 27, the specific heat of the binary molten salt nanofluid mixed with $NaNO_3$ nanostructure rods was increased when the number of the $NaNO_3$ nanostructure rod was increased at the same mass fraction (9.0 %). It shows 1.6237 kJ/kg °C with one single $NaNO_3$ nanostructure rod, 1.6278 kJ/kg °C with two $NaNO_3$ nanostructure rods, and 1.6940 kJ/kg °C with three $NaNO_3$ nanostructure rods respectively. According to the table 29, the surface area of the $NaNO_3$ nanostructure was also calculated to verify the effect of surface area when the number of the $NaNO_3$ nanostructure rod is increased at the same mass fraction. It shows the one single $NaNO_3$ nanostructure rod is 2.19 nm^2, two $NaNO_3$ nanostructure rods is 3.17 nm^2, and three $NaNO_3$ nanostructure rods is 4.44 nm^2. From this results, it confirm that the surface area is increased due to the number of $NaNO_3$ nanostructure rods and its enlarged surface area is responsible for the enhanced specific heat of nanofluids. The binary molten salt mixed with three $NaNO_3$ nanostructure rods shows the highest enhanced specific heat compared to the other cases (e.g., one, two, and three rods) due to the enlarged surface area over the interior atoms in the nanostructure. According to this results of the simulation, it confirms that the effect of the surface atoms of $NaNO_3$ nanostructure is responsible for enhanced specific heat of molten salt nanofluids at the same mass fraction. Its specific heat can be increased when the number of the surface atoms of $NaNO_3$ nanostructure is increased at the same mass fraction. It means that the surface area of nanostructure is increased when the number of the $NaNO_3$ nanostructure rods is increased at the same mass fraction. In other words, there is a close

correspondence between the contribution of the effect of the surface atoms of $NaNO_3$ nanostructure and enhanced specific heat of nanofluid at the same mass fraction. Although specific heat of nanofluid was enhanced when the number of the $NaNO_3$ structure was increased in the molten salt eutectic, this enhanced specific heat is less than the experimental results of specific heat (~2.0 kJ/kg °C) from the previous chapter in this research. The one and two $NaNO_3$ nanostructure rods were only used to calculate enhanced specific heat of nanofluid in this simulation. Moreover, it is hard to mimic complicated nanostructures observed from the actual experimental results.

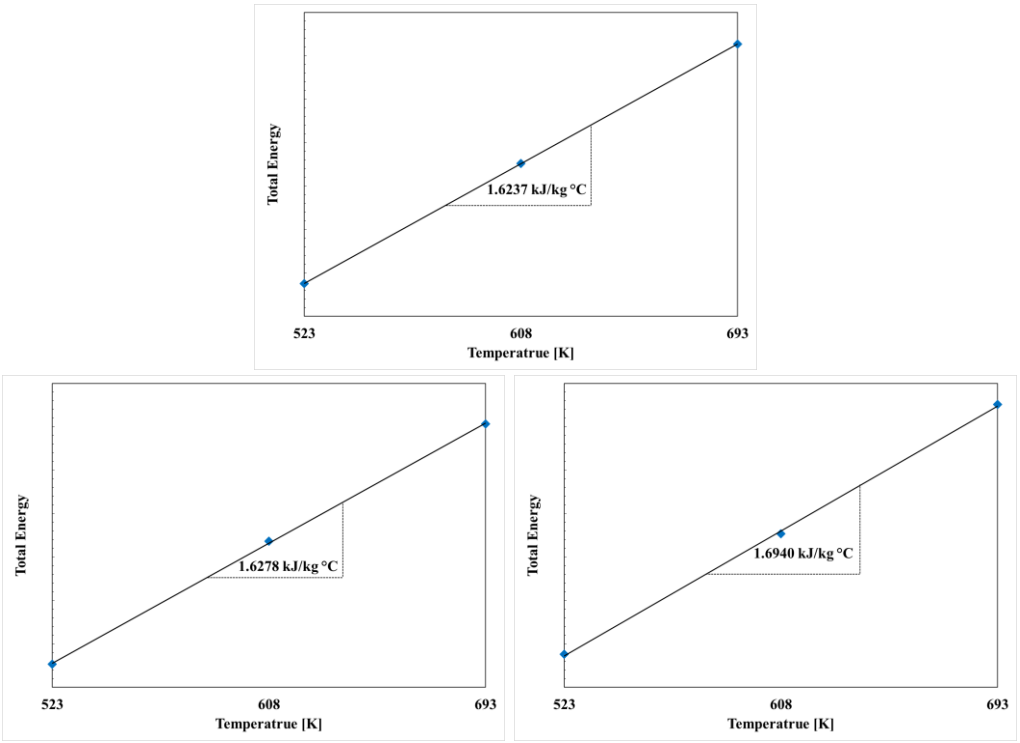

Figure 89 Slope of total energy and temperature of the binary molten salt nanofluid mixed with $NaNO_3$ rods (one rod: top, two rods: bottom left, and three rods: bottom right) between 250 °C (523 K) and 420 °C (693 K) at the same volume

Table 27 Comparison of specific heat of the binary molten salt nanofluid mixed with $NaNO_3$ rods (one rod, two rods, and three rods) at the same mass fraction (9.0 %)

Number of rod	Mass fraction (%)	Surface area (nm^2)	250 °C (523 K) to 420 °C (693 K)	
			Cp (kJ/kg °C)	Molten salt eutectic Cp (kJ/kg °C)
One $NaNO_3$ rod	9.0	2.19	1.6237	1.5756
Two $NaNO_3$ rods	9.0	3.17	1.6278	
Three $NaNO_3$ rods	9.0	4.44	1.6940	

The different size and shape (different surface area) of $NaNO_3$ nanostructure rods were used at the same mass fraction (12.0 %) in this simulation. The results of this case (e.g., at the same mass fraction) can explain how the surface atoms have an effect on the effective specific heat over the interior atoms in the nanostructure. First, the density of the molten salt nanofluid mixed with the different size (different surface area) of $NaNO_3$ nanostructure rods at the same mass fraction was calculated by 2000000 run in NPT (e.g., isothermal-isobaric ensemble). The different surface area depends on the shape of the $NaNO_3$ nanostructure rod. According to the results of the simulation, the density value converges during all computation running time and it means that this simulation system is stable enough to obtain thermophysical properties of the binary molten salt nanofluid. The temperature range of all simulation was considered between 250 °C (523 K) and 420 °C (693 K) for the density and its specific heat. The surface energy of the nanostructure may be responsible for the enhanced specific heat of nanofluid at the same mass fraction. To verify this effect, the binary molten salt eutectic (e.g., $NaNO_3$-KNO_3=60:40 by weight ratio) mixed with one, two, three, and four $NaNO_3$ nanostructure rods were used to explain the effect of the surface energy on the nanostructure at the same mass fraction (12.0 %). First, the one single $NaNO_3$ nanostructure rod was used in the system and its mass fraction is about 12.0 %. Two $NaNO_3$ nanostructure rods were inserted into the pure eutectic salt to compare the effect of the surface energy on the nanostructure. Its total mass fraction of nanostructures is about 12.0 % with two $NaNO_3$ nanostructure rods (one rod: 6.2 %) and it is the same as the one single $NaNO_3$ nanostructure rod. Three NaNO3 nanostructure rods were inserted in the domain box. The total mass fraction of nanostructures is about 12.0 % with three NaNO3 nanostructure rods (one rod: 4.1 %) and it is the same as the one single $NaNO_3$ nanostructure rod. Four $NaNO_3$ nanostructure rods were inserted in the domain. The total

mass fraction of nanostructures is about 12.0 % with four $NaNO_3$ nanostructure rods (one rod: 3.2 %) and it is the same as the one single $NaNO_3$ nanostructure rod. According to the literature [5], the density of the single chemical (e.g., $NaNO_3$ and KNO_3) was given and $NaNO_3$ is 1.80 g/cm^3 and KNO_3 is 1.81 g/cm^3 at 420 °C (693 K) respectively. As shown in figure 90 and table 28, the results shows the density of each simulation domain box. There is no fluctuation over the computation time and thus the system is stable (convergence). Its density is 1.937 g/cm^3, 1.907 g/cm^3, 1.901 g/cm^3, and 1.863 g/cm^3 at the final step (2000000 run) at 693 K (420 °C) respectively. It means that the density of the total system with the one single $NaNO_3$ nanostructure rod (larger size) is larger than the system mixed with two, three, and four $NaNO_3$ nanostructure rods (smaller size) at the same mass fraction.

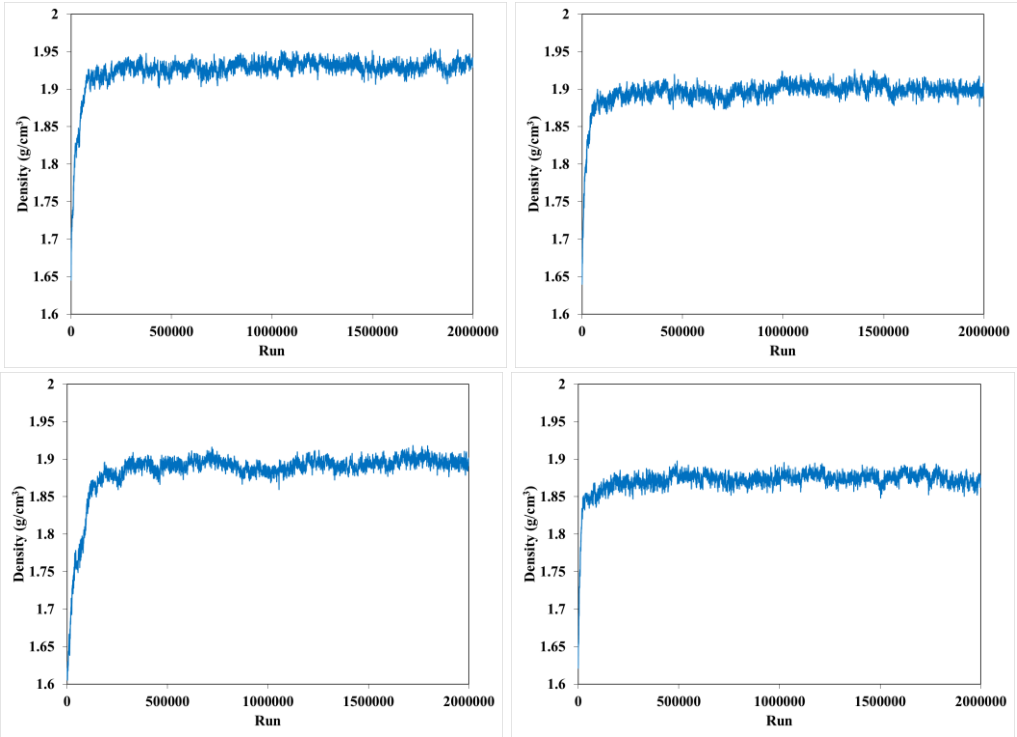

Figure 90 Density plot of the binary molten salt nanofluid mixed with $NaNO_3$ rods (one rod: top left, two rods: top right, three rods: bottom left, and four rods: bottom right) at 693 K

Table 28 Comparison of density the binary molten salt nanofluid mixed with $NaNO_3$ rods (one rod, two rods, three rods, and four rods) at 693 K

Number of rod	Mass fraction (%)	at the final step (2000000) at 693 K (420 °C)	
		Density (g/cm^3)	Molten salt eutectic Density (g/cm^3)
One $NaNO_3$ rod	12.0	1.937	1.848
Two $NaNO_3$ rods	12.0	1.907	
Three $NaNO_3$ rods	12.0	1.901	
Four $NaNO_3$ rods	12.0	1.863	

The total energy (e.g., potential energy and kinetic energy) of the binary molten salt nanofluid was computed by the NPT (the isothermal-isobaric ensemble) at the same mass fraction. This binary molten salt eutectic was mixed with the different size and shape (different surface) of $NaNO_3$ nanostructure rods. The temperature range is between 250 °C (523 K) and 420 °C (693 K). The slope was created by the temperature and the total energy to obtain the specific heat of the nanofluid. As shown in figure 91 and table 29, the specific heat of the binary molten salt nanofluid mixed with $NaNO_3$ nanostructure rods (different size and surface) was increased when the number of the $NaNO_3$ nanostructure rod was increased at the same mass fraction. As I mentioned earlier, the $NaNO_3$ nanostructure rods with different size, shape, and surface were prepared to compare specific heat of nanofluids. According to the results, it shows 1.6627 kJ/kg °C with one single $NaNO_3$ nanostructure rod, 1.6683 kJ/kg °C with two $NaNO_3$ nanostructure rods, 1.6687 kJ/kg °C with three $NaNO_3$ nanostructure rods, and 1.7328 kJ/kg °C with four $NaNO_3$ nanostructure rods respectively. According to the table 34, the surface area of the $NaNO_3$ nanostructure was also calculated to verify the effect of surface area when the number of the $NaNO_3$ nanostructure rod is increased at the same mass fraction. It shows the one single $NaNO_3$ nanostructure rod is 3.64 nm^2, two $NaNO_3$ nanostructure rods is 4.25 nm^2, three $NaNO_3$ nanostructure rods is 4.50 nm^2, and four $NaNO_3$ nanostructure rods is 5.92 nm^2. It means that the enlarged surface area is related to the enhanced specific heat and this surface area is increased when the number of $NaNO_3$ nanostructure rod is increased. The binary molten salt eutectic mixed with four $NaNO_3$ nanostructure rods shows the highest enhanced specific heat compared to the other cases (e.g., one, two, three, and four rods) due to the enlarged surface area over the interior atoms in the nanostructure. According to this results of the simulation, it confirms that the effect of the surface atoms of $NaNO_3$ nanostructures is responsible for

enhanced specific heat of molten salt nanofluids at the same mass fraction. Moreover, the effect of the surface atoms is enhanced when $NaNO_3$ nanostructure rods with the smaller size and different shape were inserted in the eutectic salt at the same mass fraction. In other words, its specific heat can be increased when the number of the surface atoms of the $NaNO_3$ nanostructure is increased at the same mass fraction. It means that the surface area of nanostructures is increased due to the number of the $NaNO_3$ nanostructure rods (different size and shape) at the same mass fraction. In other words, there is a close correspondence between the contribution of the effect of the surface atoms of $NaNO_3$ nanostructures and enhanced specific heat of nanofluid at the same mass fraction. Although enhanced specific heat of nanofluids was shown when the number of the $NaNO_3$ structure was increased in the molten salt eutectic system, this increased specific heat is less than the experimental specific heat (~2.0 kJ/kg °C) from the previous chapter in this research. It is hard to mimic complicated nanostructures observed from the actual experimental results because only one, two, three, and four $NaNO_3$ nanostructure rods were used to calculate the enhanced specific heat of nanofluid in this simulation.

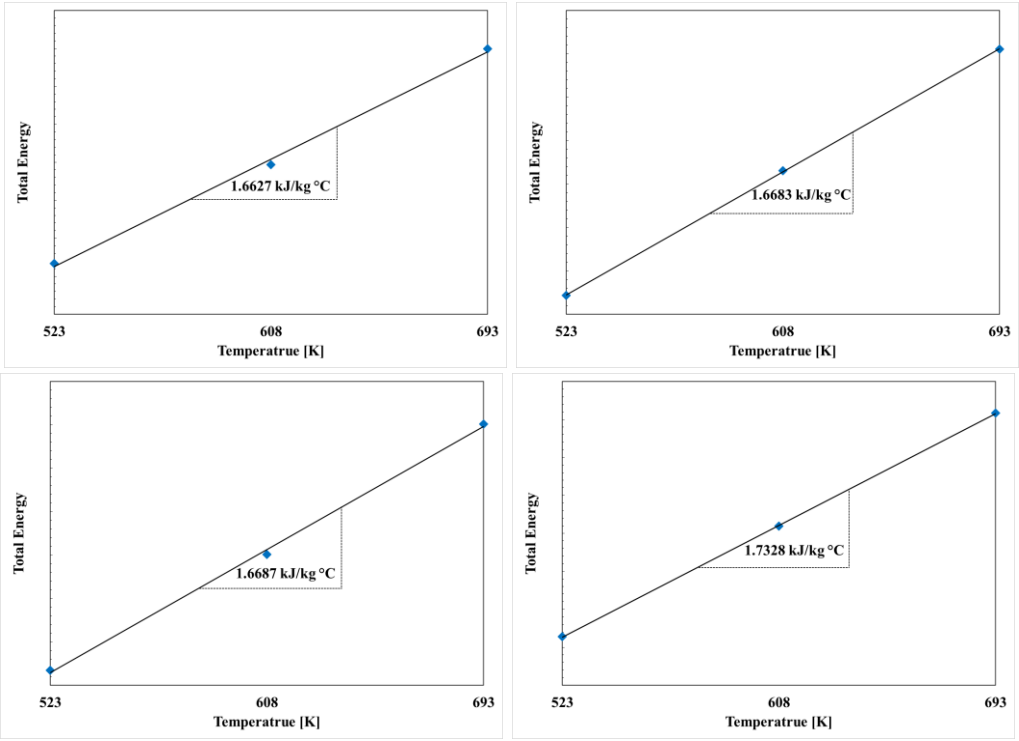

Figure 91 Slope of total energy and temperature of the binary molten salt nanofluid mixed with $NaNO_3$ rods (one rod: top left, two rods: top right, three rods: bottom left, and four rods: bottom right) between 250 °C (523 K) and 420 °C (693 K)

Table 29 Comparison of specific heat of the binary molten salt nanofluid mixed with $NaNO_3$ rods (one rod, two rods, three rods, and four rods) at the same volume (12.0 %)

Number of rod	Mass fraction (%)	Surface area (nm^2)	250 °C (523 K) to 420 °C (693 K)	
			Cp (kJ/kg °C)	Molten salt eutectic Cp (kJ/kg °C)
One $NaNO_3$ rod	12.0	3.64	1.6627	1.5756
Two $NaNO_3$ rods	12.0	4.25	1.6683	
Three $NaNO_3$ rods	12.0	4.50	1.6687	
Four $NaNO_3$ rods	12.0	5.92	1.7328	

In this simulation case, SiO_2 nanoparticle was used to confirm the effect of the surface energy between the binary molten salt eutectic and nanoparticle. The density of the molten salt nanofluid mixed with SiO_2 nanoparticle was calculated by 2000000 run in the NPT (e.g., isothermal-isobaric ensemble). The results of density converges during the simulation (2000000 run) and there is no fluctuation. This system is stable enough to calculate another thermophsical properties (e.g., specific heat) in the next step. The temperature range of all simulation was between 250 °C (523 K) and 420 °C (693 K). From this simulation set-up, the contribution of the surface energy of the nanostructure will be related to enhanced specific heat of nanofluid. The binary molten salt eutectic ($NaNO_3$-KNO_3) mixed with SiO_2 nanoparticle to verify the effect of the surface atoms between the binary molten salt and nanoparticle. The one SiO_2 nanoparticle was used in the binary molten salt eutectic and this mass fraction is fixed at 2.0 %. According to the literature [5], the density of the single chemical (e.g., $NaNO_3$ and KNO_3) was given. $NaNO_3$ is 1.80 g/cm^3 and KNO_3 is 1.81 g/cm^3 at 420 °C (693 K) respectively and the density of SiO_2 is 2.65 g/m^3. As shown in figure 92 and table 30, the results shows the density of the binary molten salt nanofluid mixed with SiO_2 nanoparticle in the simulation domain box. Its density is 1.860 g/cm^3 at the final step (2000000 run) at 693 K (420 °C). This density values is higher than the binary molten salt eutectic due to the high density value of SIO_2 nanoparticle (2.65 g/m^3).

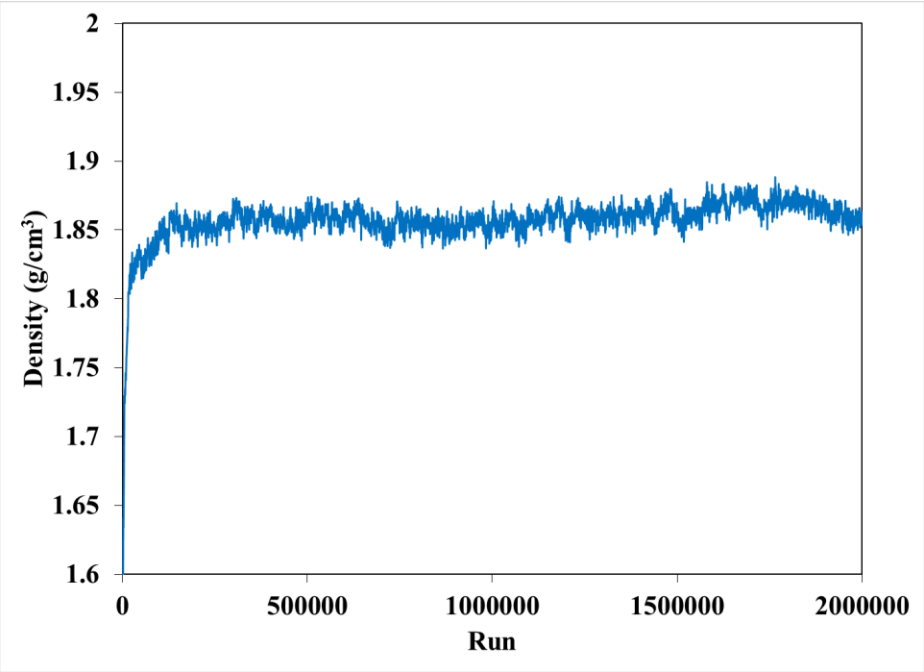

Figure 92 Density plot of the binary molten salt nanofluid mixed with SiO_2 nanoparticle at 693 K

Table 30 Comparison of density the binary molten salt eutectic and its nanofluid mixed with SiO_2 nanoparticle at 693 K

Nanoparticle	Mass fraction (%)	at the final step (2000000) at 693 K (420 °C)	
		Density (g/cm^3)	Molten salt eutectic Density (g/cm^3)
One SiO_2 nanoparticle	2.0	1.860	1.848

To calculate specific heat of this nanolfuid, the total energy (e.g., potential energy and kinetic energy) of the binary molten salt nanofluid with SiO_2 nanoparticle was computed by the NPT (the isothermal-isobaric ensemble) during the simulation step. This binary molten salt eutectic was mixed with one SiO_2 nanoparticle and its temperature range is between 250 °C (523 K) and 420 °C (693 K). The slope was created by the temperature and the total energy to obtain the specific heat of the nanofluid mixed SiO_2 nanoparticle. As shown in figure 93 and table 34, the specific heat of the binary molten salt nanofluid mixed with SiO_2 nanoparticle was decreased when the nanoparticle was added into the molten salt. According to the results, it shows 1.5455 kJ/kg °C with one SiO_2 nanoparticle and it is less than the binary molten salt eutectic. According to the literature [119], the specific heat of SiO_2 nanoparticle is 1.122 kJ/kg °C at high temperature (574 °C) and thus SiO_2 nanoparticle's specific heat is less than the specific heat of the binary molten salt eutectic under the temperature range in this simulation. The surface energy of the nanoparticle is not related to the enhanced specific heat of nanofuids. Although the enlarged surface area is related to the enhanced specific heat, this enhanced surface area of nanoparticles is not responsible for the enhanced specific heat of nanofluid. In other word, this results confirm that the effect of the surface atoms of $NaNO_3$ nanostructures, not SiO_2 nanoparticle, is responsible for enhanced specific heat of the binary molten salt ($NaNO_3$-KNO_3) eutectic nanofluids. Therefore, the specific heat of the binary molten salt nanofluid can be increased when the number of the surface energy of the $NaNO_3$ nanostructure is increased.

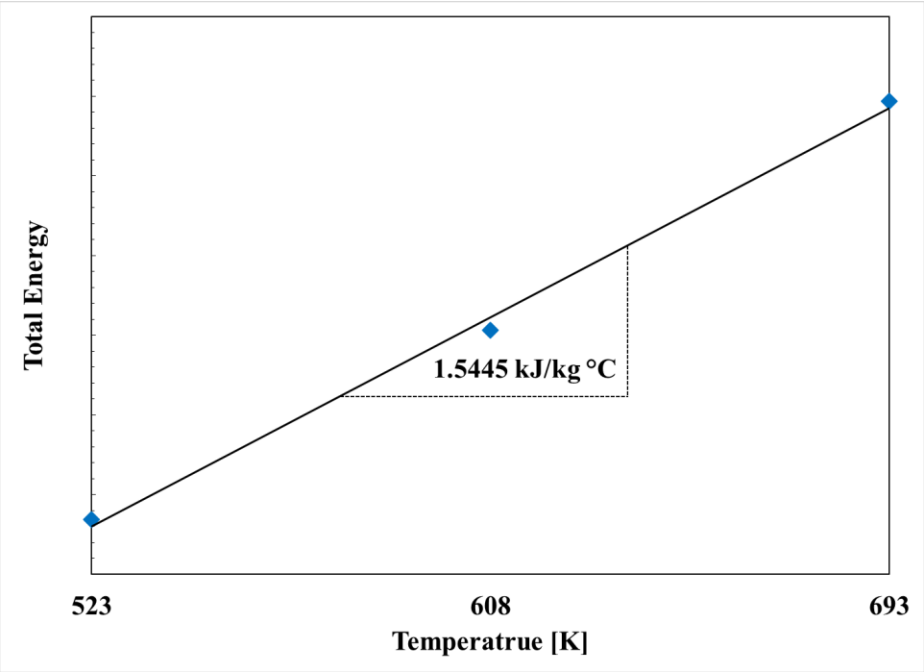

Figure 93 Slope of total energy and temperature of the binary molten salt nanofluid mixed with SiO_2 nanoparticle between 250 °C (523 K) and 420 °C (693 K)

Table 31 Comparison of specific heat of the binary molten salt eutectic and its nanofluid mixed with SiO_2 nanoparticle

Nanoparticle	Mass fraction (%)	250 °C (523 K) to 420 °C (693 K)	
		Cp (kJ/kg °C)	Molten salt eutectic Cp (kJ/kg °C)
One SiO_2 nanoparticle	2.0	1.5455	1.5756

Chapter 7 Conclusions

In this research, several commercial SiO_2 nanoparticles were dispersed into a ternary nitrate salt ($LiNO_3$–$NaNO_3$–KNO_3) to see if it can enhance its effective heat capacity. Several SiO_2 nanoparticles at different sizes were tested to investigate the effect of nanoparticle size. Fresh nanoparticles, then, were *in-situ* synthesized in a binary ($NaNO_3$-KNO_3) and ternary nitrate salts ($NaNO_3$-KNO_3-$Ca(NO_3)_2{\cdot}4(H_2O)$. $Al(NO_3)_3{\cdot}9H_2O$ (aluminum nitrate nonahydrate) and $Mg(NO_3)_2{\cdot}6H_2O$ (magnesium nitrate hexahydrate) were induced to decompose (e.g., thermal decomposition process) in a molten nitrate salt to produce Al_2O_3 and MgO nanoparticles. A figure of merit (FOM1 and FOM2) analysis was performed to predict the performance of the mixture. The new method (Liquid to Liquid) for the sample preparation was used to increase the enhancement of specific heat of a binary nitrate salt ($NaNO_3$-KNO_3) with SiO_2 nanoparticle. A modulated differential scanning calorimeter (MDSC; Q20, TA Instrument Inc.) was used to measure the effective heat capacity. A discovery hybrid rheometer (HR-2, TA Instruments Inc.) was employed to measure the mixture's viscosity. A customized apparatus was built to measure its effective thermal conductivity. A scanning electron microscope (SEM: Hitachi S-3000N and S-5000H) was used for material characterization. Moreover, molecular dynamics simulation was performed to investigate the effect of nanoparticles on the observed property measurements.

- The inhomogeneous interface between two different layers (solid and liquid) is likely to form the needle-like structure in the molten salt eutectic. This separation process (growing structure) can be used to explain how the fractal-like structure (micro-scale level) is formed physically. Molten salts possibly start to crystallize on a nanoparticle surface after separation. It

grows away from the nanoparticles and possibly form fractal-like structures (micro-scale level) in the molten salt nanofluid.

- The specific heat capacity of ternary molten salt ($LiNO_3$–$NaNO_3$–KNO_3) nanofluid with 5 nm, 10 nm, 30 nm, and 60 nm nanoparticles were enhanced by an average of 13 %-16 % compared to the pure ternary molten salt eutectic. The fractal-like nanostructures are formed by separated base molten salt. This nanostructure is responsible for enhanced specific heat of a molten salt nanofluid with SiO_2 nanoparticle.
- The nanoparticle (e.g., Al_2O_3 and MgO) was created by the thermal decomposition process of the hydrated salts ($Al(NO_3)_3 \cdot 9H_2$ and $Mg(NO_3)_2 \cdot 6H_2O$). For the binary nitrate molten salt eutectic, the size of each nanometer-size particle (Al_2O_3) was created and they show approximately 40 nm-60 nm size particle. For the ternary nitrate molten salt eutectic, the size of each nanometer-size particle (Al_2O_3) was created and they show approximately 30 nm-60 nm size particles.
- The enhancement of the specific heat capacity of the binary nitrate molten salt eutectic ($NaNO_3$-KNO_3) and nanofluid with Al_2O_3 and MgO nanoparticle is 39.7 % and 36.8 % on average respectively. The enhancement of the specific heat capacity of the ternary nitrate molten salt eutectic ($NaNO_3$-KNO_3-$Ca(NO_3)_2 \cdot 4(H_2O)$) and nanofluid with Al_2O_3 and MgO nanoparticle is 39.7 % and 36.8 % on average respectively.
- The performance of the binary nitrate molten salt eutectic ($NaNO_3$-KNO_3) with Al_2O_3 and MgO nanoparticle is enhanced by 115 %-130 % and 125 %-130 % respectively for the storage fluid point from the figure of merit (FOM1).

- The performance of the ternary nitrate molten salt eutectic ($NaNO_3$-KNO_3-$Ca(NO_3)_2{\cdot}4(H_2O)$) with Al_2O_3 and MgO nanoparticle is enhanced by 24 %-34 %and 96 %-99 % respectively for the storage fluid point from the figure of merit (FOM1).
- Thermal conductivity of this binary nitrate molten salt nanofluid with SiO_2 nanoparticle (10 nm size) were enhanced by 23 % compared to the pure eutectic salt respectively. GrPr (about 488) is definitely less than 1000 in the concentric cylinder we used. Therefore, convective heat transfer for the vertical direction can be avoided to measure thermal conductivity using the concentric cylinder type.
- The performance of the binary nitrate molten salt eutectic ($NaNO_3$-KNO_3) with SiO_2 nanoparticle is enhanced by 39 % for heat transfer fluid from the figure of merit (FOM2).
- The new method (molten mixing method) for the sample preparation shows the highest enhancement of specific heat compared to other methods (e.g., solution method and dry mixing method with liquid to solid loading process).
- For Molecular Dynamics (MD) simulation, the increase of the specific heat capacity may result from the contribution of the surface energy of the $NaNO_3$ nanostructure. To verify the effect of the surface energy, $NaNO_3$-KNO_3 molten salt eutectic mixed with one, two, three, and four $NaNO_3$ nanostructure rods and one single $NaNO_3$ nanostructure rod (3.2 %) was used to increase the number of rods in the system. The total mass fraction of each case is 3.2 %, 6.2 %, 9.0 %, and 11.7 % respectively when the number of the $NaNO_3$ nanostructure rod is increased. It shows 1.6175 kJ/kg °C with one $NaNO_3$ nanostructure rod, 1.6469 kJ/kg °C with two $NaNO_3$

nanostructure rods, 1.6940 kJ/kg °C with three $NaNO_3$ nanostructure rods, and 1.7328 kJ/kg °C with four $NaNO_3$ nanostructure rods respectively. It confirms that the effect of the surface atoms of the $NaNO_3$ nanostructure is responsible for enhanced specific heat of molten salt nanofluids and its specific heat can be increased when the number of the surface atoms of $NaNO_3$ nanostructure is increased.

- The binary molten salt eutectic ($NaNO_3$-KNO_3) mixed with one and two $NaNO_3$ nanostructure rods at the same mass fraction (6.0 %). It shows 1.6085 kJ/kg °C with one single $NaNO_3$ nanostructure rod and 1.6469 kJ/kg °C with two $NaNO_3$ nanostructure rods (one rod: 3.2 %) respectively. The binary molten salt mixed with two $NaNO_3$ nanostructure rods shows the highest enhanced specific heat compared to the one single $NaNO_3$ nanostructure rod at the same mass fraction (6.0 %) due to the enlarged surface area over the interior atoms in the nanostructure.
- The binary molten salt eutectic ($NaNO_3$-KNO_3) mixed with one, two, and three $NaNO_3$ nanostructure rods at the same mass fraction (9.0 %). The one single $NaNO_3$ nanostructure rod was used. Two $NaNO_3$ nanostructure rods were used to compare the effect of the surface atoms and its total mass fraction of nanostructures is about 9.0 % with two $NaNO_3$ nanostructure rods (one rod: 4.9 %). Three NaNO3 nanostructure rods were inserted in the domain and its total mass fraction of nanostructure is 9.0% with three NaNO3 nanostructure rods (one rod: 3.2 %). The binary molten salt mixed with three $NaNO_3$ nanostructure rods shows the highest enhanced specific heat compared to the other cases (e.g., one, two, and three rods) at the same

mass fraction (9.0 %) due to the enlarged surface area over the interior atoms in the nanostructure.

- The binary molten salt eutectic ($NaNO_3$-KNO_3) mixed with one, two, three, and four $NaNO_3$ nanostructure rods at the same mass fraction (12.0 %). The one single $NaNO_3$ nanostructure rod was used and this mass fraction is about 12.0 %. Two $NaNO_3$ nanostructure rods were used to compare the effect of the surface atoms and its total mass fraction of nanostructures is about 12.0 % with two $NaNO_3$ nanostructure rods (one rod: 6.2 %). Three NaNO3 nanostructure rods were inserted in the domain and its total mass fraction of nanostructure is about 12.0% with three $NaNO_3$ nanostructure rods (one rod: 4.1 %). Four $NaNO_3$ nanostructure rods were inserted in the domain and its total mass fraction of nanostructure is about 12.0 % with four NaNO3 nanostructure rods (one rod: 3.2 %). It shows 1.6627 kJ/kg °C with one single $NaNO_3$ nanostructure rod, 1.6683 kJ/kg °C with two $NaNO_3$ nanostructure rods, 1.6687 kJ/kg °C with three $NaNO_3$ nanostructure rods, and 1.7328 kJ/kg °C with four $NaNO_3$ nanostructure rods respectively. The binary molten salt mixed with four $NaNO_3$ nanostructure rods shows the highest enhanced specific heat compared to the other cases (e.g., one, two, three, and four rods) at the same mass fraction (12.0 %) due to the enlarged surface area over the interior atoms in the nanostructure.
- The enlarged surface area of the $NaNO_3$ nanostructure rod is related to the enhanced specific heat of nanofluids. The surface area of the $NaNO_3$ nanostructure was calculated to verify the effect of surface area when the number of the $NaNO_3$ nanostructure rod is increased. The surface area of the $NaNO_3$ nanostructure was enlarged due to the number of the $NaNO_3$

nanostructure rod at the same mass fraction as well as different mass fraction with the number of the $NaNO_3$ nanostructure rod (same size and shape).

- The specific heat of the binary molten salt nanofluid mixed with SiO_2 nanoparticle was decreased when the nanoparticle was added into the molten salt due to the low specific heat of SiO_2 nanoparticle. It shows 1.5455 kJ/kg °C with one SiO_2 nanoparticle and it is less than the specific heat of the binary molten salt eutectic.
- Although the enhanced specific heat was shown when the number of the $NaNO_3$ structure was increased in the molten salt eutectic, this enhanced specific heat is less than the experimental results of specific heat (~2.0 kJ/kg °C) from the previous chapter in this research. It is hard to mimic complicated nanostructures observed from the actual experiment because only few $NaNO_3$ nanostructure rods (one, two, three, and four rods) were used to calculate enhanced specific heat of nanofluid in this simulation.

References

[1] D. R. Malik, *Evaluation of Composite Alumina Nanoparticle and Nitrate Eutectic Materials for use in Concentrating Solar Power Plants,* 2010.

[2] R. I. Dunn, P. J. Hearps and M. N. Wright, "Molten-salt power towers: newly commercial concentrating solar storage," *Proc IEEE,* vol. 100, *(2),* pp. 504-515, 2012.

[3] R. Guédez, J. Spelling and B. Laumert, "Reducing the number of turbine starts in concentrating solar power plants through the integration of thermal energy storage," *Journal of Solar Energy Engineering,* vol. 137, *(1),* pp. 011003, 2015.

[4] G. Glatzmaier, *Summary Report for Concentrating Solar Power Thermal Storage Workshop: New Concepts and Materials for Thermal Energy Storage and Heat-Transfer Fluids, may 20, 2011,* 2011.

[5] G. J. Janz *et al*, *Physical Properties Data Compilations Relevant to Energy Storage.II.Molten Salts: Data on Single and Multi-Component Salt Systems,* 1979.

[6] D. Kearney *et al*, "Engineering aspects of a molten salt heat transfer fluid in a trough solar field," *Energy,* vol. 29, *(5),* pp. 861-870, 2004.

[7] C. Zhao and Z. Wu, "Thermal property characterization of a low melting-temperature ternary nitrate salt mixture for thermal energy storage systems," *Solar Energy Mater. Solar Cells,* vol. 95, *(12),* pp. 3341-3346, 2011.

[8] U. EIA, *Direct Federal Financial Interventions and Subsidies in Energy in Fiscal Year 2010,* 2015.

[9] Y. He *et al*, "Experimental investigation on turbulent heat transfer characteristics of molten salt in a shell-and-tube heat exchanger," *Appl. Therm. Eng.,* vol. 108, pp. 1206-1213, 2016.

[10] Q. Liu *et al*, "Thermodynamics investigation of a solar power system integrated oil and molten salt as heat transfer fluids," *Appl. Therm. Eng.,* vol. 93, pp. 967-977, 2016.

[11] H. Riazi *et al*, "The effect of nanoparticle morphology on the specific heat of nanosalts," *Int. J. Heat Mass Transfer,* vol. 94, pp. 254-261, 2016.

[12] C. Yang *et al*, "NOx emissions and the component changes of ternary molten nitrate salts in thermal energy storage process," *Appl. Energy,* vol. 184, pp. 346-352, 2016.

[13] Y. Luo *et al*, "Thermal energy storage enhancement of a binary molten salt via in-situ produced nanoparticles," *Int. J. Heat Mass Transfer,* vol. 104, pp. 658-664, 2017.

[14] P. Zhang, F. Ma and X. Xiao, "Thermal energy storage and retrieval characteristics of a molten-salt latent heat thermal energy storage system," *Appl. Energy,* vol. 173, pp. 255-271, 2016.

[15] Y. Jiang *et al*, "Eutectic Na 2 CO 3–NaCl salt: a new phase change material for high temperature thermal storage," *Solar Energy Mater. Solar Cells,* vol. 152, pp. 155-160, 2016.

[16] M. Wu, C. Xu and Y. He, "Cyclic behaviors of the molten-salt packed-bed thermal storage system filled with cascaded phase change material capsules," *Appl. Therm. Eng.,* vol. 93, pp. 1061-1073, 2016.

[17] D. Zhou and P. Eames, "Thermal characterisation of binary sodium/lithium nitrate salts for latent heat storage at medium temperatures," *Solar Energy Mater. Solar Cells,* vol. 157, pp. 1019-1025, 2016.

[18] M. C. Morrison and K. J. Bateman, "Transfer and Storage of Molten Salt for the Pyroprocessing of Used Nuclear Fuel," *Journal of Nuclear Engineering and Radiation Science,* vol. 3, *(1),* pp. 011001, 2017.

[19] H. Tiznobaik and D. Shin, "Enhanced specific heat capacity of high-temperature molten salt-based nanofluids," *Int. J. Heat Mass Transfer,* vol. 57, *(2),* pp. 542-548, 2013.

[20] J. Seo and D. Shin, "Enhancement of specific heat of ternary nitrate (LiNO3-NaNO3-KNO3) salt by doping with SiO2 nanoparticles for solar thermal energy storage," *Micro & Nano Letters,* vol. 9, *(11),* pp. 817-820, 2014.

[21] J. Seo and D. Shin, "Size effect of nanoparticle on specific heat in a ternary nitrate (LiNO 3–NaNO 3–KNO 3) salt eutectic for thermal energy storage," *Appl. Therm. Eng.,* vol. 102, pp. 144-148, 2016.

[22] H. Tiznobaik, D. Banerjee and D. Shin, "Effect of formation of “long range” secondary dendritic nanostructures in molten salt nanofluids on the values of specific heat capacity," *Int. J. Heat Mass Transfer,* vol. 91, pp. 342-346, 2015.

[23] B. Dudda and D. Shin, "Effect of nanoparticle dispersion on specific heat capacity of a binary nitrate salt eutectic for concentrated solar power applications," *International Journal of Thermal Sciences,* vol. 69, pp. 37-42, 2013.

[24] A. Fritsch *et al*, "Conceptual study of central receiver systems with liquid metals as efficient heat transfer fluids," *Energy Procedia,* vol. 69, pp. 644-653, 2015.

[25] M. Z. Hossain *et al*, "A new model for the thermal conductivity of molten salts," *Int. J. Thermophys.,* vol. 35, *(2),* pp. 246-255, 2014.

[26] S. U. Choi and J. A. Eastman, *Enhancing Thermal Conductivity of Fluids with Nanoparticles,* 1995.

[27] P. Keblinski, J. A. Eastman and D. G. Cahill, "Nanofluids for thermal transport," *Materials Today,* vol. 8, *(6),* pp. 36-44, 2005.

[28] X. Wang and A. S. Mujumdar, "Heat transfer characteristics of nanofluids: a review," *International Journal of Thermal Sciences,* vol. 46, *(1),* pp. 1-19, 2007.

[29] J. A. Eastman *et al*, "Anomalously increased effective thermal conductivities of ethylene glycol-based nanofluids containing copper nanoparticles," *Appl. Phys. Lett.,* vol. 78, *(6),* pp. 718-720, 2001.

[30] J. Eapen *et al*, "Mean-field versus microconvection effects in nanofluid thermal conduction," *Phys. Rev. Lett.,* vol. 99, *(9),* pp. 095901, 2007.

[31] N. Putra, P. Thiesen and W. Roetzel, "Temperature dependence of thermal conductivity enhancement for nanofluids," *Journal of Heat Transfer,* vol. 125, pp. 567-574, 2003.

[32] C. H. Li and G. Peterson, "Experimental investigation of temperature and volume fraction variations on the effective thermal conductivity of nanoparticle suspensions (nanofluids)," *J. Appl. Phys.,* vol. 99, *(8),* pp. 084314, 2006.

[33] H. Xie *et al*, "Thermal conductivity enhancement of suspensions containing nanosized alumina particles," *J. Appl. Phys.,* vol. 91, *(7),* pp. 4568-4572, 2002.

[34] T. Hong, H. Yang and C. Choi, "Study of the enhanced thermal conductivity of Fe nanofluids," *J. Appl. Phys.,* vol. 97, *(6),* pp. 064311, 2005.

[35] P. Keblinski *et al*, "Mechanisms of heat flow in suspensions of nano-sized particles (nanofluids)," *Int. J. Heat Mass Transfer,* vol. 45, *(4),* pp. 855-863, 2002.

[36] S. P. Jang and S. U. Choi, "Role of Brownian motion in the enhanced thermal conductivity of nanofluids," *Appl. Phys. Lett.,* vol. 84, *(21),* pp. 4316-4318, 2004.

[37] W. Evans, J. Fish and P. Keblinski, "Role of Brownian motion hydrodynamics on nanofluid thermal conductivity," *Appl. Phys. Lett.,* vol. 88, *(9),* pp. 093116, 2006.

[38] W. Yu and S. Choi, "The role of interfacial layers in the enhanced thermal conductivity of nanofluids: a renovated Maxwell model," *Journal of Nanoparticle Research,* vol. 5, *(1-2),* pp. 167-171, 2003.

[39] L. Xue *et al*, "Effect of liquid layering at the liquid–solid interface on thermal transport," *Int. J. Heat Mass Transfer,* vol. 47, *(19),* pp. 4277-4284, 2004.

[40] J. Buongiorno *et al*, "A benchmark study on the thermal conductivity of nanofluids," *J. Appl. Phys.,* vol. 106, *(9),* pp. 094312, 2009.

[41] P. Keblinski, R. Prasher and J. Eapen, "Thermal conductance of nanofluids: is the controversy over?" *Journal of Nanoparticle Research,* vol. 10, *(7),* pp. 1089-1097, 2008.

[42] W. Evans *et al*, "Effect of aggregation and interfacial thermal resistance on thermal conductivity of nanocomposites and colloidal nanofluids," *Int. J. Heat Mass Transfer,* vol. 51, *(5),* pp. 1431-1438, 2008.

[43] S. Li and J. Eastman, "Measuring thermal conductivity of fluids containing oxide nanoparticles," *J.Heat Transf,* vol. 121, *(2),* pp. 280-289, 1999.

[44] H. Xie *et al*, "Thermal conductivity of suspensions containing nanosized SiC particles," *Int. J. Thermophys.,* vol. 23, *(2),* pp. 571-580, 2002.

[45] Y. Xuan and Q. Li, "Heat transfer enhancement of nanofluids," *Int J Heat Fluid Flow,* vol. 21, *(1),* pp. 58-64, 2000.

[46] H. Xie *et al*, "Nanofluids containing multiwalled carbon nanotubes and their enhanced thermal conductivities," *J. Appl. Phys.,* vol. 94, *(8),* pp. 4967-4971, 2003.

[47] X. Wang, X. Xu and S. U. Choi, "Thermal conductivity of nanoparticle-fluid mixture," *J. Thermophys. Heat Transfer,* vol. 13, *(4),* pp. 474-480, 1999.

[48] J. Fan and L. Wang, "Review of heat conduction in nanofluids," *Journal of Heat Transfer,* vol. 133, *(4),* pp. 040801, 2011.

[49] A. Lenert, Y. Nam and E. N. Wang, "Heat transfer fluids," *Annual Review of Heat Transfer,* vol. 15, *(15),* 2012.

[50] I. C. Nelson, D. Banerjee and R. Ponnappan, "Flow loop experiments using polyalphaolefin nanofluids," *J. Thermophys. Heat Transfer,* vol. 23, *(4),* pp. 752, 2009.

[51] M. R. Betts, *The Effects of Nanoparticle Augmentation of Nitrate Thermal Storage Materials for use in Concentrating Solar Power Applications,* 2011.

[52] L. Wang *et al*, "Enhancement of molar heat capacity of nanostructured Al2O3," *Journal of Nanoparticle Research,* vol. 3, *(5),* pp. 483-487, 2001.

[53] D. Chen and X. He, "Synthesis of nickel ferrite nanoparticles by sol-gel method," *Mater. Res. Bull.,* vol. 36, *(7),* pp. 1369-1377, 2001.

[54] J. Buongiorno, "Convective transport in nanofluids," *Journal of Heat Transfer,* vol. 128, *(3),* pp. 240-250, 2006.

[55] B. Wang, L. Zhou and X. Peng, "Surface and size effects on the specific heat capacity of nanoparticles," *Int. J. Thermophys.,* vol. 27, *(1),* pp. 139-151, 2006.

[56] I. Avramov and M. Michailov, "Specific heat of nanocrystals," *Journal of Physics: Condensed Matter,* vol. 20, *(29),* pp. 295224, 2008.

[57] P. Andreu-Cabedo *et al*, "Increment of specific heat capacity of solar salt with SiO2 nanoparticles," *Nanoscale Research Letters,* vol. 9, *(1),* pp. 582, 2014.

[58] M. Chieruzzi *et al*, "Effect of nanoparticles on heat capacity of nanofluids based on molten salts as PCM for thermal energy storage," *Nanoscale Research Letters,* vol. 8, *(1),* pp. 448, 2013.

[59] M. Schuller, Q. Shao and T. Lalk, "Experimental investigation of the specific heat of a nitrate–alumina nanofluid for solar thermal energy storage systems," *International Journal of Thermal Sciences,* vol. 91, pp. 142-145, 2015.

[60] M. Lasfargues *et al*, "Mechanical dispersion of nanoparticles and its effect on the specific heat capacity of impure binary nitrate salt mixtures," *Nanomaterials,* vol. 5, *(3),* pp. 1136-1146, 2015.

[61] R. Devaradjane and D. Shin, "Nanoparticle dispersions on ternary nitrate salts for heat transfer fluid applications in solar thermal power," *Journal of Heat Transfer,* vol. 138, *(5),* pp. 051901, 2016.

[62] D. Shin and D. Banerjee, "Enhanced specific heat of silica nanofluid," *Journal of Heat Transfer,* vol. 133, *(2),* pp. 024501, 2011.

[63] H. Tiznobaik and D. Shin, "Experimental validation of enhanced heat capacity of ionic liquid-based nanomaterial," *Appl. Phys. Lett.,* vol. 102, *(17),* pp. 173906, 2013.

[64] D. Shin and D. Banerjee, "Enhanced specific heat capacity of nanomaterials synthesized by dispersing silica nanoparticles in eutectic mixtures," *Journal of Heat Transfer,* vol. 135, *(3),* pp. 032801, 2013.

[65] D. Shin and D. Banerjee, "Specific heat of nanofluids synthesized by dispersing alumina nanoparticles in alkali salt eutectic," *Int. J. Heat Mass Transfer,* vol. 74, pp. 210-214, 2014.

[66] D. Shin and D. Banerjee, "Enhancement of specific heat capacity of high-temperature silica-nanofluids synthesized in alkali chloride salt eutectics for solar

thermal-energy storage applications," *Int. J. Heat Mass Transfer,* vol. 54, *(5),* pp. 1064-1070, 2011.

[67] M. X. Ho and C. Pan, "Optimal concentration of alumina nanoparticles in molten Hitec salt to maximize its specific heat capacity," *Int. J. Heat Mass Transfer,* vol. 70, pp. 174-184, 2014.

[68] B. Jo and D. Banerjee, "Viscosity measurements of multi-walled carbon nanotubes-based high temperature nanofluids," *Mater Lett,* vol. 122, pp. 212-215, 2014.

[69] M. Lasfargues *et al*, "Rheological Analysis of Binary Eutectic Mixture of Sodium and Potassium Nitrate and the Effect of Low Concentration CuO Nanoparticle Addition to Its Viscosity," *Materials,* vol. 8, *(8),* pp. 5194-5204, 2015.

[70] H. Chen *et al*, "Rheological behaviour of ethylene glycol based titania nanofluids," *Chemical Physics Letters,* vol. 444, *(4),* pp. 333-337, 2007.

[71] C. F. Bonilla, "Nuclear engineering," 1957.

[72] G. Qiao *et al*, "Simulation and experimental study of the specific heat capacity of molten salt based nanofluids," *Appl. Therm. Eng.,* vol. 111, pp. 1517-1522, 2017.

[73] G. Qiao, A. Alexiadis and Y. Ding, "Simulation study of anomalous thermal properties of molten nitrate salt," *Powder Technol,* vol. 314, pp. 660-664, 2017.

[74] S. Jayaraman *et al*, "Molecular simulation of the thermal and transport properties of three alkali nitrate salts," *Ind Eng Chem Res,* vol. 49, *(2),* pp. 559-571, 2009.

[75] R. Prasher, P. Bhattacharya and P. E. Phelan, "Brownian-motion-based convective-conductive model for the effective thermal conductivity of nanofluids," *Journal of Heat Transfer,* vol. 128, *(6),* pp. 588-595, 2006.

[76] L. Li *et al*, "Molecular dynamics simulation of effect of liquid layering around the nanoparticle on the enhanced thermal conductivity of nanofluids," *Journal of Nanoparticle Research,* vol. 12, *(3),* pp. 811-821, 2010.

[77] S. H. Oh *et al*, "Ordered liquid aluminum at the interface with sapphire," *Science,* vol. 310, *(5748),* pp. 661-663, 2005. . DOI: 1118611 [pii].

[78] P. Namburu *et al*, "Experimental investigation of viscosity and specific heat of silicon dioxide nanofluids," *Micro & Nano Letters,* vol. 2, *(3),* pp. 67-71, 2007.

[79] S. Zhou and R. Ni, "Measurement of the specific heat capacity of water-based Al 2 O 3 nanofluid," *Appl. Phys. Lett.,* vol. 92, *(9),* pp. 093123, 2008.

[80] R. S. Vajjha and D. K. Das, "Specific heat measurement of three nanofluids and development of new correlations," *Journal of Heat Transfer,* vol. 131, *(7),* pp. 071601, 2009.

[81] W. Luo, W. Hu and S. Xiao, "Size effect on the thermodynamic properties of silver nanoparticles," *The Journal of Physical Chemistry C,* vol. 112, *(7),* pp. 2359-2369, 2008.

[82] M. Saeedian *et al*, "Specific heat capacity of TiO2 nanoparticles," *Journal of Computational and Theoretical Nanoscience,* vol. 9, *(4),* pp. 616-620, 2012.

[83] D. Shin, H. Tiznobaik and D. Banerjee, "Specific heat mechanism of molten salt nanofluids," *Appl. Phys. Lett.,* vol. 104, *(12),* pp. 121914, 2014.

[84] M. Salanne and P. A. Madden, "Polarization effects in ionic solids and melts," *Mol. Phys.,* vol. 109, *(19),* pp. 2299-2315, 2011.

[85] B. Chakraborty, J. Wang and J. Eapen, "Multicomponent diffusion in molten LiCl-KCl: Dynamical correlations and divergent Maxwell-Stefan diffusivities," *Physical Review E,* vol. 87, *(5),* pp. 052312, 2013.

[86] M. Chemla and I. Okada, "Ionic mobilities of monovalent cations in molten salt mixtures," *Electrochim. Acta,* vol. 35, *(11-12),* pp. 1761-1776, 1990.

[87] I. Okada, "The Chemla effect---from the separation of isotopes to the modeling of binary ionic liquids," *Journal of Molecular Liquids,* vol. 83, *(1-3),* pp. 5-22, 1999.

[88] M. C. Ribeiro, "On the Chemla effect in molten alkali nitrates," *J. Chem. Phys.,* vol. 117, *(1),* pp. 266-276, 2002.

[89] M. C. Ribeiro, "Chemla effect in molten LiCl/KCl and LiF/KF mixtures," *The Journal of Physical Chemistry B,* vol. 107, *(18),* pp. 4392-4402, 2003.

[90] B. Morgan and P. A. Madden, "Ion mobilities and microscopic dynamics in liquid (Li, K) Cl," *J. Chem. Phys.,* vol. 120, *(3),* pp. 1402-1413, 2004.

[91] D. A. Porter, K. E. Easterling and M. Sherif, *Phase Transformations in Metals and Alloys, (Revised Reprint).* 2009.

[92] C. Martin, T. Bauer and H. Müller-Steinhagen, "An experimental study of a non-eutectic mixture of KNO 3 and NaNO 3 with a melting range for thermal energy storage," *Appl. Therm. Eng.,* vol. 56, *(1),* pp. 159-166, 2013.

[93] R. O. Suzuki *et al*, "Titanium powder prepared by magnesiothermic reduction of Ti 2 in molten salt," *Metallurgical and Materials Transactions B,* vol. 30, *(3),* pp. 403-410, 1999.

[94] K. Coscia *et al*, "Thermophysical Properties of LiNO3–NaNO3–KNO3 Mixtures for Use in Concentrated Solar Power," *Journal of Solar Energy Engineering,* vol. 135, *(3),* pp. 034506, 2013.

[95] E. El-Shereafy *et al*, "Mechanism of thermal decomposition and γ-pyrolysis of aluminum nitrate nonahydrate [Al (NO3) 3· 9H2O]," *J. Radioanal. Nucl.,* vol. 237, *(1-2),* pp. 183-186, 1998.

[96] F. Paulik *et al*, "Investigation on the thermal behaviour of Mg (NO3) 2· 6H2O I. The decomposition behaviour," *Journal of Thermal Analysis and Calorimetry,* vol. 34, *(3),* pp. 627-635, 1988.

[97] T. Bauer, D. Laing and R. Tamme, "Characterization of sodium nitrate as phase change material," *Int. J. Thermophys.,* vol. 33, *(1),* pp. 91-104, 2012.

[98] D. Kearney *et al*, "Evaluation of a molten salt heat transfer fluid in a parabolic trough solar field," *Proc.of Solar 2002,* 2002.

[99] R. Serrano-López, J. Fradera and S. Cuesta-López, "Molten salts database for energy applications," *Chemical Engineering and Processing: Process Intensification,* vol. 73, pp. 87-102, 2013.

[100] L. Moens *et al*, "Advanced thermal storage fluids for solar parabolic trough systems," *Transactions-American Society of Mechanical Engineers Journal of Solar Energy Engineering,* vol. 125, *(1),* pp. 112-116, 2003.

[101] J. C. Gomez *et al*, "Ca (NO3) 2—NaNO3—KNO3 Molten Salt Mixtures for Direct Thermal Energy Storage Systems in Parabolic Trough Plants," *Journal of Solar Energy Engineering,* vol. 135, *(2),* pp. 021016, 2013.

[102] A. A. Balandin *et al*, "Superior thermal conductivity of single-layer graphene," *Nano Letters,* vol. 8, *(3),* pp. 902-907, 2008.

[103] S. Ramirez *et al*, "Thermal and magnetic properties of nanostructured densified ferrimagnetic composites with graphene-graphite fillers," *Mater Des,* vol. 118, pp. 75-80, 2017.

[104] X. Zhang and M. Fujii, "Simultaneous measurements of the thermal conductivity and thermal diffusivity of molten salts with a transient short-hot-wire method," *Int. J. Thermophys.,* vol. 21, *(1),* pp. 71-84, 2000.

[105] R. DiGuilio and A. Teja, "The thermal conductivity of the molten NaNO3-KNO3 eutectic between 525 and 590 K," *Int. J. Thermophys.,* vol. 13, *(4),* pp. 575-592, 1992.

[106] A. G. Vilella and S. Yesilyurt, "Analysis of heat storage with a thermocline tank for concentrated solar plants: Application to AndaSol I," in *Industrial Technology (ICIT), 2015 IEEE International Conference On,* 2015, .

[107] N. V. Tsederberg and R. D. Cess, *Thermal Conductivity of Gases and Liquids.* 1965*229*.

[108] L. R. White and H. T. Davis, "Thermal conductivity of molten alkali nitrates," *J. Chem. Phys.,* vol. 47, *(12),* pp. 5433-5439, 1967.

[109] C. W. Smith, "Pilot test results utilizing polymeric dispersants for control of silica," in *Water Soluble Polymers*Anonymous 2002, .

[110] T. Bauer *et al*, "Overview of molten salt storage systems and material development for solar thermal power plants," in *Proceedings of the 2012 National Solar Conference for (SOLAR 2012), Denver,* 2012, .

[111] N. Singh, *Computational Analysis of Thermo-Fluidic Characteristics of a Carbon Nano-Fin.* 2010.

[112] V. B. Pawar, *Computational Analysis of Nanostructures Formed in Molten Salt Nanofluids.* 2014.

[113] A. Rajabpour *et al*, "Molecular dynamics simulation of the specific heat capacity of water-Cu nanofluids," *International Nano Letters,* vol. 3, *(1),* pp. 58, 2013.

[114] Y. Hu *et al*, "Effect of Al 2 O 3 nanoparticle dispersion on the specific heat capacity of a eutectic binary nitrate salt for solar power applications," *Energy Conversion and Management,* vol. 142, pp. 366-373, 2017.

[115] D. C. Rapaport *et al*, "The art of molecular dynamics simulation," *Comput. Phys.,* vol. 10, *(5),* pp. 456-456, 1996.

[116] G. Yuan, Z. Wei and G. Li, "A modified Polak–Ribière–Polyak conjugate gradient algorithm for nonsmooth convex programs," *J. Comput. Appl. Math.,* vol. 255, pp. 86-96, 2014.

[117] L. Li *et al*, "An investigation of molecular layering at the liquid-solid interface in nanofluids by molecular dynamics simulation," *Physics Letters A,* vol. 372, *(25),* pp. 4541-4544, 2008.

[118] A. Stukowski, "Visualization and analysis of atomistic simulation data with OVITO–the Open Visualization Tool," *Modell Simul Mater Sci Eng,* vol. 18, *(1),* pp. 015012, 2009.

[119] J. J. Reed, "The NIST Chemistry Webbook," 2009.

Biographical Information

Joohyun Seo was a doctoral student at the department of Materials Science and Engineering (MSE) in the University of Texas at Arlington. He earned his PhD in December 2017 and he completed the doctoral dissertation on investigation of thermophysical properties of enhanced molten salt nanofluids for thermal energy storage (TES) in concentrated solar power (CSP) systems. He has a Master of Science degree in Mechanical Engineering from Inha University in 2009 and he also received a Bachelor of Science degree in Mechanical and System Design Engineering from Hongik University in 2007. He is interested in nitrate-based and carbonate-based nanofluids for thermal energy storage (TES) applications in concentrated solar power (CSP) systems, high-temperature nanomaterials, fractal nanostructures, molecular dynamics (MD) simulation, and formation of different phases at nanoscale interfaces in enhanced molten salt nanofluids.